LEGIBILITY NOTICE

A major purpose of the Technical Information Center is to provide the broadest dissemination possible of information contained in DOE's Research and Development Reports to business, industry, the academic community, and federal, state and local governments.

Although a small portion of this report is not reproducible, it is being made available to expedite the availability of information on the research discussed herein.

EPA-230-04-84-006

United States
Environmental Protection
Agency

Stategic Studies Staff
Office of Policy Analysis
Office of Policy, Planning
and Evaluation

April 1984

EPA

Potential Climatic Impacts of Increasing Atmospheric CO_2 with Emphasis on Water Availability and Hydrology in the United States

MASTER

POTENTIAL CLIMATIC IMPACTS OF INCREASING ATMOSPHERIC CO_2 WITH EMPHASIS ON WATER AVAILABILITY AND HYDROLOGY IN THE UNITED STATES

EPA--230-04-84-006

DE85 901081

REPORT PREPARED FOR
THE ENVIRONMENTAL PROTECTION AGENCY

BY

NASA GODDARD SPACE FLIGHT CENTER
INSTITUTE FOR SPACE STUDIES
NEW YORK, N.Y. 10025

Principal contributors: David Rind and Sergej Lebedeff

CAUTION: The state of the art of climate modeling is inadequate to accurately forecast climate changes on the regional level. The grid estimates contained in this report are for study purposes only and should not be relied upon or used for the purposes of planning.

NOTICE
PORTIONS OF THIS REPORT ARE ILLEGIBLE.
It has been reproduced from the best available copy to permit the broadest possible availability.

DISTRIBUTION OF THIS DOCUMENT IS UNLIMITED

JSW

TABLE OF CONTENTS

SECTION	TITLE	PAGE
	PREFACE	i
	INTRODUCTION	1
I	CLIMATE MODEL ASSESSMENT OF THE HYDROLOGICAL CHANGES ASSOCIATED WITH DOUBLING ATMOSPHERIC CO_2	3
II	DIFFERENCE OF PRECIPITATION BETWEEN WARM AND COLD PERIODS IN THIS CENTURY	55
III	FUTURE REFINEMENTS TO CLIMATE MODELS	78
APPENDIX A	ESTIMATING ANNUAL CHANGES IN TEMPERTATURES	82
	REFERENCES	94

PREFACE

By

John S. Hoffman* and Stephen Seidel**

Water planners, coastal engineers, and agronomists as part of their jobs necessarily make assumptions about future water supplies, temperature, droughts, and storms. In general, they assume that in the future these conditions will repeat those of the past -- there will be the same amount of water available, the worst storm during the next hundred years will be similar to the worst storm during the past 100 years, and droughts will be of similar frequency and duration. Such assumptions are used to design public works, to demarcate flood plains, and to establish safety and growth margins for project and planning purposes. In agriculture, such assumptions form the basis for developing more productive strains of crops and for establishing planting and irrigation practices.

Unfortunately, the underlying assumption that future climate will essentially repeat the past no longer appears valid. Research efforts since the turn of the century have produced considerable scientific support for the belief that increases in atmospheric levels of carbon dioxide and other greenhouse gases will increase global temperature and alter precipitation patterns by trapping infrared radiation.

---

*Director, Strategic Studies Staff, Office of Policy Analysis, U.S. Environmental Protection Agency

**Senior Policy Analyst, Strategic Studies Staff, Office of Policy Analysis, U.S. Environmental Protection Agency

Although a significant rise in temperature appears likely, much uncertainty still surrounds the timing and magnitude of a greenhouse warming. Moreover, less confidence exists about effects other than temperature, including potentially critical changes in regional rainfall, evaporation, storms, droughts, run-off, and soil moisture. Yet the importance of possible shifts in the hydrologic cycle on future agricultural practices, public works, and development patterns underscores the need to improve our ability to project likely changes.

This study focuses specifically on possible shifts in a range of hydrologic conditions that could accompany a doubling of atmospheric carbon dioxide. It reports on an experiment done with the Goddard Institute for Space Study's general circulation model (GCM) -- a complex computer simulation of the physical forces that produce weather patterns. GCMs are the most sophisticated tool used to project climatic changes resulting from increases in greenhouse gases. Past reporting of GCM experiments has dealt primarily with likely changes in temperature accompanying a doubling of atmospheric CO_2 levels; this analysis shows how these models can be used to examine potential hydrologic effects. THIS STUDY REPRESENTS A FIRST ATTEMPT AT PROVIDING DETAILED REGIONAL HYDROLOGIC EFFECTS. THE VALUES GIVEN FOR HYDROLOGIC CONDITIONS IN PARTICULAR GRIDS SHOULD NOT BE USED FOR PLANNING PURPOSES.

Section I reports on a range of hydrologic conditions (e.g., precipitation, evaporation, soil moisture, run-off) for a "control" run that seeks to duplicate existing conditions. It then compares these results with output from a model run where atmospheric CO_2 levels are doubled. Section II shifts the focus of analysis from the future to the past. It compares hydrologic conditions during a particularly cold period (1900-20) with a particularly warm period (1940-60). The final section discusses future research efforts needed to advance our understanding and to improve GCMs and thus enhance our ability to respond to changes resulting from the greenhouse effect. It also describes an important project underway at GISS to further this effort. The remainder of this foreward sets the context for this analysis.

Scientific Evidence of the Greenhouse Effect

Greenhouse gases in the atmosphere allow the sun's energy to penetrate and warm the earth, but then block the escape of some of the infrared energy given off by our planet. In effect, these gases form a thermal blanket around the earth. Carbon dioxide is an important greenhouse gas. Others exhibiting the same property include water vapor, nitrous oxide, methane, and the chlorofluorocarbons.

A small amount of these greenhouse gases in the atmosphere is partly responsible for the climatic conditions under which our civilization has prospered. For example, the earth is 30°C (58°F) warmer than it would be without the presence of any greenhouse gases. In contrast, the atmosphere surrounding Venus is 97 percent CO_2 and it is much warmer than earth, while Mars with little CO_2 or water vapor in its atmosphere is much colder.

Although CO_2 constitutes only .03% of our atmosphere, it has increased more than 20% since the beginning of the Industrial Revolution. Much of this increase is directly linked to expanded use of coal, oil, and natural gas. In addition, past reductions in forests -- trees absorb and store carbon dioxide during photosynthesis -- may also have contributed to historical increases in atmospheric CO_2 levels.

Despite this sizable increase in CO_2 levels, the complexity and time lags built into our climatic system prevent scientists from stating unequivocably that the global warming experienced since 1850 can be attributed to the rise in CO_2. The amount of warming that should accompany the past rise in CO_2 is too small compared to unexplained natural variation in global temperature to yield statistically significant proof that CO_2 is responsible. Nonetheless, this warming is consistent with expectations.

In an effort to illuminate this issue, the National Academy of Sciences has conducted two extensive reviews (1979, 1983) of what we know and don't know about the greenhouse effect. In each case, they concluded that temperatures would ultimately increase somewhere between 1.5°C (2.7° F) and 4.5°C (8.1° F) for a doubling of pre-industrial atmospheric CO_2 levels (to 600 ppm). Increases in other greenhouse gases could increase the overall warming by an additional 50-100 percent. Current estimates of fossil fuel usage suggest that we could reach atmospheric levels of 600 ppm by 2075 (NAS, 1983).

This rate of temperature change would be unprecendented. For example, a temperature increase of 2.0°C (3.8° F) by 2050 would be roughly comparable to the highest temperature of the last 100,000 years. At the height of the last Ice Age, approximately 15,000 years ago, the earth was only about 5°C (9.0° F) colder.

Rising temperatures would produce many other climatic changes. As the difference in temperature between the equator and the poles shifts -- the poles will warm at a faster rate because melting ice changes their albedo -- weather patterns may be radically altered, resulting in changes in precipitation.

Potential Changes in the Hydrologic Cycle

This study first looks at aggregate measures of changes in the hydrologic cycle such as annual average precipitation and evaporation for the entire North American continent. These changes provide a broad sense of whether we are likely to experience more or less rainfall.

However, most decisions based on assumptions about hydrologic conditions require more specific data. Annual averages across a large geographic scale are not detailed enough in two respects. They may mask critically important changes in the seasonality of precipitation. For example, moderate rainfall just before spring planting is far more important to agricultural productivity than the same rainfall in the fall. Similarly, rainfall concentrated in a single season would require different design standards for many public works than the same amount dispersed throughout the year.

To be useful to decisionmakers, projections of hydrologic changes must also be tied to specific locations. Precipitation can vary dramatically within a hundred miles depending on the location of mountains, lakes, and oceans, and on prevailing wind patterns. Other important factors such as soil moisture and run-off also are linked to conditions at a specific location.

This study seeks to address these issues by examining possible changes in specific hydrologic characteristics including ground moisture, lenghth of growing season, frequency and severity of droughts, run-off, and ground moisture. Changes in these factors may be particularly relevant to decisionmakers concerned with long-term projects (25 years or more) that are sensitive to assumptions concerning hydrologic conditions.

Caveats to This Analysis

The GISS results suggest substantial changes throughout the hydrologic cycle. If changes of this magnitude were to occur in the future, the assumption that future hydrologic conditions would repeat the past would fall far wide of its mark. However, the results of this modeling effort should be considered only the first step in the process of planning for future changes. Because of current limitations, the model does not resolve many important issues. Model input and resolution must be enhanced in several important respects.

To minimize computer time, the GCM developed by GISS simulates the weather for rather large grid areas. The whole earth was divided into grids, each consisting of approximately 17,000 sq. miles. The grid size used in GCMs covers a large area of land that may include diverse topography. Not only does this prevent a completely reliable representation of the physical processes that determine weather, but it also makes interpretation of the output somewhat difficult. Conditions at a specific location within a grid may vary considerably from the average for the grid.

The GISS model produces a warming of 4.1°C, a temperature increase at the higher end of the current NAS temperature range (1.5-4.5°C) for a doubling of atmospheric CO_2. As we learn more about the processes producing climate, it is possible that this number will shift, though it probably will remain within the NAS range. Narrowing this range will require more extensive data from observed characteristics of the oceans and clouds as they effect our climate system and improvements in the representation of the processes in models. Changes also will be needed in detailing ground hydrology, vegetation response, and the changes in these systems over time as climatic conditions shift. More accurate model results will become available only as quickly as support is given to efforts to observe the climate system adequately to enhance and validate the GCM models.

As they now stand, GCMs are able to accurately recreate existing climatic conditions only at a very aggregate level. Thus, when run with existing concentrations of greenhouse gases, they will produce current global temperature, rainfall, and seasonal changes in reasonably accurate fashion. Today's models cannot, however, recreate existing conditions in each grid -- essential information for decisionmakers. For example, in the control run for this study, efforts to recreate existing hydrolgic conditions produced results that were generally consistent for the entire North American continent, but showed 50-100 percent excessive rainfall in the western part of the continent and half the observed rainfall around Tennessee. Clearly, improvements to the model will be required to increase the reliability of its output, particularly where information from individual grids is being used.

Finally, the model run examined in this report looks only at changes that will occur once CO_2 levels have doubled and temperatures have reached equilibrium. Steady state conditions are useful to simplify the analysis, but focus attention on changes that probably will not occur before 2075. In the interim significant hydrologic changes are likely to accompany increases in CO_2 and other greenhouse gases. Nor is there a basis for simply stating that the transitional period will be a linear interpolation based on the results from a doubling of CO_2. In fact, a region shown to be drier after a doubling of CO_2 has occurred could, in fact, first become wetter before beginning to dry.

As mentioned above, Section III of this report discusses efforts currently underway to improve the ability of GCM's to reliably predict climatic changes associated with annual increases in levels of greenhouse gases. Appendix A details some of the assumptions that will be made in a first effort to simulate the yearly evolution of climate. These results should be available by the end of 1984 and provide a better basis for assessing the short and long-term vulnerability of decisions to climatic change.

Potential Response by Decisionmakers

Given the uncertainties surrounding the results of this study, water planners, engineers and agronomists face a difficult situation. Based on the output presented here and elsewhere, it is clear that future hydrologic conditions should diverge from past conditions and that decisions involving long-term projects may be vulnerable to such changes. Nonetheless, we are currently limited in our ability to project future hydrologic conditions at the required geographic scale. WE CAN SAY WITH SOME CERTAINTY THAT CHANGES WILL OCCUR, BUT WE CANNOT YET ASSIGN A VALUE TO THOSE CHANGES.

In light of these uncertainties, decisionmakers need to begin assessing the vulnerability of their decisions (e.g., design, sizing, and location of long-term projects) to a range of potential changes in hydrologic conditions. In many cases, low cost changes can be made that will reduce future risks. This analysis can also show the value of reducing existing uncertainties in projections -- whether the costs to narrow these uncertainties are justified by the potential value of reducing the accompanying risks. Finally, decisionmakers must develop an ongoing dialogue with climate modelers to effectively communicate their priorities and to make certain that useful and timely information is made available to them.

INTRODUCTION

The increase of CO_2 in the atmosphere resulting from fossil fuel combustion is expected to have a profound climatic effect, due to the ability of carbon dioxide to absorb radiation emitted from the earth atmosphere system. It is expected that increasing CO_2 will warm the atmosphere. The magnitude of this warming, and the consequences for the other aspects of the climate system -e.g. precipitation patterns, clouds, winds, etc. -are currently being investigated by a variety of scientific researchers.

Two recent reviews of the evidence by the National Academy of Sciences (1979, 1981) concluded that a doubling of carbon dioxide would probably lead to an increase in mean global surface temperature of between 1.5°C and 4.5°C. This range was determined primarily from reviewing results of several mathematical models of the earth's climate, the most sophisticated models of which, the General Circulation Models, incorporate representations of many physical processes in a three dimensional framework. These models are also capable of indicating changes in the other climate variables, and, in particular, can assess expected alterations in components of the hydrological cycle.

This report concentrates on analyzing the hydrologic changes over the North American continent that were produced by doubling the carbon dioxide in the Goddard Institute for Space Studies (GISS) general circulation model. The first section of this report describes the model and provides a comparison between the model output and the actual current climate. The changes that the model produces with a doubling of the atmospheric carbon dioxide are then presented. The second section attempts to put the results in perspective by examining historical variations in precipitation.

The results presented in this report, while giving plausible estimates of potential hydrological changes at the regional level, should be used and interpreted with great care. Many aspects of the GCM lead to uncertainty in the reliability of the results. The computation of changes at a relatively coarse geographic scale necessarily introduces uncertainty as to the magnitude of the change on a smaller scale. Other uncertainties are introduced because some relevant processes -- ocean transports and cloud process, for example-are modeled very crudely. Consequently the certainty that can be attached to various results is problematical. In some grid boxes and regions there may be large errors. Thus even though it is possible to conclude that climatic normals, whether they be thirty year or one hundred year averages, cannot be reliably used as predictors of future means or variation in climate it is as yet impossible to project future conditions accurately.

RESEARCHERS USING THE RESULTS OF THIS GCM EXPERIMENT IN THEIR STUDIES MUST RECOGNIZE THAT THE OUTPUTS OF THE GCM CANNOT BE CONSIDERED AS ACCURATELY DEFINING FUTURE CONDITIONS. More reliable estimate of hydrological change will become available only as further research, scientific effort, and data collection allow the scientific community to improve the GCM's representations of the actual climate processes. The speed at which this is done will directly depend on the overall level of effort the whole scientific community is able to devote to this problem. THIS REPORT, IN EFFECT, PRESENTS A METHODOLOGY FOR ESTIMATING THE HYDROLOGIC IMPACT OF INCREASED ATMOSPHERIC CO_2, AND SHOULD BE LOOKED UPON AS A FIRST APPROACH TO A COMPLEX PROBLEM.

The results presented herein apply only to a doubled CO_2 climate, once the system comes to equilibrium. CO_2 amounts are not expected to double until approx-imately the middle of the next century, and it will take additional decades before the equibrium is attained. Furthermore the doubling simulation does not consider the increases taking place in other greenhouse gases, -- methane, chloro-flurocarbons, and nitrous oxide -- which will significantly enhance the expected warming. In order to consider the transient response of the climate system between now and then and to consider the increases in trace gases, GISS is conducting an experiment in which CO_2 and these other greenhouse gases are increased gradually in the model atmosphere, starting from 1958 values. This later experiment will not only provide a more realistic estimate of expected decadel changes, but will also provide insight into the expected response of the climate system in a world of doubled CO_2 in which the climate system is in disequilibrium. In the third section we describe details of this experiment.

I. CLIMATIC MODEL ASSESSMENT OF THE HYDROLOGICAL CHANGES ASSOCIATED WITH DOUBLED ATMOSPHERIC CO_2

Model Description

The general circulation model used for this work has been developed at Goddard Institute for Space Studies (GISS) over the last several years. Global in extent, the model has realistic topography, 8° x 10° resolution in the horizontal, and nine layers in the vertical. Climate is simulated by solving the fundamental equations for conservation of mass, momentum, energy and water, using numerical schemes developed by Arakawa (1972). Parameterizations for the source terms in these equations represent the physical processes of radiation, turbulent transfers at the ground-atmosphere boundary, cloud formation, and condensation of rain. A complete description of the model appears in Monthly Weather Review (Hansen et al., April, 1983).

The only difference between the version of the model used for the experiment and the one documented in the literature is in the determination of sea surface temperatures and sea ice. In the documented version these values are specified climatologically based on monthly-mean values with linear interpolation once per day. If a calculation is made in that run of the net heat gain or loss from each ocean grid box, it is then possible to specify what heat gain or loss from each ocean grid box, it is then possible to specify what heat convergence or divergence in the ocean would be necessary to reproduce the observed ocean temperatures. Assuming that these heat fluxes represent horizontal transports, one can calculate the implied meridional ocean heat transport, and compare these values with observations. As shown in Hansen et al. (Fig. 15) the close agreement of model II, used in these experiments, with the observations indicates that the ocean heat exchange with the atmosphere on an annual and zonal average is realistic in the model. An expanded discussion of this technique and its results, including a detailed geographical presentation, can be found in Miller et al. (1983).

In the control run, and the climate change experiments, it was necessary to allow the sea surface temperatures to change. A simple thermal response which ignores ocean heat transport would result in the low latitude ocean (and atmosphere) being excessively warm, while high latitudes would be too cold, unless the atmospheric transport increased substantially. Either alternative would be unrealistic, in comparison with the current climate. It was thus decided to include the ocean transports which were calculated from the specified sea surface temperature model as necessary to reproduce the observed temperatures, given the fluxes in or out of the ocean which prevailed in that model. Thus to first order, the sea surface temperatures would be allowed to vary as radiative, sensible or latent heat fluxes varied, but would be kept realistic in the current climate simulation by the specified fixed transports. To the extent that the control run experienced fluxes which differed from the specified SST model, the sea surface temperatures would vary from the climatological average, but not to the extreme that would occur if no transport were included. The specified transport, with varying sea surface temperatures, was thus a standard part of the control run and experiment. Sea ice was also allowed to vary, forming when the ocean temperature drops below -1.6°C, and melting when it rises above 0°C.

For the purpose of this report we will compare observations and model simulations of the hydrologic cycle. This comparison must be labeled preliminary; more thorough comparison is expected in a later report.

Three situations will be described:

(1) Observed climate, which represents averages for forty years or more (depending on location). For the longest averages (80 years) they cover a time period during which a climatic change of 0.3°C occurred, for global mean temperature.

(2) The control run, the model's simulation of the current climate, a period of 10 modeled years with CO_2 at 315 ppm, with no climate trend (the only exception to this is shown and explained below, for Figure 1).

(3) The doubled CO_2 or "experiment" run, in which the world is treated as if the CO_2 had doubled and it had time to reach equilibrium.

Comparisons of Model Control Run and Observed Climate

Fig. 1 presents the annually averaged precipitation produced by a five year run of the model with specified climatological sea surface temperatures along with observations of actual precipitation (left hand side). (Year to year standard deviations of 25% occur in the model in certain regions, so while five years are sufficient to show the general patterns of rainfall, the exact values might vary somewhat for a longer time average). The distributions are similar, with both showing relatively little precipitation in desert areas (Sahara, Gobi, Australian deserts) and off the west coasts of continents (South America, North America and the southern portion of Africa). Regions of large rainfall occur in the tropics in the Amazon and African rainforests and in the central Pacific. The model produces too much rain over the Bay of Bengal and New Guinea, and somewhat more than observed over certain portions of North America. A more detailed comparison with observations over North America will be presented below.

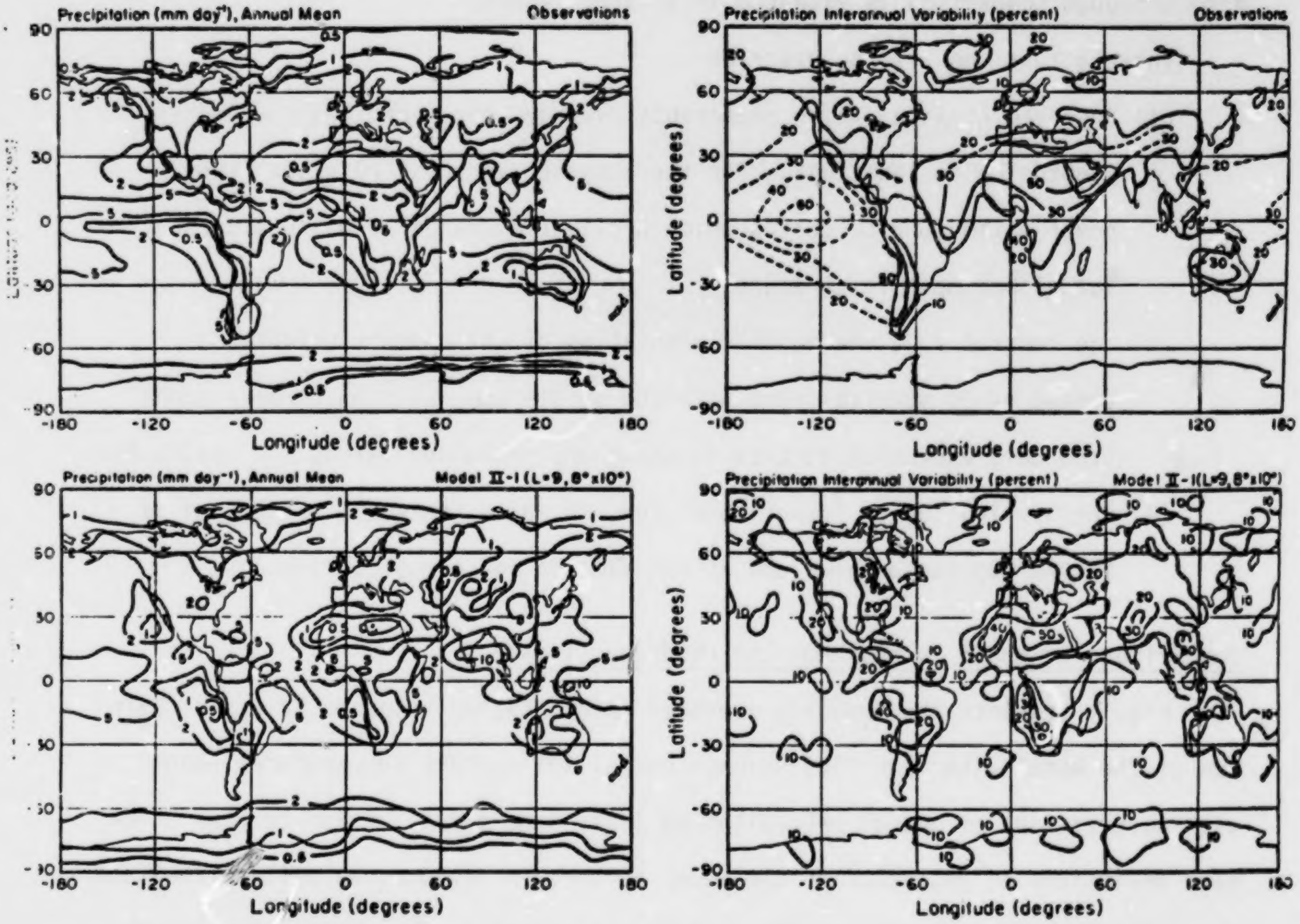
Precipitation (mm day⁻¹), Annual Mean
Observations
Precipitation Interannual Variability (percent)
Observations
Precipitation (mm day⁻¹), Annual Mean
Model II-1 (L=9, 8°x10°)
Precipitation Interannual Variability (percent)
Model II-1 (L=9, 8°x10°)
Latitude (degrees)
Longitude (degrees)
90
60
30
0
-30
-60
-90
-180
-120
-60
0
60
120
180

Fig. 1 . Global distribution of annual-mean precipitation (left) and its interannual relative variability (right). Observed annual-mean precipitation is from Schutz and Gates (1971) and interannual variability from Berry et al. (1973).

In addition to the annual mean precipitation, Fig. 1 also indicates the relative variability of precipitation from year to year in the model and in observations (right hand side). This is an important aspect of the model simulations because it indicates whether the model's natural variability is representative of the real variability, and implies something about the sensitivity of the model to internal climate forcings relative to that of the real world. As can be seen in the figure, the model's relative variability is similar to that which is observed both in magnitude and pattern, except for underestimating the variations that occur in the tropical Pacific and Atlantic. This deviation is presumably related to the use of specified sea surface temperatures in that area; in reality there is strong interannual variability in the sea surface temperatures in this region associated with the El Nino phenomenon, which occurs together with large fluctuations in rainfall. Over land, the model appears to have the proper degree of natural variability.

The control run was extended for 35 years allowing the ocean temperatures to change in response to thermal forcing, while incorporating inputs or outputs of heat into each ocean grid box representative of the influence of ocean currents. This procedure kept the ocean temperatures at reasonable values, while allowing them to respond to radiative and other thermal variations. A complete description of this technique is available in Miller and Russell (1982). The following comparisons with observations are from the last ten years of this run unless otherwise stated. Fig. 2 shows the model grid, numbered for reference.

Fig. 3a and 3b show the annual rainfall in the model grids over North America and the observed rainfall on a much finer scale. This comparison is meant to emphasize the subgrid-scale variation which exists in the observed rainfall pattern, which the model cannot directly reproduce. Fig. 3c shows as estimate of the observation on the model grid scale. Given the inhomogeniety

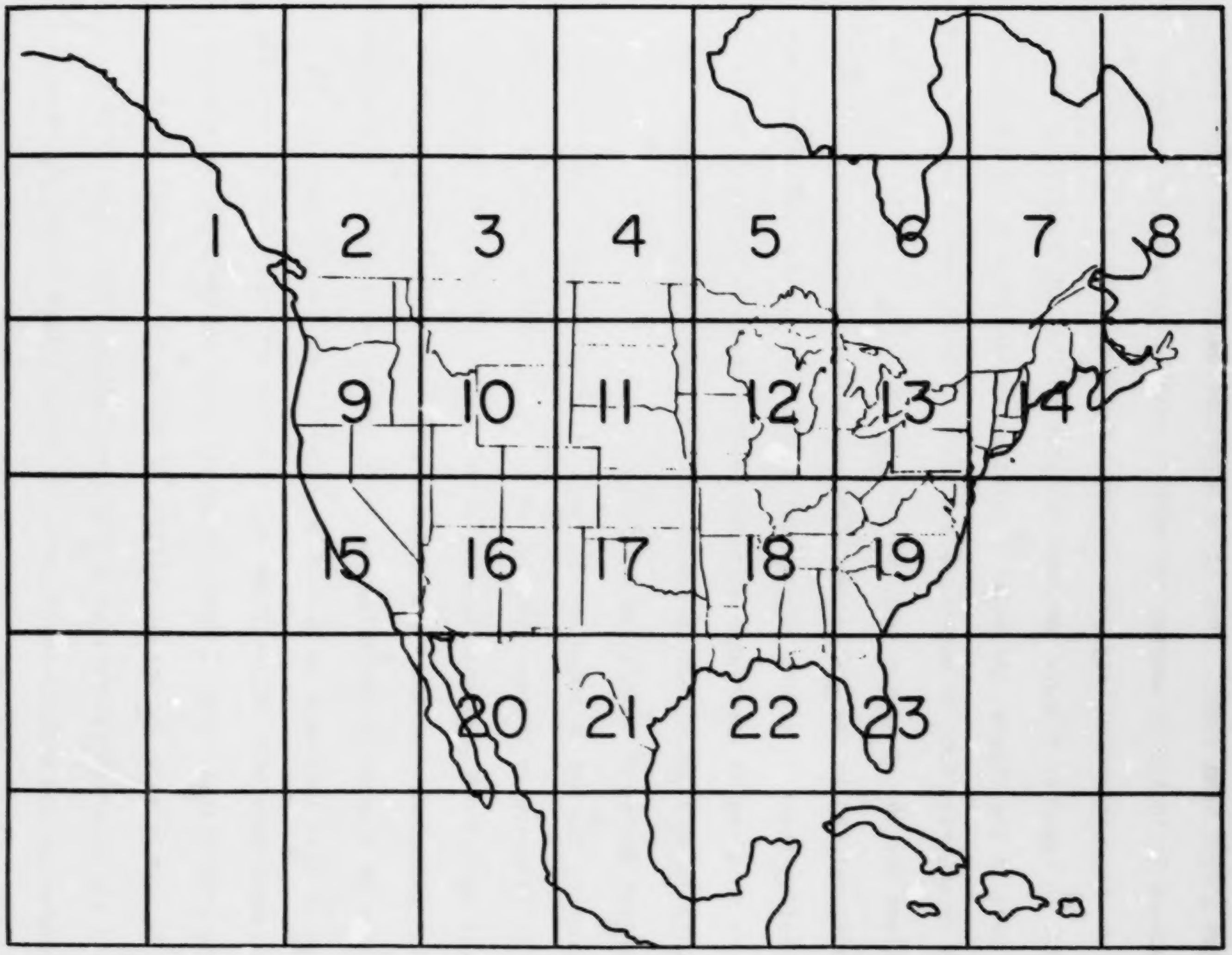
1
2
3
4
5
6
7
8
9
10
11
12
13
14
15
16
17
18
19
20
21
22
23

Fig. 2. Grid boxes over North America and the surrounding ocean in the GISS $8^{\circ} \times 10^{\circ}$ global climate model. Grid boxes are numbered for reference.

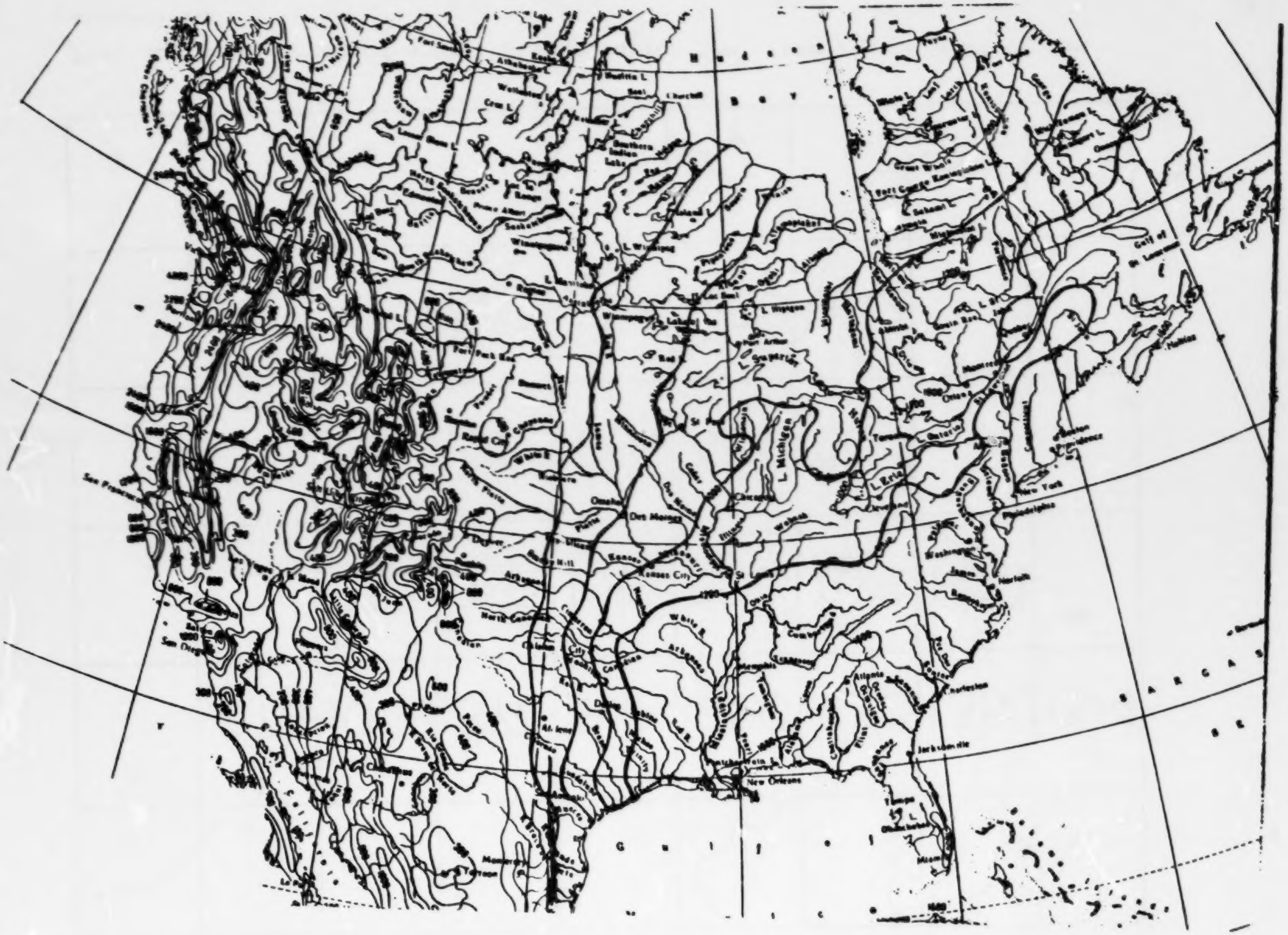

Fig. 3a. Observed annual precipitation (mm) over North America (Korzoun et al 1977).

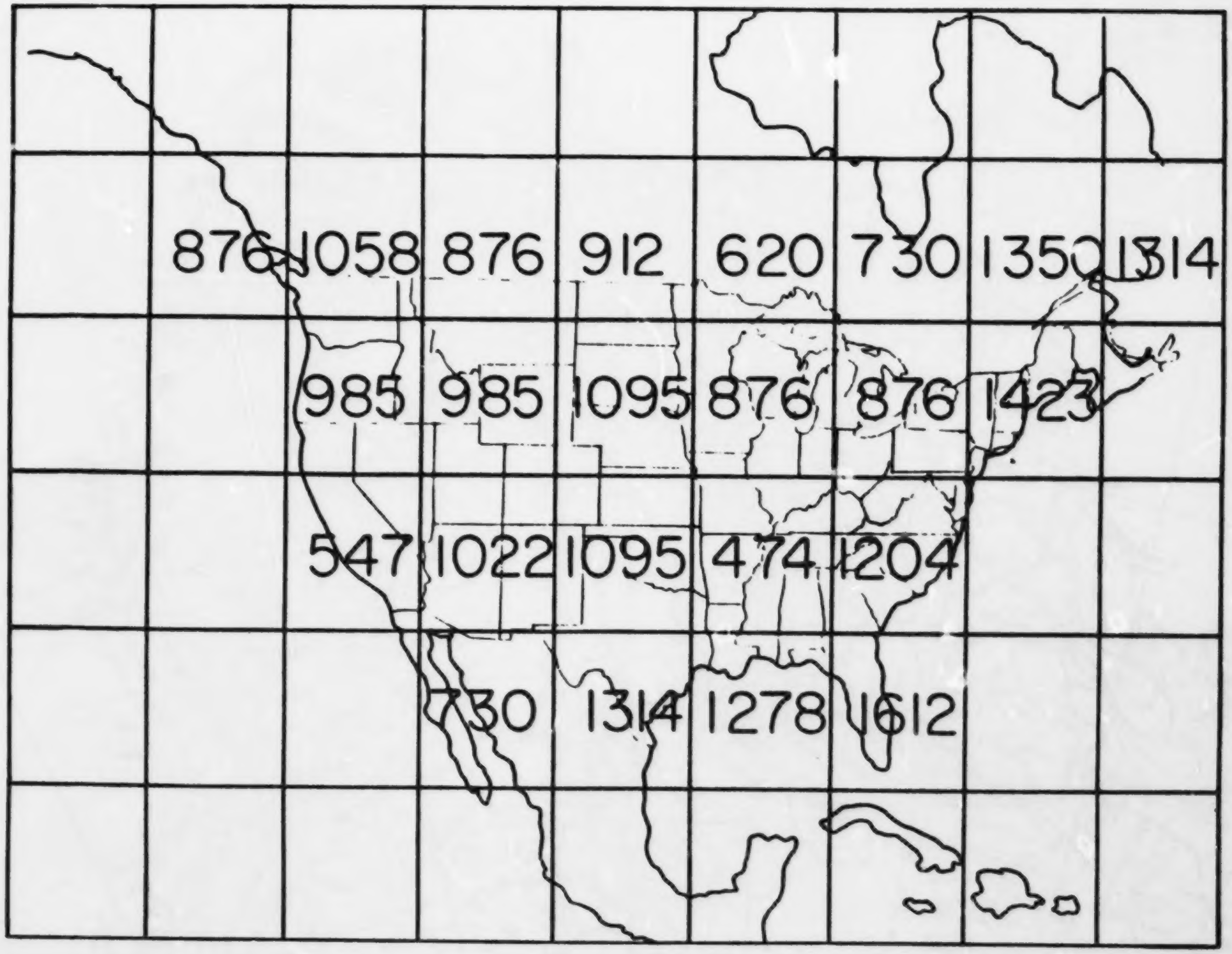

876 1058 876 912 620 730 1350 1314
985 985 1095 876 876 1423
547 1022 1095 474 1204
730 1314 1278 1612

Fig. 3b. Model produced annual precipitation (mm) from years 26-35 of the control run.

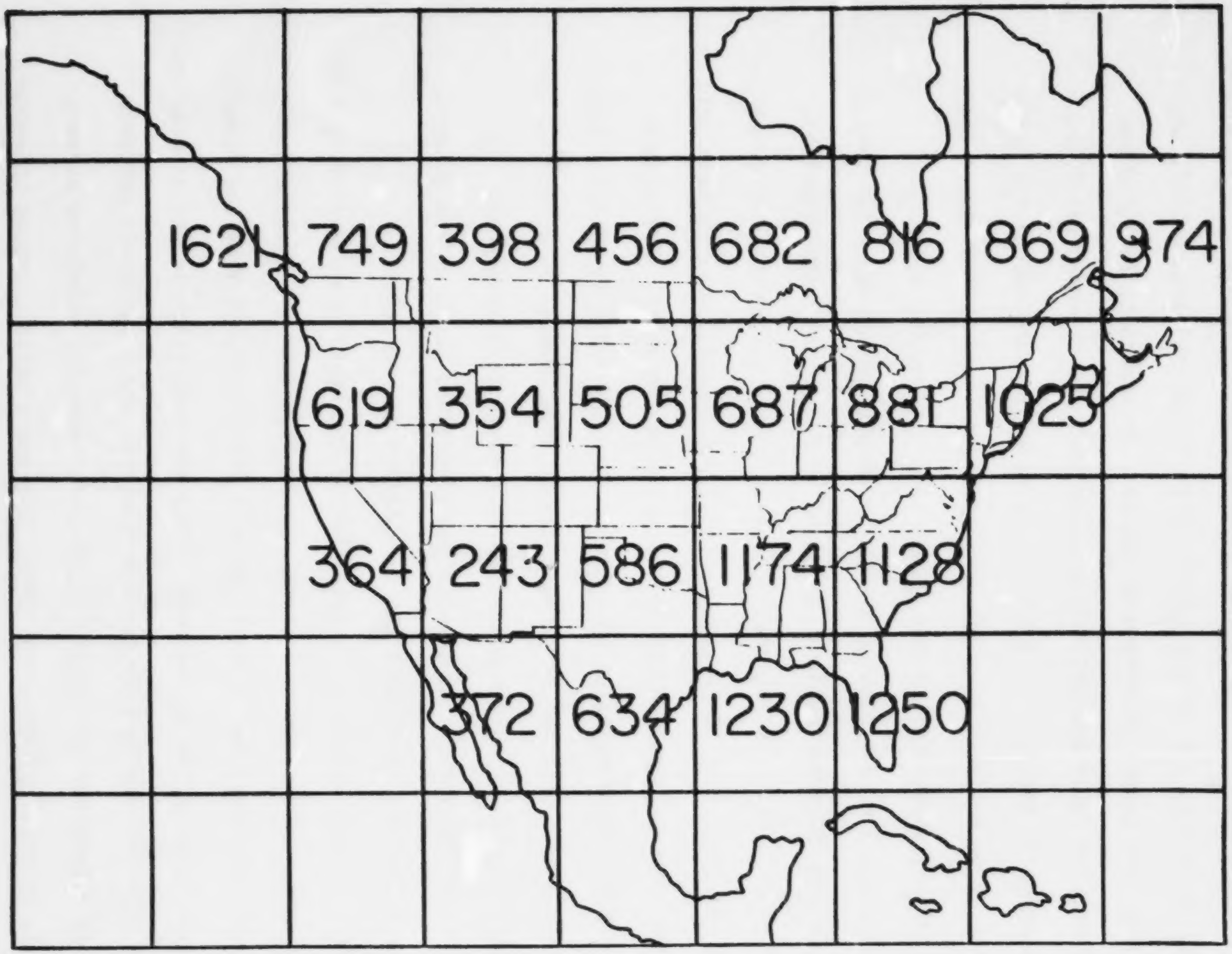
1621
749
398
456
682
816
869
974
619
354
505
687
881
1025
364
243
586
1174
1128
372
634
1230
1250

Fig. 3c. Estimated observed annual precipitation (mm) on the model grid.

evident in Fig. 3a the value for a given grid box is probably only accurate to about 20%. Comparison between these presentations shows that the model produces realistic rainfall except for the following deficiencies: rainfall is exceesive in general, by about 50%-100% in the longitude belt centered around 100°W and 110°W stretching from Canada southward to Mexico. In contrast, the grid box centered in Tennessee (grid box 18) has only one-half the observed rainfall. Detailed discussion of the reasons for these deficiencies are beyond the scope of this report; it is believed they are principally related to the larger than actual water holding capacities of the ground specified in the model.

This emphasizes the necessity to treat the results given below for individual grid boxes with extreme caution. As shown in Fig. 1 the model simulation of precipitation on global and regional scales is quite realistic. The comparison in Fig. 3 indicates that in certain regions, and especially in certain grid boxes, the model does not produce precipitation values in accord with observations. This introduces a degree of uncertainty into the validity of the changes produced for any single grid box in climate change experiments. The results for a given grid box should not be considered to be the expected change for that particular physical location. The greater the geographic scale of the expected climatic change, the more confidence can be attached to the result.

Fig. 4a and 4b show the annual evaporation in the model over land along with the "observed" evaporation. It is important to realize that the observations are deduced from a mathematical formula, which differs somewhat from the formula used to calculate evaporation in the model; thus the comparison is not as meaningful as was the case for precipitation. Nevertheless, the large-scale patterns agree with those determined for precipitation, with somewhat excessive evaporation west of the Mississippi River (by about 30%) and a deficit around Tennessee.

Fig. 5 shows the runoff calculated in the model, and observed river runoff. Again the question of the similarity of the two diagnostics arises and will be

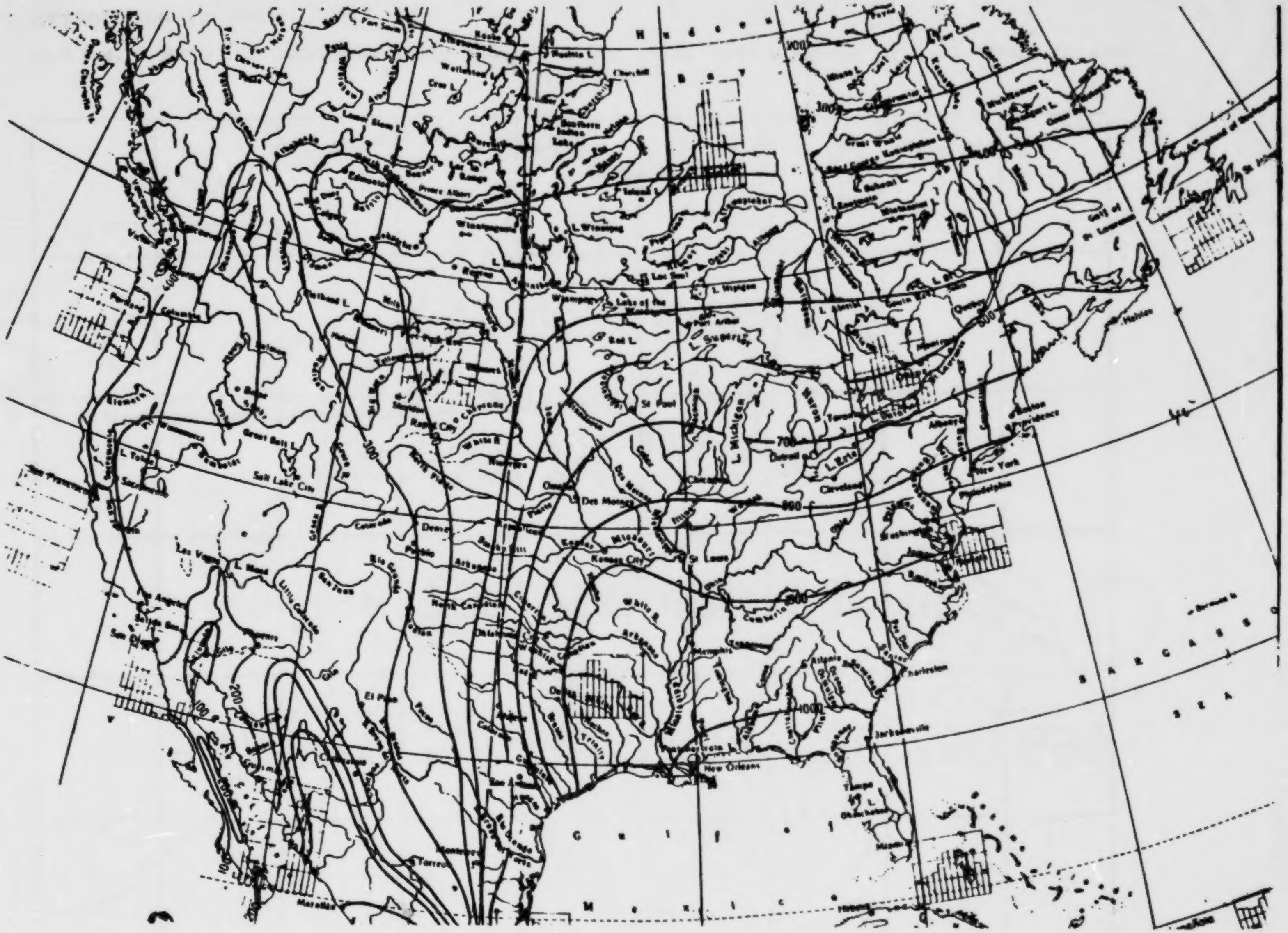
Hudson
Bay
Gulf of St Lawrence
Sargasso Sea
Gulf of Mexico
L. Superior
L. Michigan
Huron
L. Erie
Ontario
Great Salt L.
Salt Lake City
San Francisco
Las Vegas
Denver
Pueblo
El Paso
Des Moines
Kansas City
St Louis
St Paul
Detroit
Cleveland
Toronto
Albany
New York
Philadelphia
Boston
Providence
Washington
Charleston
Jacksonville
Tampa
Miami
New Orleans
Memphis
Halifax
Quebec
Edmonton
Winnipeg
Regina
100
200
300
400
500
700
800
900
1000

Fig. 4a. Observed annual evaporation (mm) over North America (Korzoun et al 1977)

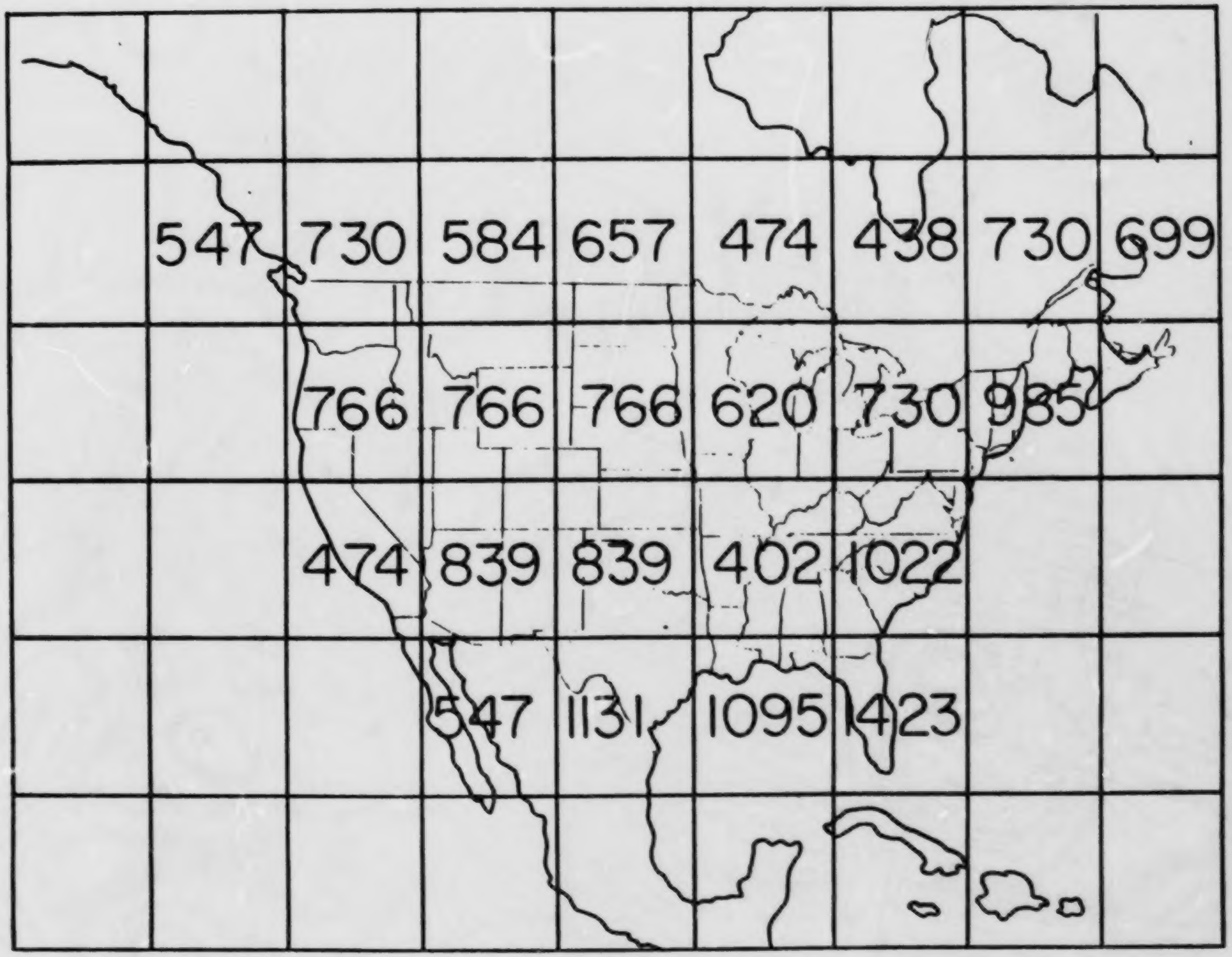
547
730
584
657
474
438
730
699
766
766
766
620
730
985
474
839
839
402
1022
547
1131
1095
1423

Fig. 4b. Model produced annual evaporation from years 26-35 of the control run. Values are in mm.

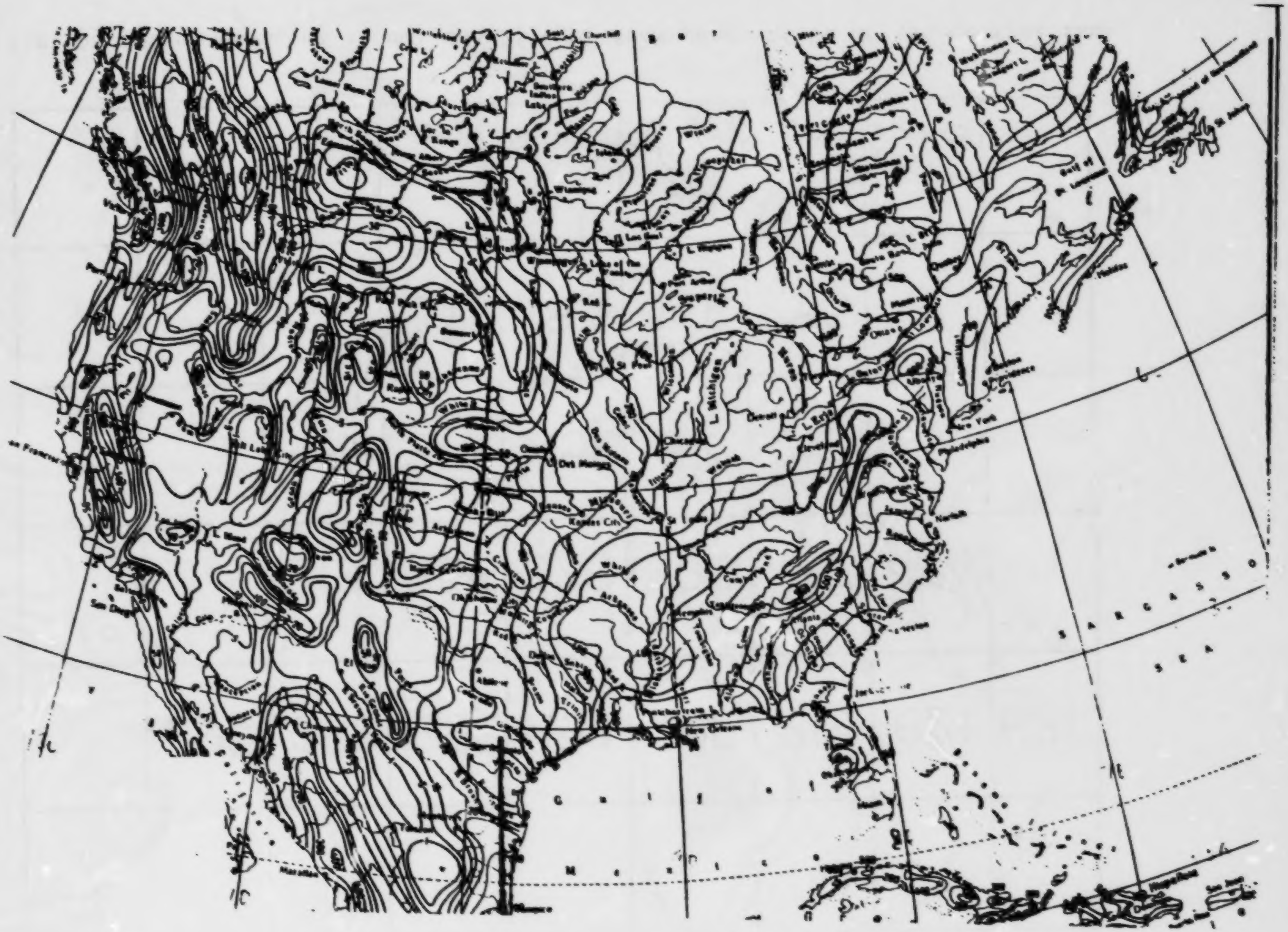
SARGASSO
SEA
L. Michigan
New Orleans
Philadelphia
New York

Fig. 5a. Observed annual runoff over North America (Korzoun et al 1977).

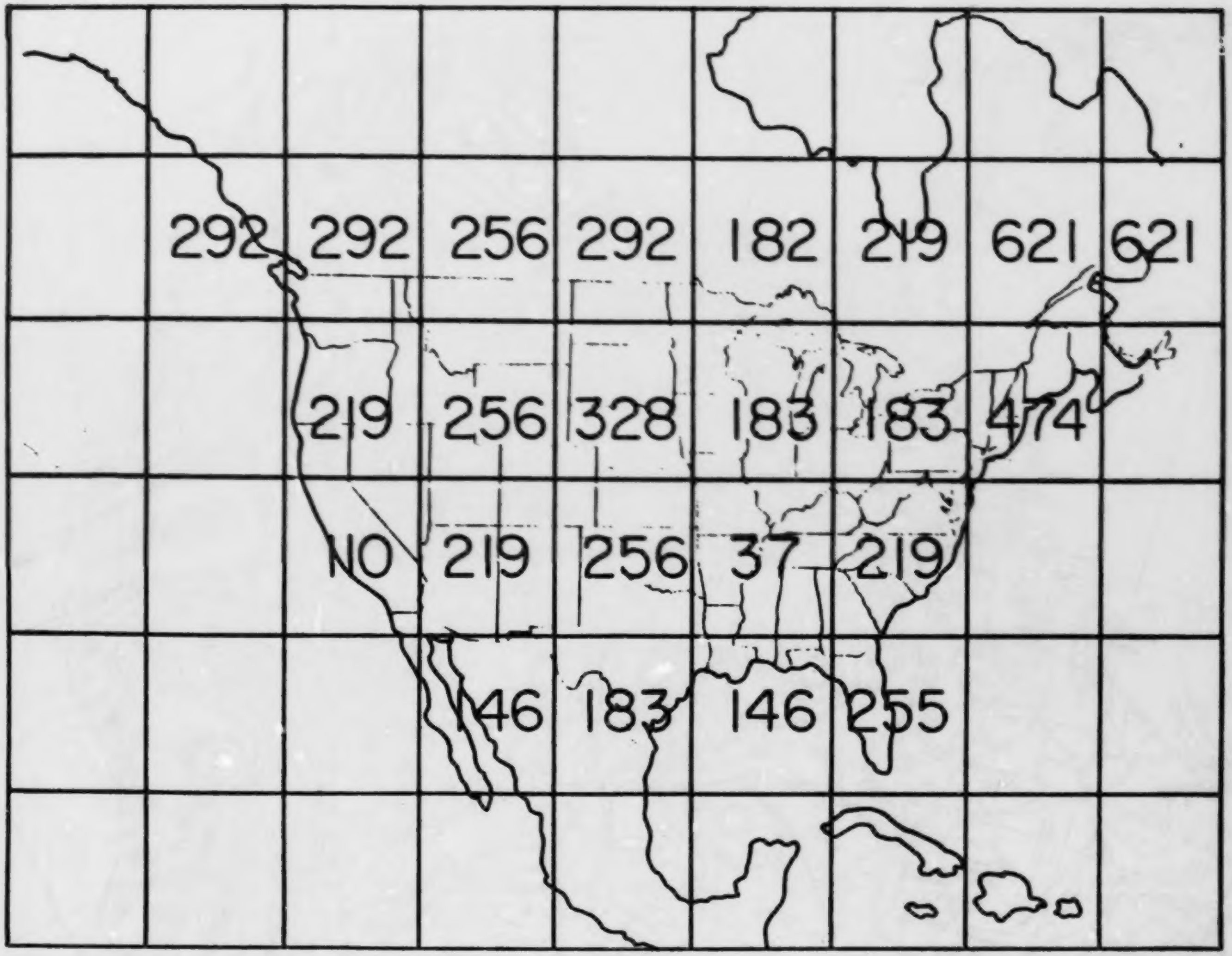
292
292
256
292
182
219
621
621
219
256
328
183
183
474
110
219
256
37
219
146
183
146
255

Fig. 5b. Model produced annual runoff (mm) from years 26-35 of the control run.

commented upon further in a later report. As shown here the model runoff is excessive (by a factor of two or more) in the same grid boxes that precipitation was excessive, while being deficient in the Tennessee area, so the pattern is qualitatively consistent.

The comparisons presented indicate the extent to which the model reproduces the annual average hydrologic cycle. THESE DEFICIENCIES DIRECTLY AFFECT THE ACCURACY OF ESTIMATES FOR INDIVIDUAL GRIDS AND MUST BE REMEMBERED WHEN EVALUATING THE RESULTS OF THE DOUBLED CO_2 EXPERIMENT.

Experiment Results

The amount of atmospheric CO_2 in the model was doubled and the run was integrated for 35 years, enough time to produce an equilibrium climate. The results discussed in this section are for a comparison of the last ten years of the experiment with the last ten years of the control run unless otherwise stated.

The doubled CO_2 world has an annual average surface temperature increase of 4.16°C in this experiment. Over the United States the temperatures rise by 4.2°C in the eastern part of the country, and 4.9°C in the central and western parts. There is some seasonal variation to this rise, with the increase in winter being about 40% larger than the increase in summer. One way to appreciate the magnitude of this increase is to consider the maximum temperatures observed on an average daily basis, and for the month as a whole, for different cities in the United States during July with the model-predicted doubled CO_2 climate. Fig. 6a shows the average daily temperature maximum to be expected in degrees Fahrenheit obtained by adding the model calculated temperature change due to doubled CO_2 to the currently observed value. These values average 5-7°F higher than is currently observed. Fig. 6b shows the monthly maximum temperature which would be expected; again, the difference is 5-7°F above current expectations.

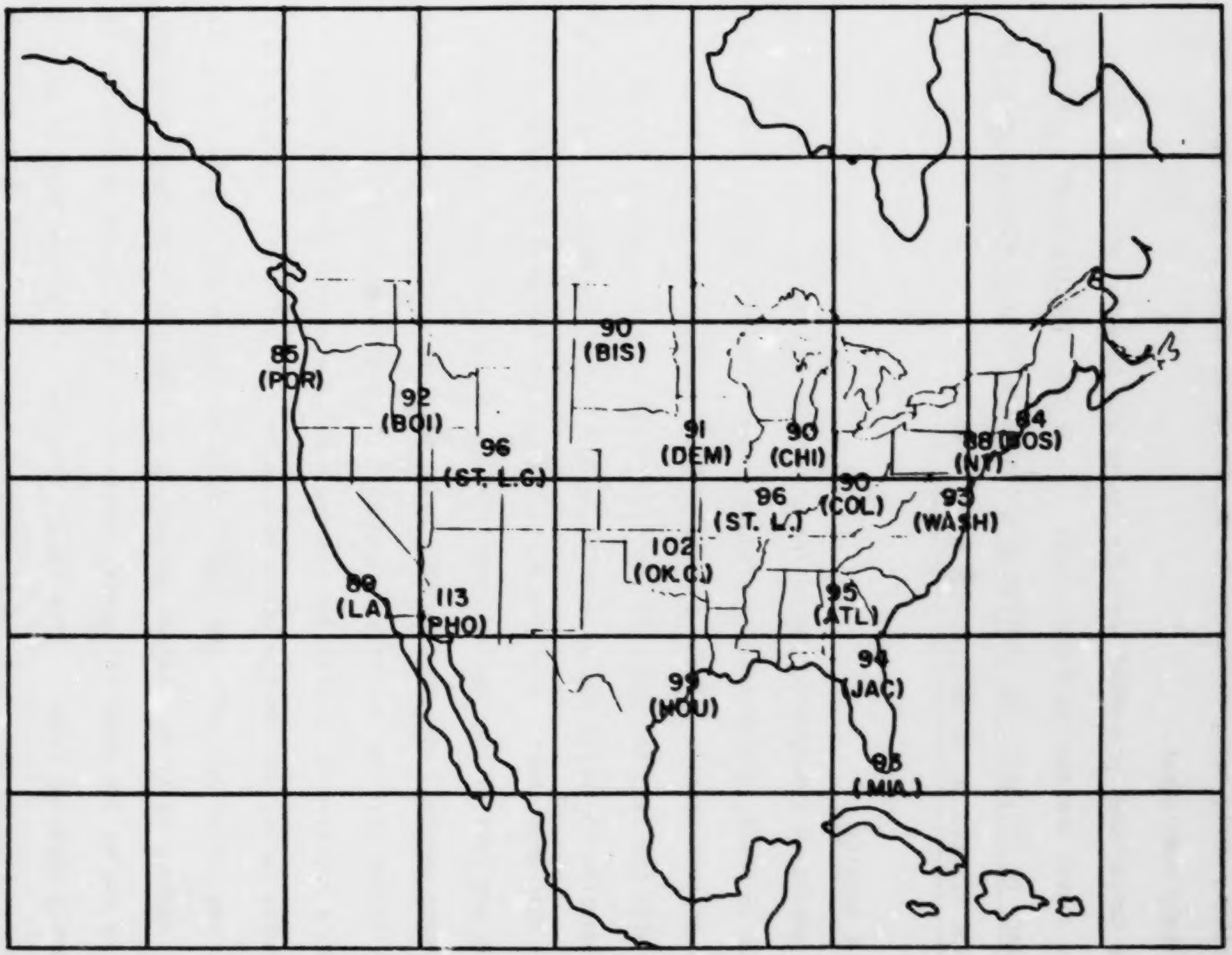
85
(POR)
92
(BOI)
96
(ST. L.C.)
90
(BIS)
91
(DEM)
90
(CHI)
96
(ST. L.)
90
(COL)
88
(NY)
84
(BOS)
93
(WASH)
102
(OK.C.)
88
(LA)
113
(PHO)
95
(ATL)
94
(JAC)
99
(HOU)
95
(MIA)

Fig. 6a. Average daily temperature maximum in July in doubled CO_2 climate. The current average daily temperature maximum for these cities is 5^{o}- $7^{o}F$ less.

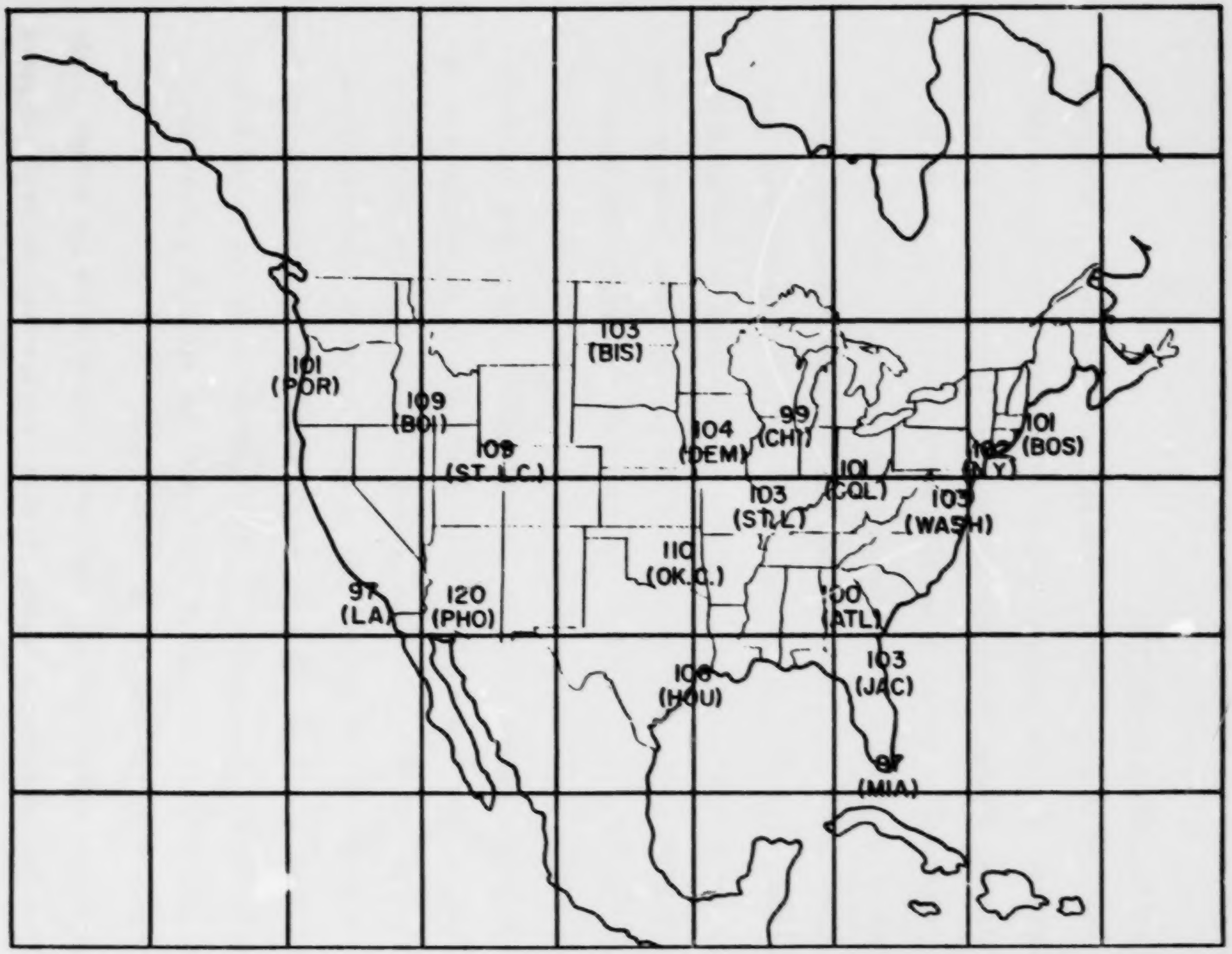
101
(POR)
109
(BOI)
108
(ST.L.C.)
97
(LA)
120
(PHO)
103
(BIS)
104
(DEM)
110
(OK.C.)
106
(HOU)
99
(CHI)
103
(ST.L)
101
(COL)
100
(ATL)
103
(JAC)
97
(MIA)
103
(WASH)
102
(NY)
101
(BOS)

Fig. 6b. Average monthly temperature maximum to be expected in July in doubled CO_2 climate.

In the following discussion we will concentrate on the effects of doubling the CO_2 on factors related to the hydrologic cycle over North America. A more complete discussion of the results of this experiment will be published elsewhere.

1. Annual Results: Basic Diagnostics

Fig. 7 shows the change in annually averaged precipitation for grid boxes over North America. Positive numbers indicate precipitation increase in the doubled CO_2 climate compared to the control run. The general pattern shows that precipitation increased in the north and northwestern portions of the domain, with variations of alternating sign elsewhere. The numbers in parenthesis at the bottom of each grid box indicate the percentage change of the annual precipitation relative to the ten years of the control run. Fifteen to twenty percent increases are common in the north and west. An increase in precipitation on the annual average is characteristic of the doubled CO_2 world, as warmer temperatures lead to greater evaporation of moisture from the ocean. The global average precipitation increases by 11% when CO_2 is doubled.

The change in evaporation, along with the percentage change from the control are shown in Fig. 8. The change refers to the difference in evaporation over the land portions of the grid box, while the percentage change relative to the control run uses evaporation from the grid box as a whole, but it should be representative, for those grid boxes which are mostly land. The pattern noted for precipitation is repeated for evaporation with increases of 15-20% (or more) occurring over the northern and western portions of the map. On a global basis evaporation increased by 11% similar, to the rainfall.

Fig. 9 shows the change in runoff over land, along with the percentage change from the control run. Assuming no change in water storage over the last ten years this would be equal to the difference between the precipitation and evaporation changes (Fig. 7 and 8). The values shown in Fig. 9 are close to this difference,

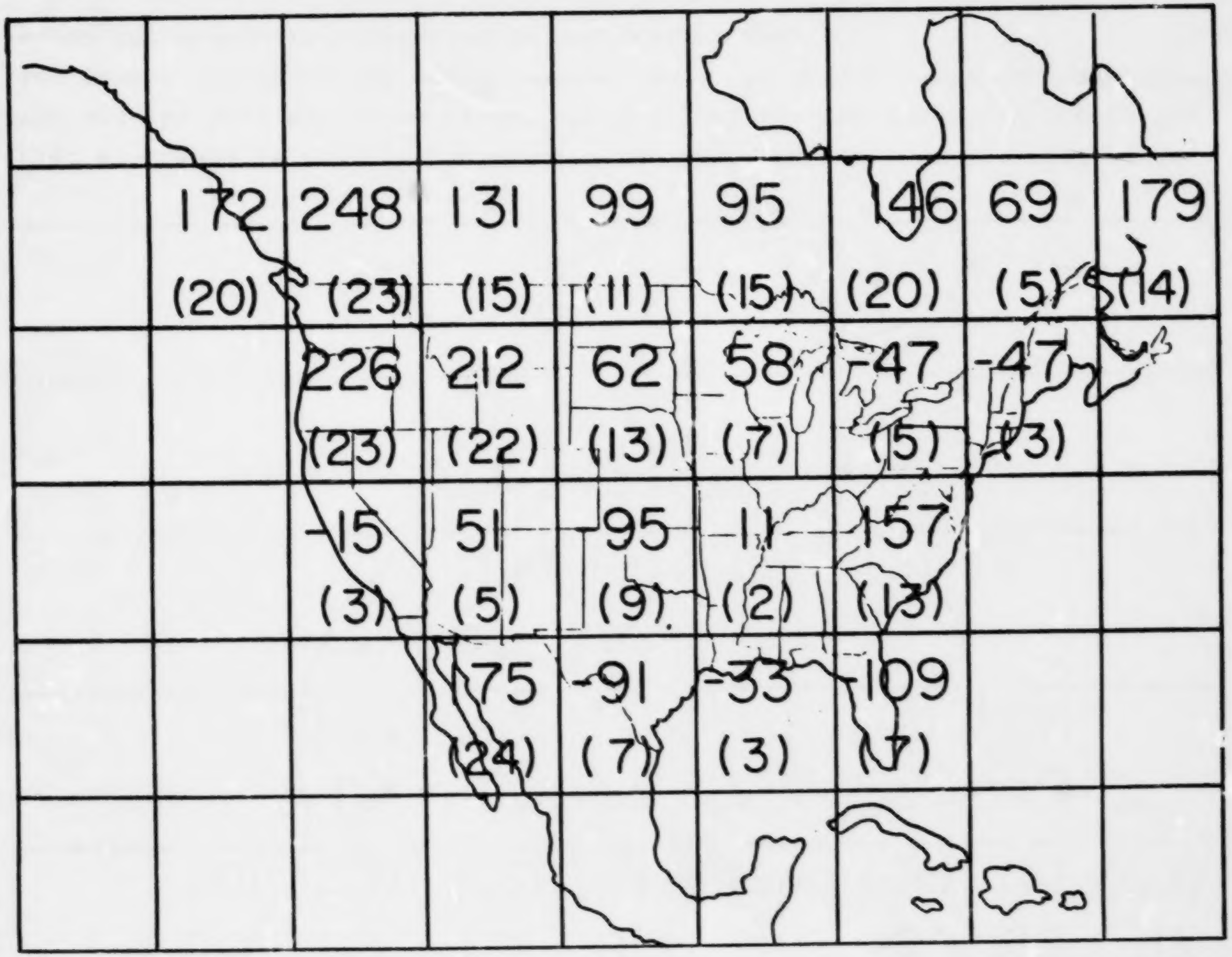
172
(20)
248
(23)
131
(15)
99
(11)
95
(15)
146
(20)
69
(5)
179
(14)
226
(23)
212
(22)
62
(13)
58
(7)
-47
(5)
-47
(3)
-15
(3)
51
(5)
95
(9)
11
(2)
157
(13)
75
(24)
-91
(7)
-33
(3)
-109
(7)

Fig. 7. Change in precipitation between the last ten years of the doubled CO_2 run and the last ten years of the control run, for the annual average. The top number indicates the actual change (mm), the bottom number in parenthesis gives the change in % relative to the control run.

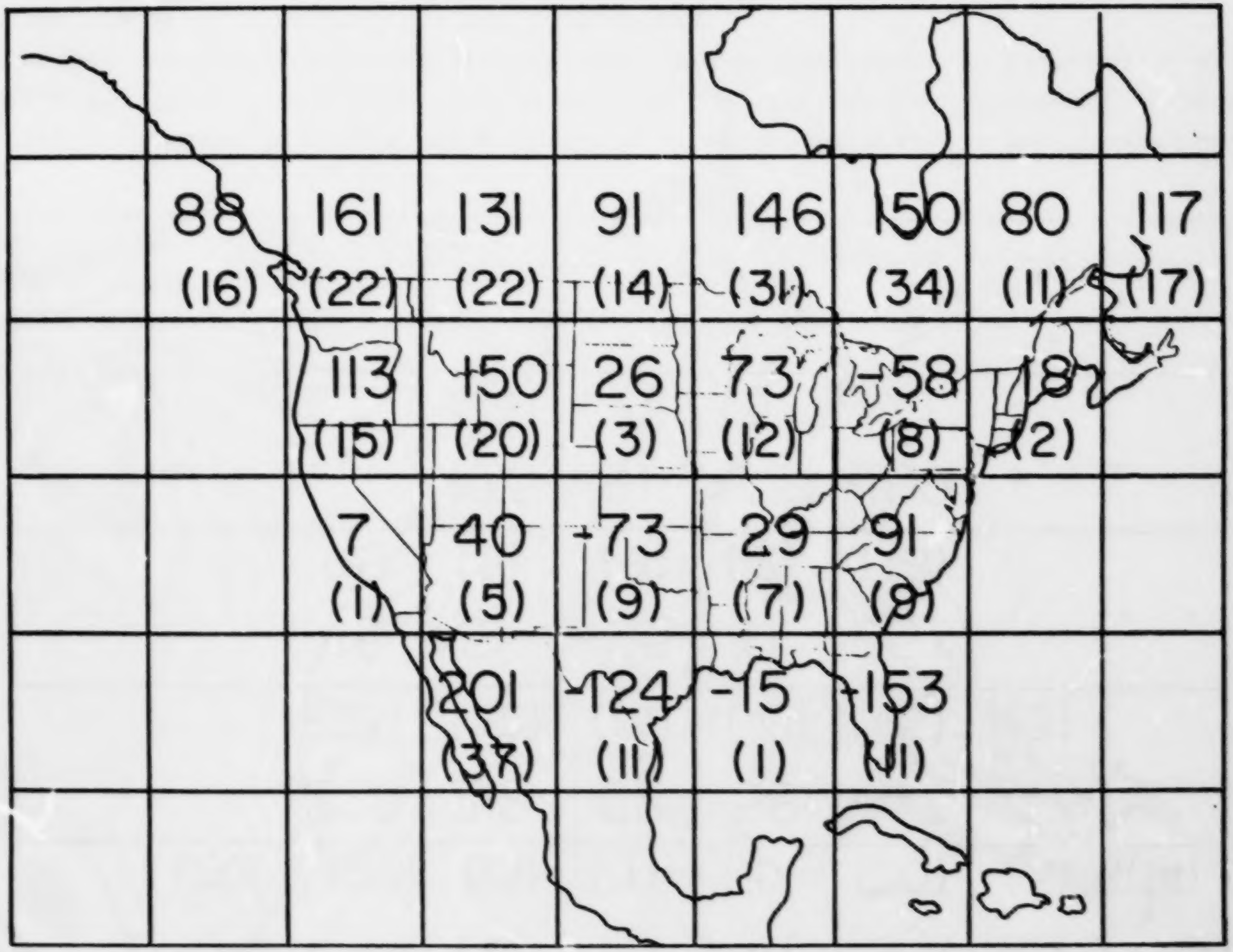
88
(16)
161
(22)
131
(22)
91
(14)
146
(31)
150
(34)
80
(11)
117
(17)
113
(15)
150
(20)
26
(3)
73
(12)
-58
(8)
18
(2)
7
(1)
40
(5)
-73
(9)
29
(7)
91
(9)
201
(37)
-124
(11)
-15
(1)
-153
(11)

Fig. 8. Change in evaporation between the last ten years of the doubled CO_2 run and the last ten years of the control run, for the annual average. The top number indicates the actual change (mm), the bottom number in parenthesis gives the change in % relative to the control run.

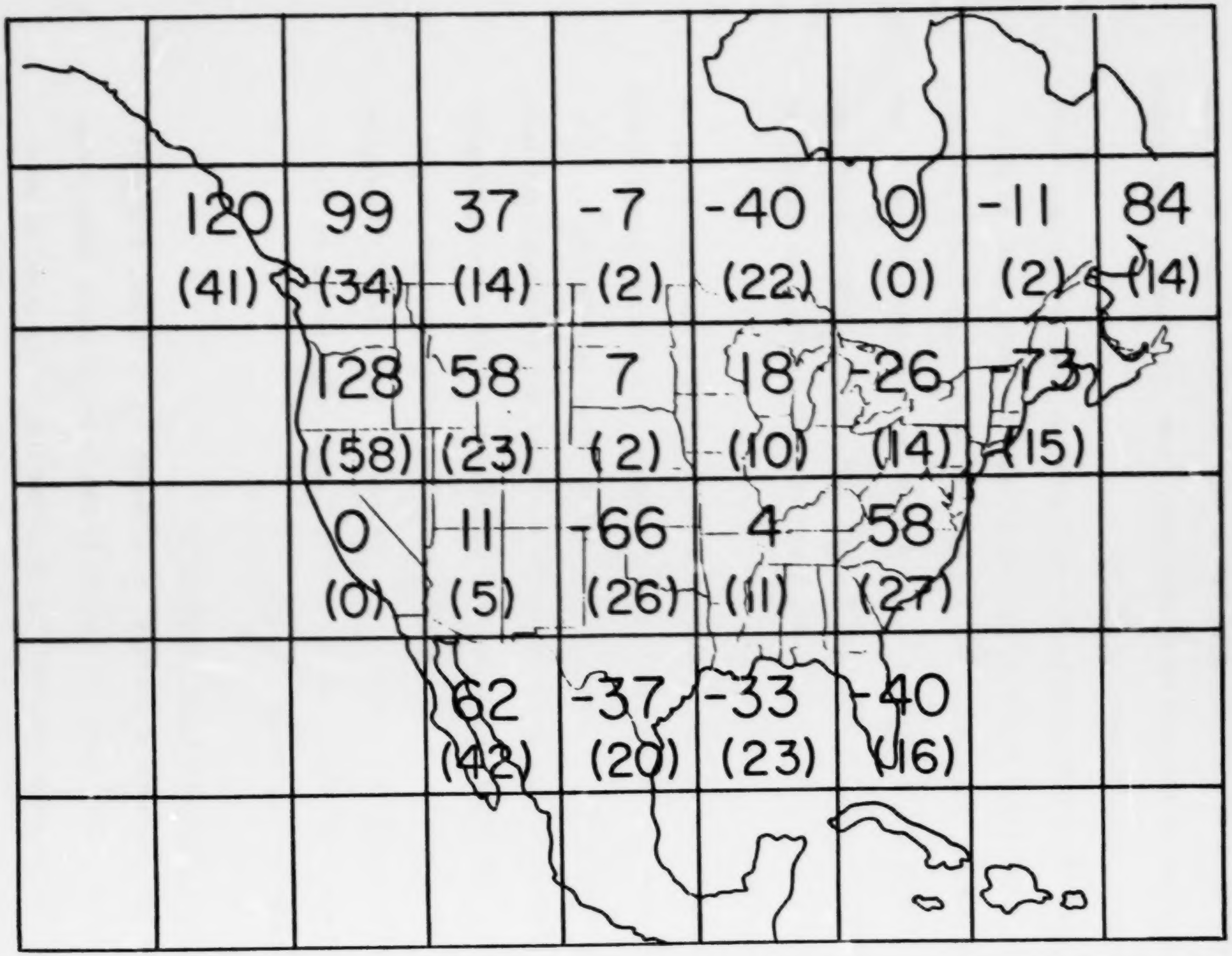
120 (41)
99 (34)
37 (14)
-7 (2)
-40 (22)
0 (0)
-11 (2)
84 (14)
128 (58)
58 (23)
7 (2)
18 (10)
-26 (14)
-73 (15)
0 (0)
11 (5)
-66 (26)
4 (11)
58 (27)
62 (42)
-37 (20)
-33 (23)
-40 (16)

Fig. 9. Change in runoff between the last ten years of the doubled CO_2 run and the last ten years of the control run, for the annual average. The top number indicates the actual change (mm), the bottom number in parenthesis gives the change in % relative to the control run.

although not exactly equal, indicative of the ground moisture changing somewhat on the annual average during the period (or perhaps a numerical resolution effect). The general pattern is one of increased runoff over the northwestern and extreme southwestern portions of the continent of 20-60%. Some grid boxes in the central and eastern regions have decreases of 15-20%.

Fig. 10 gives the ground wetness for each grid box, the percentage of soil moisture in the first layer in the ground relative to the total water holding capacity of the earth. The control run values (the lower number) were generally less than 25% of what could potentially be held in the southwest, rising to over 50% in the northeast. In the doubled CO_2 experiment, small changes (upper number) in this quantity occur, with a small reduction over most of the area except for the extreme northeast.

Fig. 11 shows the total earth water (and ice) for the ground extending down to a depth of 4 meters. The change is the top number, and the percentage change relative to the control run is shown as the bottom number is parenthesis. The values in the control run are greatest in the northwest and northeast, and least in the southwest. The northern and western portions of the continent generally increase their total water content, by 20-60%, while the southern and eastern sections generally experience some drying. The results shown in Fig. 11 represent a concise summary of the direct hydrologic changes experienced in the doubled CO_2 climate for the annual average.

2. Annual Results: Interpretative Diagnostics

To evaluate the increase or decrease of extended dry episodes, a drought index was formulated. This index is similar to the Palmer drought index except that it relates current water availability to climatologically expected water availability, rather than to water use. If P-E is the difference between precipitation and evaporation for a month, $\overline{P-E}$ the mean difference for the same ten

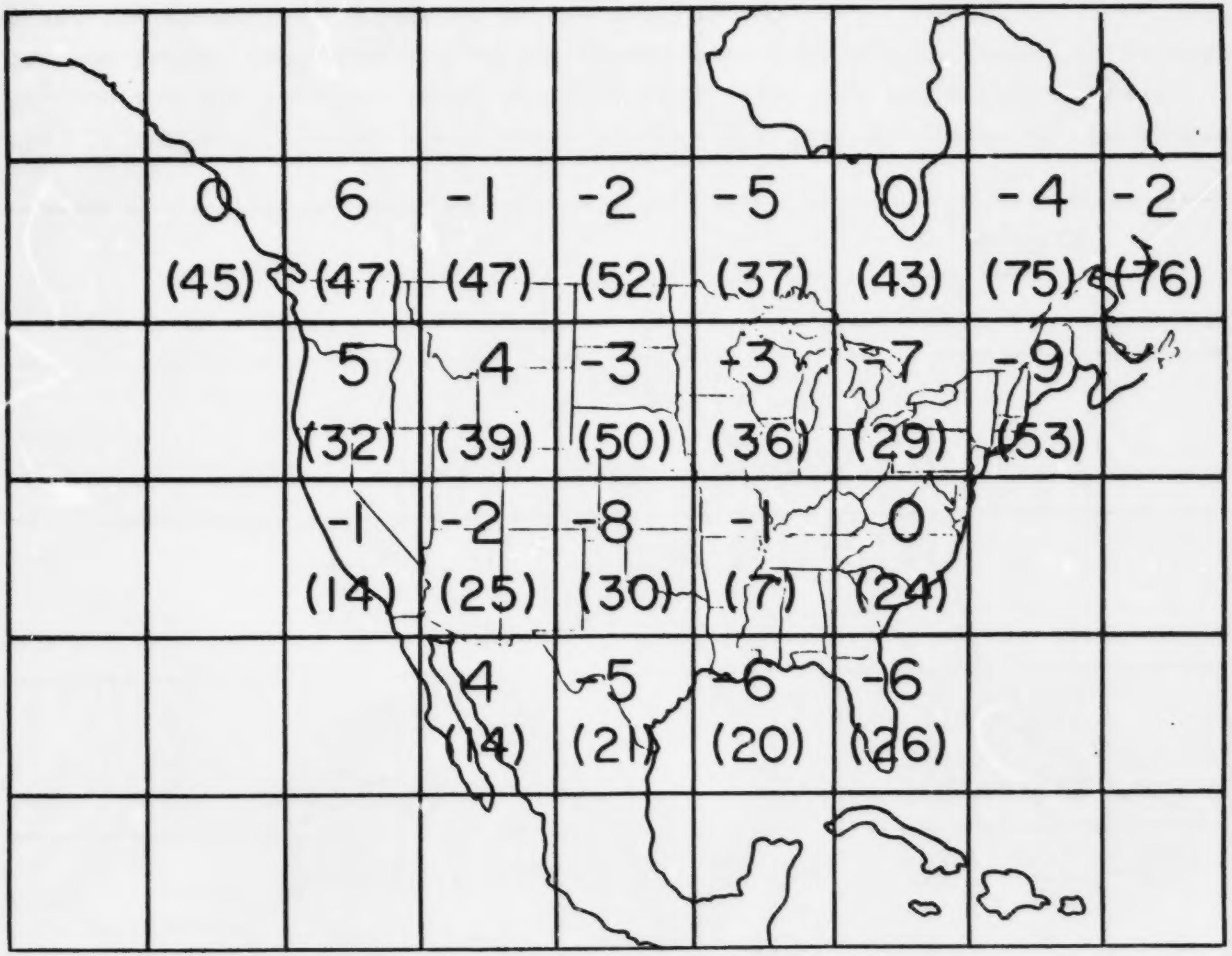
0 (45)
6 (47)
-1 (47)
-2 (52)
-5 (37)
0 (43)
-4 (75)
-2 (76)
5 (32)
4 (39)
-3 (50)
-3 (36)
-7 (29)
-9 (53)
-1 (14)
-2 (25)
-8 (30)
-1 (7)
0 (24)
4 (14)
-5 (21)
-6 (20)
-6 (26)

Fig. 10. Change in ground wetness between the last ten years of the doubled CO_2 run and the last ten years of the control run, for the annual average. The top number gives the actual change (in %), the bottom number in parenthesis gives the ground wetness (in %) for the control run.

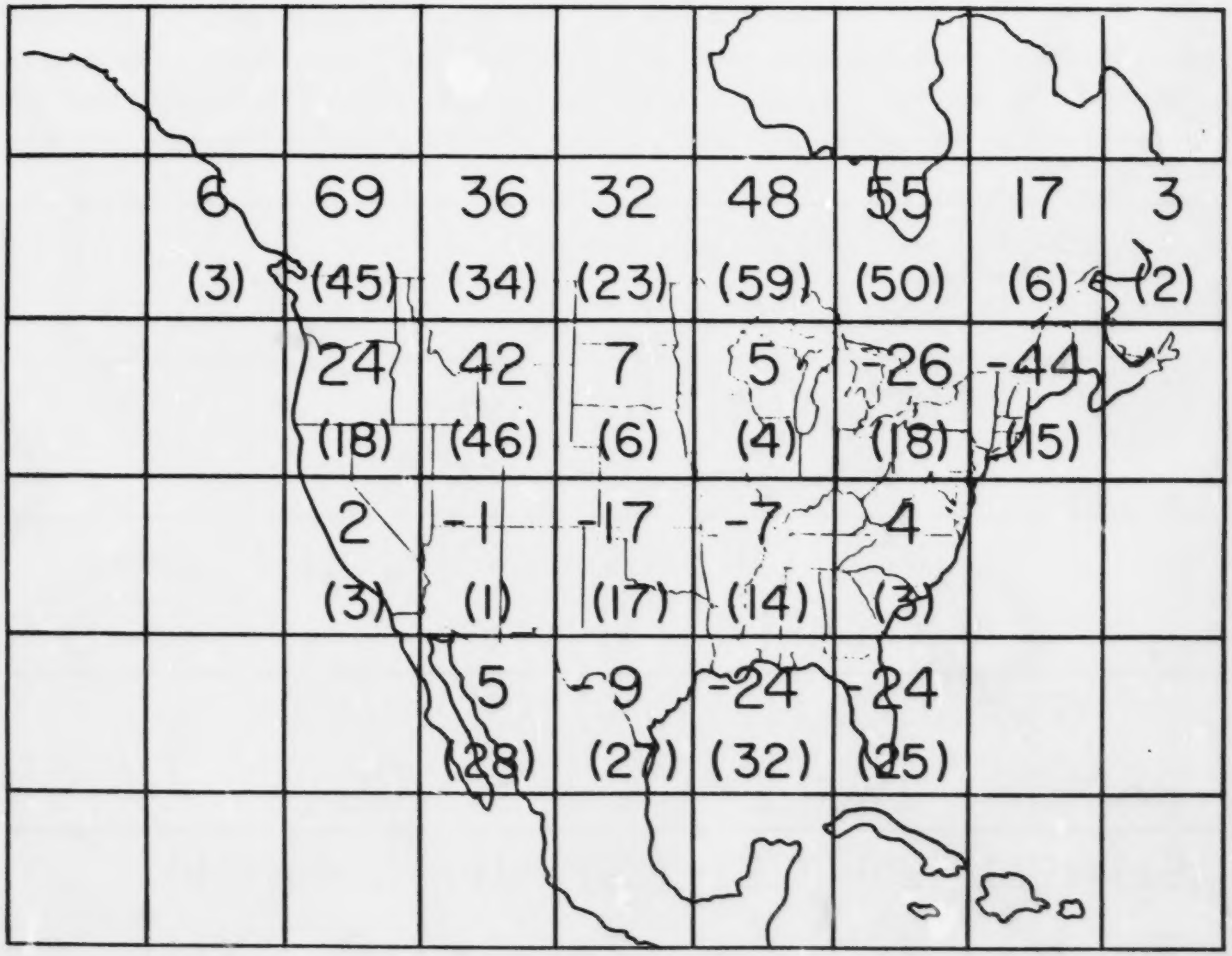
6
(3)
69
(45)
36
(34)
32
(23)
48
(59)
55
(50)
17
(6)
3
(2)
24
(18)
42
(46)
7
(6)
5
(4)
-26
(18)
-44
(15)
2
(3)
-1
(1)
-17
(17)
-7
(14)
4
(3)
5
(28)
-9
(27)
-24
(32)
-24
(25)

Fig. 11. Change in total earth water between the last ten years of the doubled CO_2 run and the last ten years of the control run, for the annual average. The top number indicates the actual change (mm), the bottom number in parenthesis gives the change in % relative to the control run.

calendar months in the control run, and S.D. the standard deviation of this difference from the control run, then the index is:

$$I_{current} = .897 I_{previous\ month} + \left(\frac{(P-E) - \overline{(P-E)}}{S.D.} \right)$$

The relationship between the current index and that for the previous month is the same as that used for the Palmer drought index. Positive values of the index indicate greater precipitation relative to evaporation than was experienced in the control run, with a deviation of one standard deviation two months in a row augmenting the index by 1.897. The index is normalized for each grid box so that the control run has a distribution for each category similar to that for the Palmer index. Table 1 shows the categories for the Palmer Index, and the distribution for each category for the control run with the drought index as defined above. This drought index differs from the Palmer index in that it uses actual evaporation rather than expected demand as the water loss process.

The difference in the drought index due to doubling CO_2 is shown in Fig. 12. The results show a tendency for droughts to persist longer, on the annual average, in the south and east, with sequences of wetter than normal months more likely in the northwest. Since by definition all grid boxes have distributions corresponding approximately to that shown in Table 1, a change in the drought index of -2 would in the mean shift all categories two divisions to the left, and increase extreme dryness from 2% to 10% in occurrence. Similarly an increase in the index of +2 would increase the occurrences of extreme wet periods in the same fashion. However, there is no way of telling from the numerical change alone in what situations the index changed, and thus it is necessary to look at the change in distribution for any particular grid box. This will be done for specific grid boxes in the next section. The changes shown in this figure are consistent with the pattern of effects that has become visible during the course of our review of

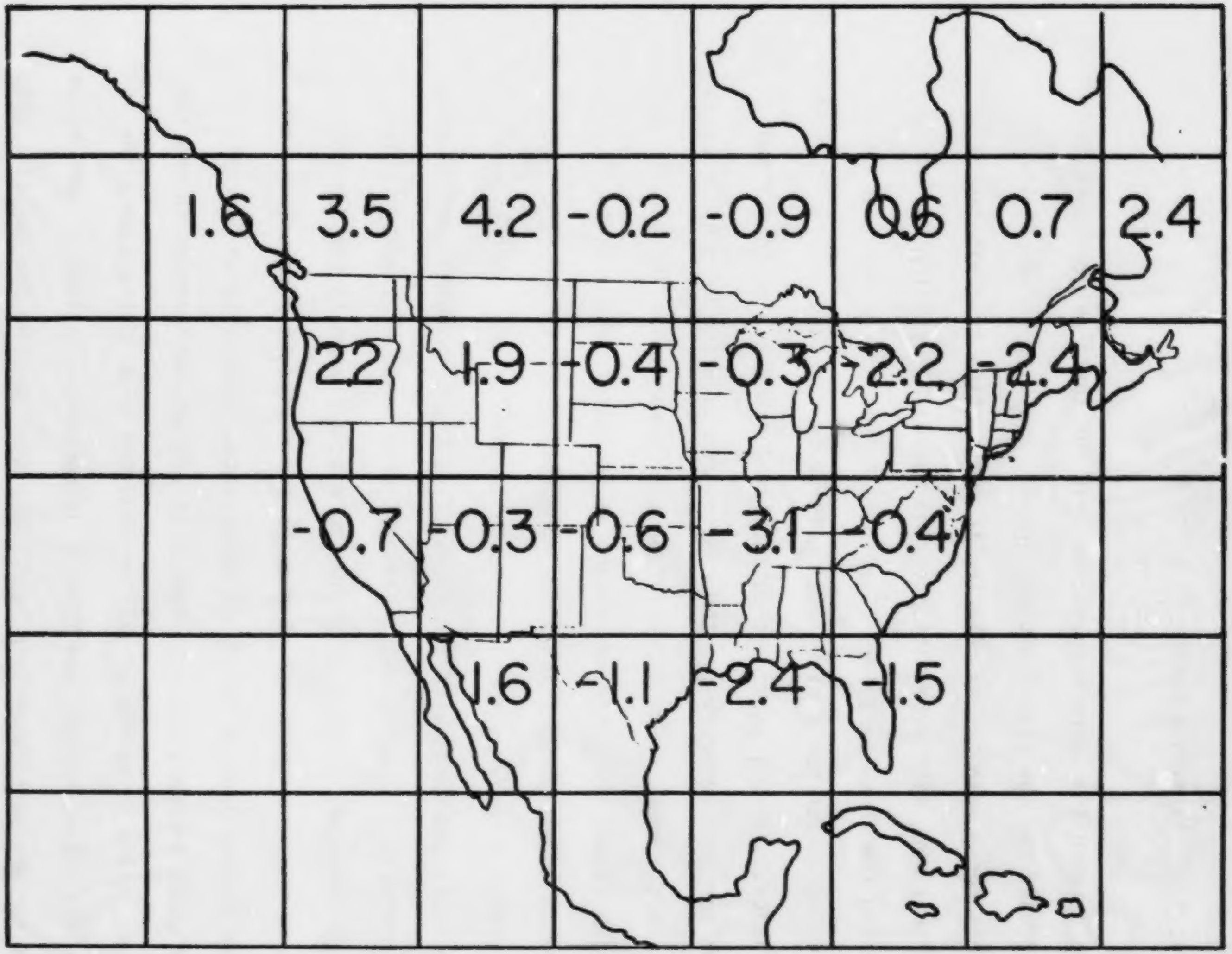
1.6
3.5
4.2
-0.2
-0.9
0.6
0.7
2.4
2.2
1.9
-0.4
-0.3
-2.2
-2.4
-0.7
-0.3
-0.6
-3.1
-0.4
1.6
-1.1
-2.4
-1.5

Fig. 12. Change in the drought index between the last ten years of the doubled CO_2 run and the last ten years of the control run, for the annual average. A negative value implies increasing drought frequency; see the text for an exact definition.

the previous diagnostics.

A diagnostic directly related to the influence of climate on agriculture is the plant water stress, which is defined by the formula

$$PWS = \sum 18 \left(\frac{TGmax - TGmin}{TSmax - TSmin} -1 \right)$$

where TG is the temperature of the top layer of the ground (10 cm), TS is the surface air temperature, and max and min refer to the maximum and minimum values of these two temperatures recorded during the day. The plant water stress is thus accumulated daily; if the ground temperature variation is twice that of the surface air temperature, then 18° accumulate per day. With the ground temperature exceeding the surface air temperature there can be expected to be a flux of heat and moisture out of the ground which is assumed to "stress" local vegetation. In general, plant water stress decreases somewhat from south to north. (It should be noted that the legitimacy of using this index in a higher CO_2 world, is ques-

Table 1

DROUGHT INDEX	DROUGHT	% OCCURRENCE IN CONTROL RUN
$DI < -4.0$	Extremely Dry	2
$-4.0 < DI < -3.0$	Severely Dry	6
$-3.0 < DI < -2.0$	Moderately Dry	10
$-2.0 < DI < -1.0$	Mildly Dry	15
$-1.0 < DI < 1.0$	Near Normal	33
$1.0 < DI < 2.0$	Mildly Wet	15
$2.0 < DI < 3.0$	Moderately Wet	10
$3.0 < DI < 4.0$	Severely Wet	6
$4.0 < DI$	Extremely Wet	3

tionable. Higher CO_2 will change stomal behavior in plants, and plant transpiration. Consequently the degree to which plants are stressed will change. The results given here do not include these effects).

Fig. 13 shows the change of plant water stress and the percentage change in the experiment relative to the control run. In the experiment the stress increased in both the southern and northern portions of the region. This of course is the yearly average result; the changes for different seasons will be discussed in the next section.

Another element of the climate system which is of importance to agriculture is the length of the growing season. This is defined in the model as the duration between days that the surface air temperature drops below 0°C during August-January (in the Northern Hemisphere). The change in the growing season, and the percentage change relative to the control run are shown in Fig. 14. The changes are quite dramatic and unambiguous - the growing season increases throughout, by values approaching 50% in the northern grid boxes. This occurs because of the general warming experienced due to increasing CO_2, which is apparently much more pronounced statistically than the precipitation changes, at least on the yearly average.

One additional factor which might be expected to influence plant growth is the cloud cover, or equivalently, the amount of sunlight reaching the surface. The change in this proved to be insignificant. Cloud cover changed by only a few percent from the range of 30-70% for different grid boxes in the control run.

To summarize the results from this section: the annually averaged hydrologic cycle increased in intensity over the northwestern portions of the continent, with greater precipitation, evaporation and runoff. Specific aspects of the hydrologic cycle increased also in the northern regions (precipitation, total earth water, evaporation) and western portions (precipitation, evaporation, runoff).

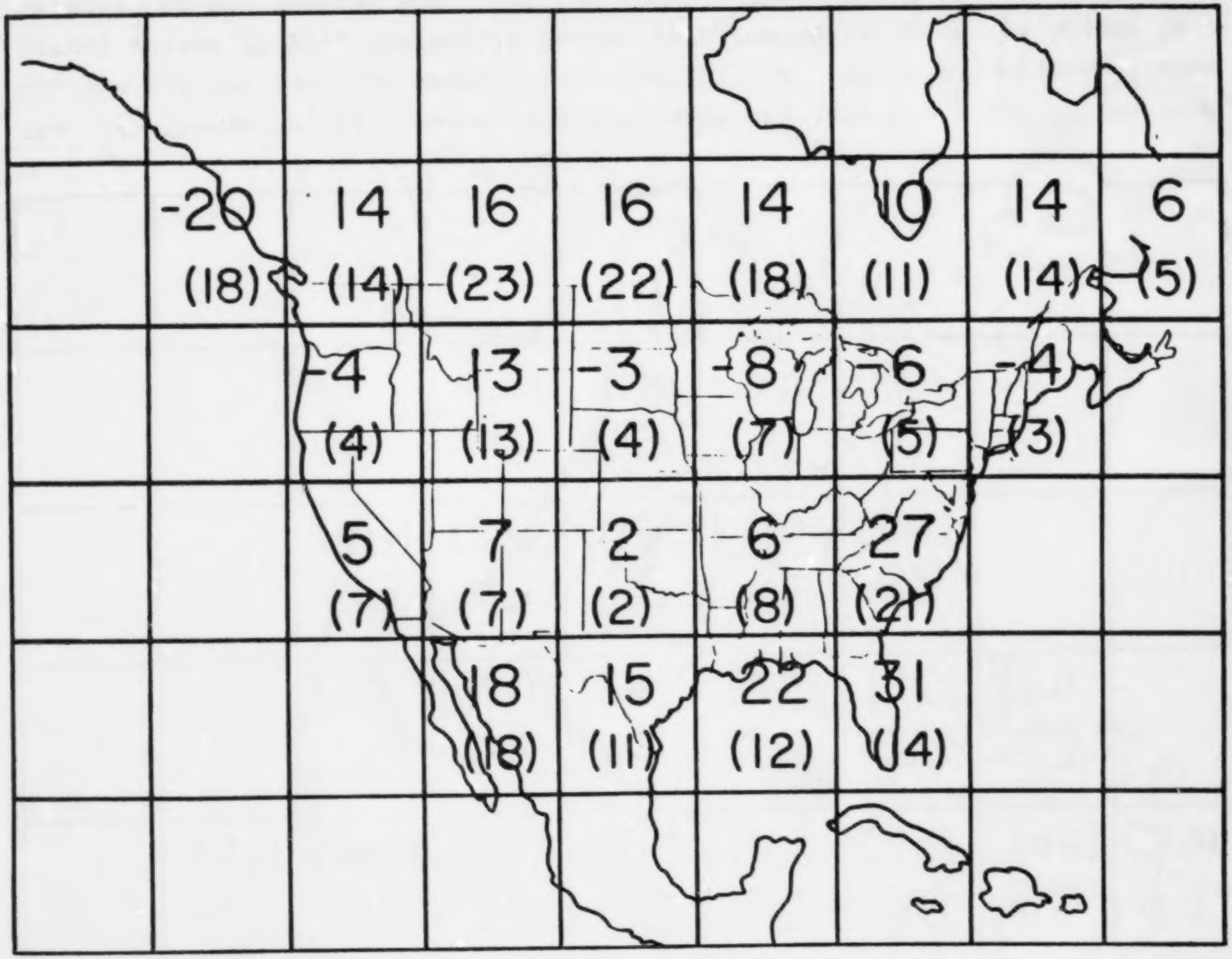
-20
(18)
14
(14)
16
(23)
16
(22)
14
(18)
10
(11)
14
(14)
6
(5)
-4
(4)
13
(13)
-3
(4)
-8
(7)
-6
(5)
-4
(3)
5
(7)
7
(7)
2
(2)
6
(8)
27
(21)
18
(18)
15
(11)
22
(12)
31
(14)

Fig. 13. Change in plant water stress between the last ten years of the doubled CO_2 run and the last ten years of the control run, for the annual average. The top number indicates the actual change, the bottom number in parenthesis gives the change in % relative to the control run. See the text for an exact definition.

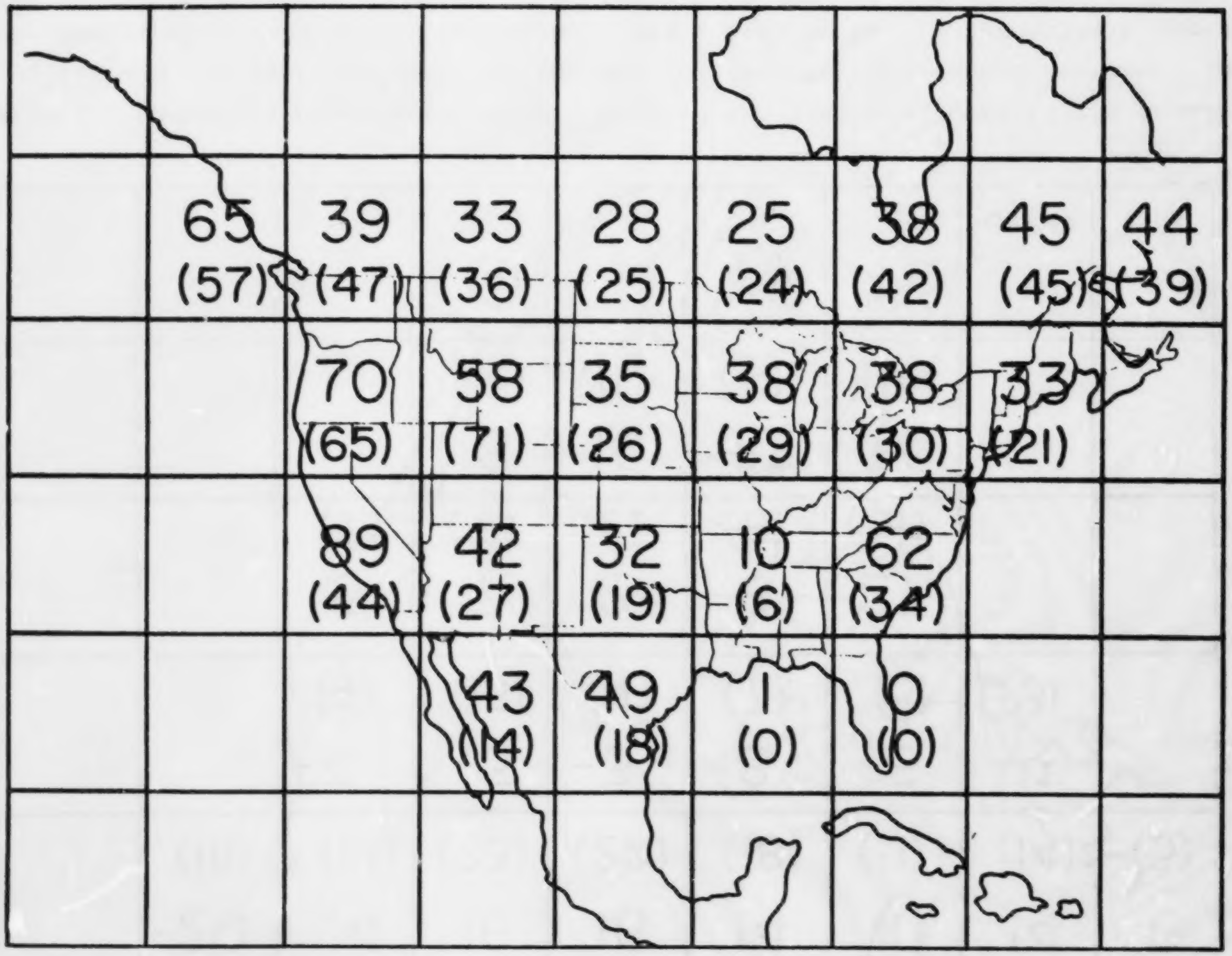
65 (57)
39 (47)
33 (36)
28 (25)
25 (24)
38 (42)
45 (45)
44 (39)
70 (65)
58 (71)
35 (26)
38 (29)
38 (30)
33 (21)
89 (44)
42 (27)
32 (19)
10 (6)
62 (34)
43 (14)
49 (18)
1 (0)
0 (0)

Fig. 14. Change in the growing season between the last ten years of the doubled CO_2 run and the last ten years of the control run. The top number indicates the actual change (days), the bottom number in parenthesis gives the change in % relative to the control run. See the text for an exact definition.

The southern and eastern portions of the continent had either mixed changes, or a tendency towards drying.

The warming associated with doubled CO_2 occurred throughout the continent and produced a longer growing season everywhere and increased plant water stress in the northern and southern sections.

3. Monthly Variation

While the annually averaged results present a picture of the variations on the continental scale for the climate in general, for many applications it is necessary to know variations on a monthly basis. In this section we will look at how various parameters changed monthly in four specific grid boxes: the grid boxes labeled 9, 16, 17, and 14 in Fig. 2. Grid box 9, which encompasses all or parts of such states as Idaho, Washington and Oregon experienced the precipitation increase noted for the northwestern section of the continent in Fig. 7. Grid box 16 includes the major portion of the Colorado River. Grid box 17, which includes the states of Kansas and Oklahoma, takes in the wheat growing region of the southern plains. Finally, grid box 14 covers the heavily populated regions of the northeast, New York and New England.

It is important to again emphasize the uncertain nature of climate change results for an individual grid box. The seasonal variation of changes for precipitation are shown for the entire country in the next section; the changes which occur on regional or larger scales are of more certainty than those which vary from grid box to grid box. The individual grid boxes chosen provide an indication of the range and character of changes that are likely to occur due to doubled CO_2, and, once again, should not be thought of as necessarily applying to that particular location.

Changes in a grid box with increased wetness

Grid box 9, which the control run had about 50% wetter than the observed values, experienced an overall increase in the hydrologic cycle, as indicated in the previous section. Fig. 15 shows the monthly variation of precipitation, evaporation and runoff as the change from the control run values for each month; an increase of all three parameters occurs in all months except September and April. The rainfall and runoff changes are small from July through September when both parameters are at their minimum in the control run. Thus to some extent the largest increases occur when the hydrologic cycle in the control run is largest, which indicates that the climate change is amplifying an already existing pattern.

Fig. 16 presents the monthly variation of other parameters, related both to the hydrologic cycle and to vegetation. The total earth water, which is affected by the difference between evaporation and precipitation, increases except for the time period August through October, mirroring with a one month phase lag the effects noted in Fig. 15. The drought index, defined in the previous section, shows that months with precipitation greater than evaporation, relative to the control run, occurred more consecutively throughout the year.

The change in the percent occurrence of extreme dry and wet periods for this grid box, as defined in Table 1, can be seen in Table 2. In the control run severe and extreme droughts occurred 12% of the time, while severe and extreme wet periods occurred 8% of the time. In the doubled CO_2 climate, extreme and severe dryness occurred only 6% of the time, while extreme and severe wet periods now occurred 37% of the time. As can be seen from the figure the increase occurred throughout the year, although somewhat less often in summer.

The plant water stress increased throughout the summer months (as did evaporation as in Fig. 15) due to the general warming of the ground. The snow cover decreased by up to 20% in winter or 80% relative to the control run, indi-

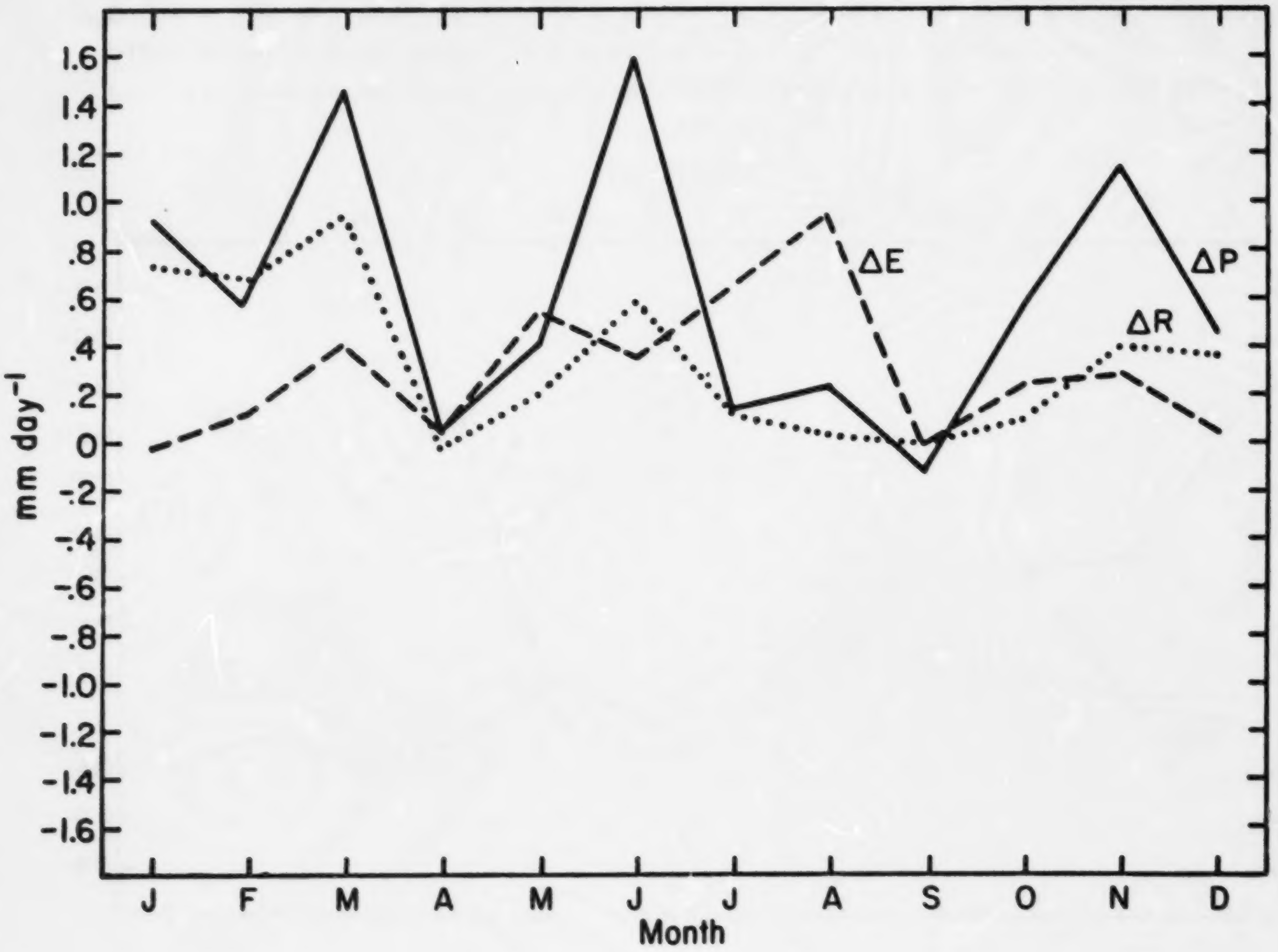

Fig. 15. Change of precipitation (P), evaporation (E) and runoff (R) between the doubled CO_2 run and the control run as a function of month for grid box 9.

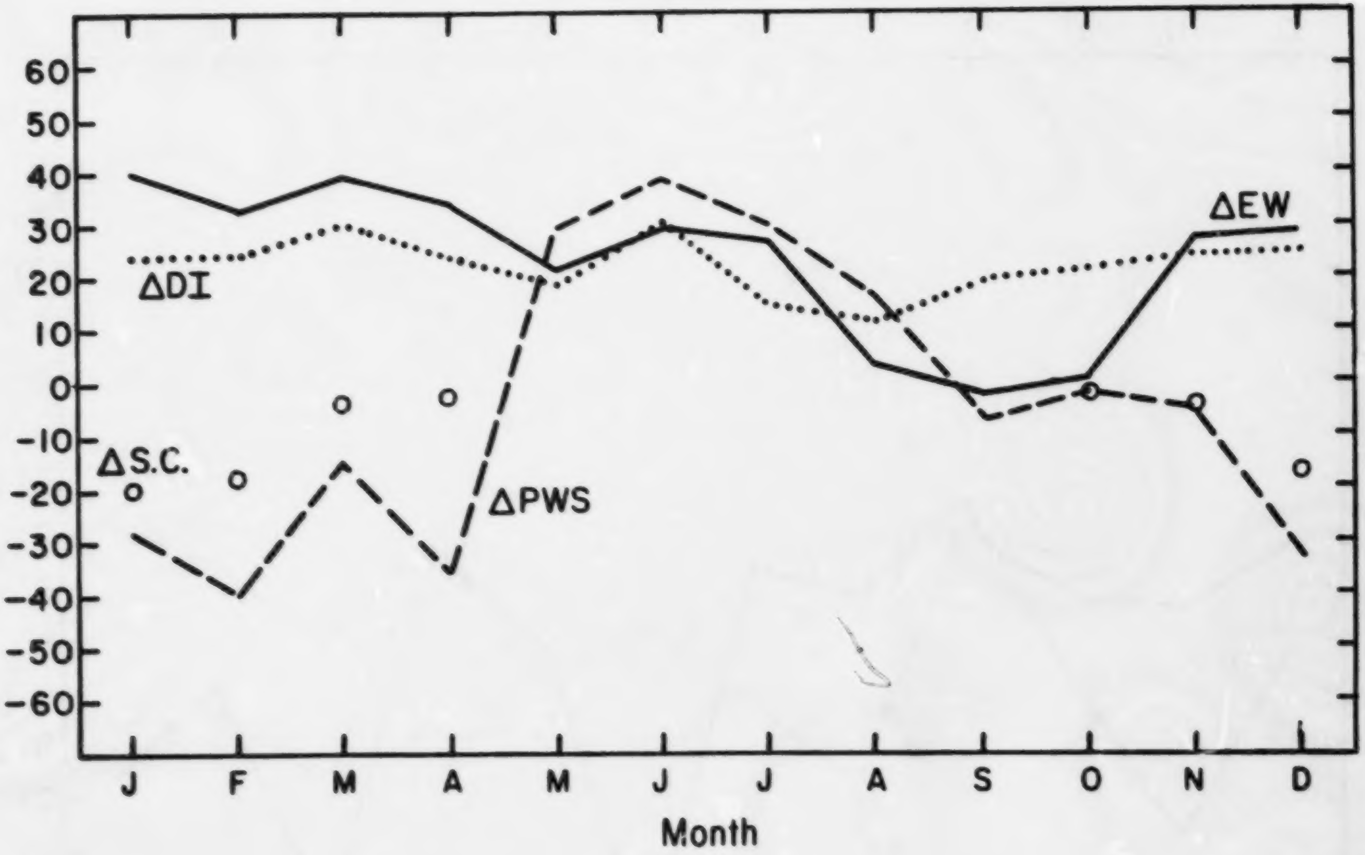

Fig. 16. Change in total earth water (EW) (mm), drought index (DI) (times ten), plant water stress (PWS), and snow cover (S.C.) (%) between the doubled CO_2 run and the control run as a function of month for grid box 9.

Table 2

	Extremely Dry	Severely Dry	Moderately Dry	Mildly Dry	Near Normal	Mildly Wet	Moderately Wet	Severely Wet	Extremely Wet
Grid Box 9									
Control	4	8	13	13	38	8	8	7	1
2'd CO_2	2	4	9	11	16	9	11	10	27
Grid Box 16									
Control	4	4	13	13	26	19	8	8	5
2'd CO_2	1	8	12	17	23	19	10	12	0
Grid Box 17									
Control	0	0	3	21	37	18	7	11	3
2'd CO_2	0	2	16	18	40	12	5	5	2
Grid Box 14									
Control	0	3	13	10	33	18	6	10	7
2'd CO_2	22	13	12	12	20	18	0	2	1

cating that the warmer temperatures offset the increased wintertime precipitation in their influence on snow cover. These diagnostics emphasize the warmer and better quality of the climate in this area, with the hydrologic cycle least affected in late summer and early fall.

Changes in a grid box with autumn dryness

Fig. 17 shows the changes in the hydrologic cycle in grid box 16. In the control run this grid was much wetter than observed, by about a factor of three. The seasonal cycle in rainfall change noted for the northwest region continues here, in amplified form. The small change in April seen in Fig. 15 has expanded into little change throughout the spring; the slight decrease in September has expanded into decreases from August through October. This grid box is normally wettest in the months of November through June, so the decrease in spring relative to winter and summer change the seasonal cycle somewhat; the dryness in fall accentuates the prevalent pattern. In fact, the rainfall in September decreases to only 20% its normal value. Also shown is the evaporation which has a similar, although not identical, monthly variation. The runoff change therefore tends to be small, with a slight increase in winter, and a slight decrease in fall.

Fig. 18 gives the monthly variation for the changes in diagnostics related to the hydrologic cycle or vegetation. The earth water increases during the first half of the year, and decreases during the second half. The first half increases amount to 10% of the values in the control run, but the decreases exceed 50% in some months (Sept. and Oct.) and thus, like the rainfall, indicate a substantial drying of the climate in the fall. The drought index showed there was a tendency for consecutive dry months to occur in the fall. Reference to Table 2 shows that dry periods tended to occur 8% of the time in the control run, with very wet periods 13%; in the doubled CO_2 climate there is little change in these percentages.

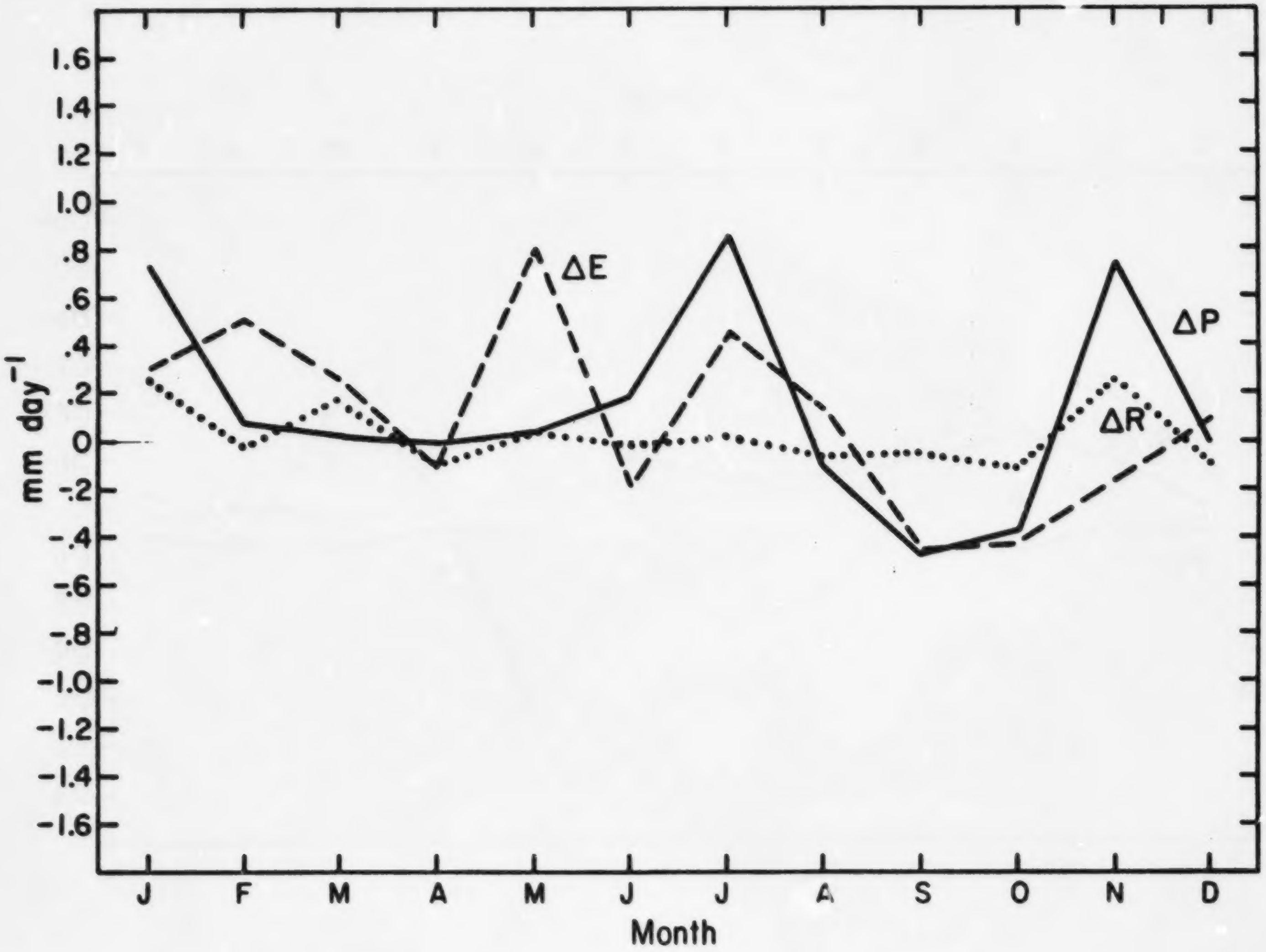

Fig. 17. As in Fig. 15 for grid box 16.

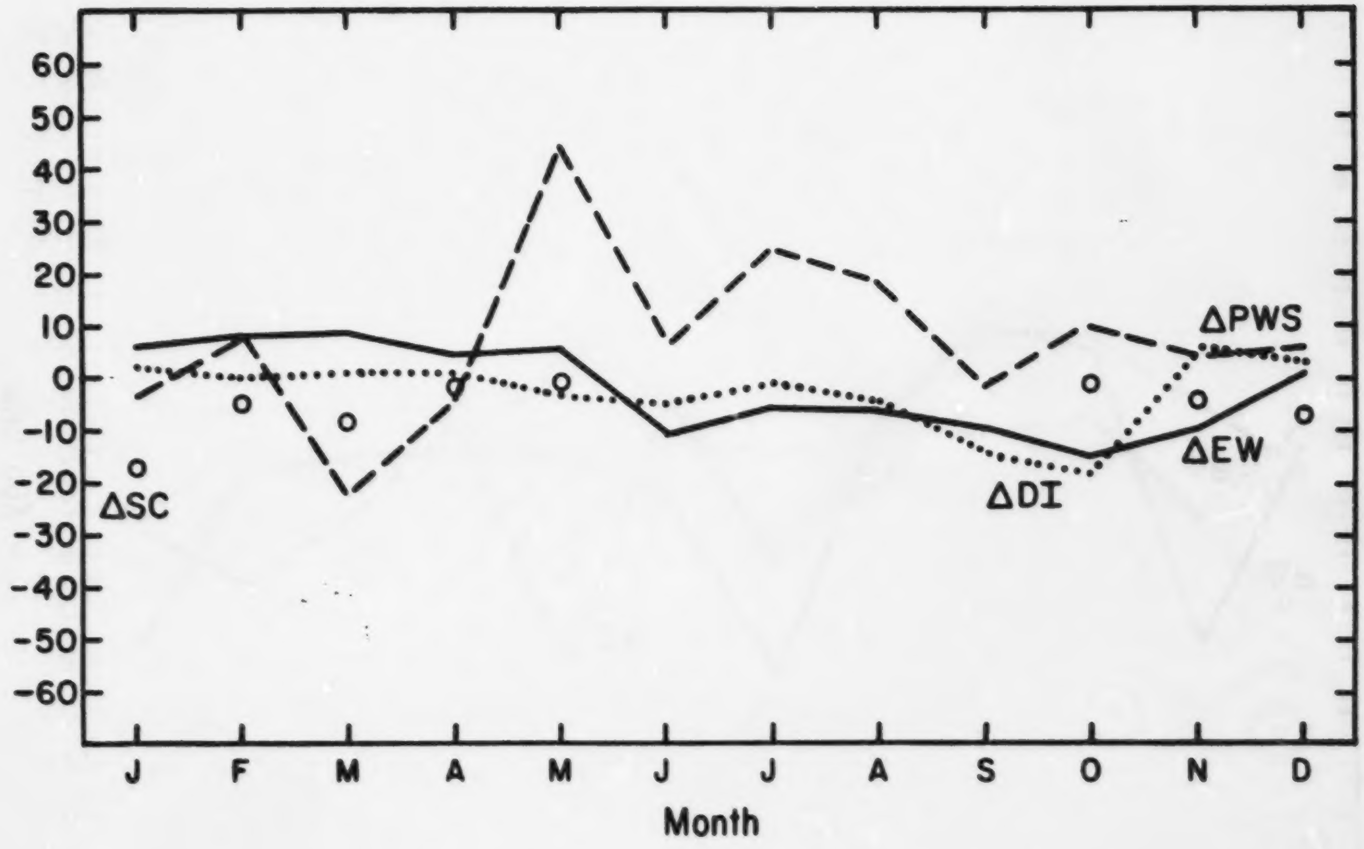

Fig. 18. As in Fig. 16 for grid box 16.

The plant water stress increases throughout all the warm months, associated with the greater temperatures; and the snow cover decreased in winter, with the deficit reaching 17% of the grid box area in January which is an 85% decrease relative to the control run. For the winter as a whole this grid box is covered with snow only 5% of the time, compared to 15% in the control run.

Changes in a grid box with increased autumn wetness

The changes in the hydrologic cycle that occurred in grid box 17 are shown in Fig. 19. In the control run this grid box had about 50% more rainfall than observed. The results for this grid are quite different from those discussed previously, especially for autumn. Large decreases in precipitation occur during the spring and the first half of summer, with strong increases in late summer and early fall. The precipitation decreases are on the order of 20% of the control run values, while the increases are as much as 30%. (Remember that this grid received about 50% more rainfall on the yearly average in the control run than is observed). The runoff changes follow a similar pattern, although the percentage reduction relative to the control run reaches 50%. The evaporation changes in a less predictable fashion.

The change of the total earth water is shown in Fig. 20, and emphasizes the reduction of water except in the fall. The value in late spring has been reduced by a factor of 33% compared to the control run. The drought index indicates the tendency for consecutive dry months to occur from March through July. As shown in Table 2 droughts did not occur at all in the control run in this grid box, while wet periods occurred 14% of the time. In the doubled CO_2 climate droughts now occur 2% of the time, with wet periods 7%. (These changes are likely within the noise limit of precipitation variability.)

The plant water stress increases around the equinoxes and decreases in June and July (along with evaporation, as in Fig. 19). The snow cover area decreases

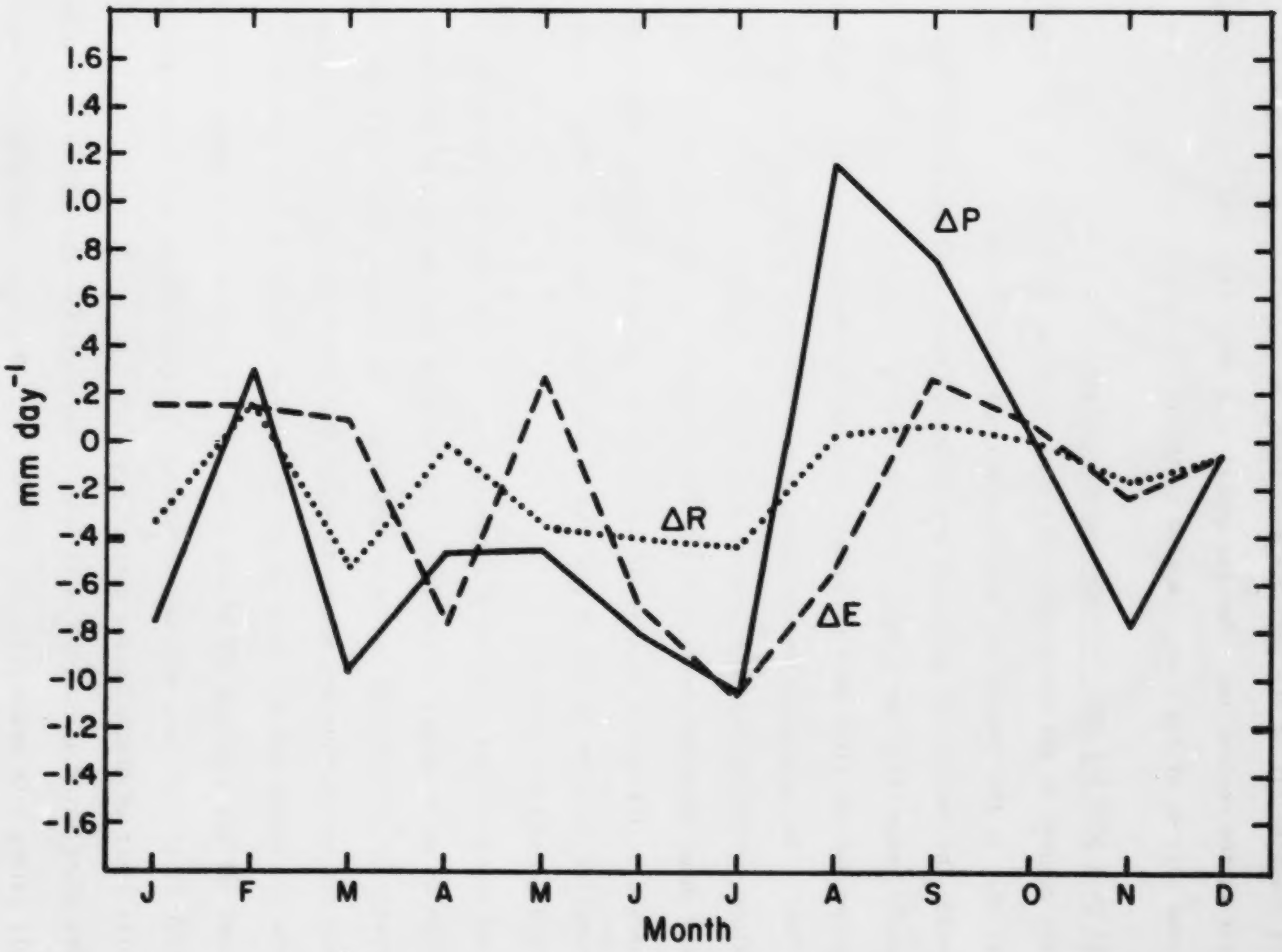

Fig. 19. As in Fig. 15 for grid box 17.

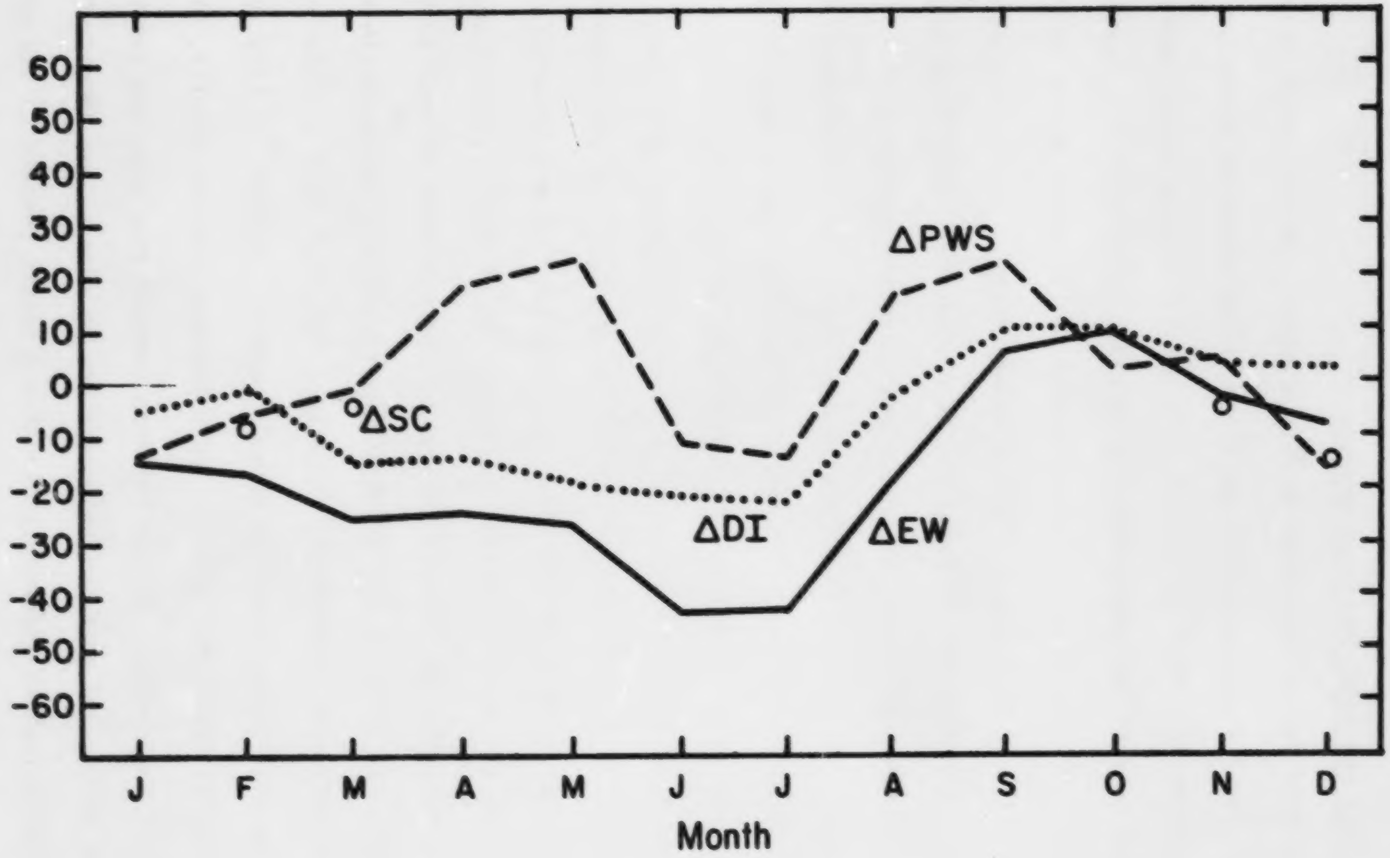

Fig. 20. As in Fig. 16 for grid box 17.

by up to 14% in January; for the winter as a whole, this amounted to a 75% reduction in snow coverage relative to the control run.

Changes in a grid box with increased dryness

The final grid box to be looked at with a monthly resolution is grid box 14. In the control run its precipitation was close to the observed amounts. The hydrologic cycle changes are shown in Fig. 21. In general precipitation decreases during the last half of the year, with the decrease being most noticeable in early summer and fall. The decreases in June, October and November amount to 20-30% of the normal rainfall in the control run for these months. Runoff follows a similar change; however the reduction in these months reaches 90%, indicating that runoff has virtually disappeared due to the large precipitation decreases.

Fig. 22 shows the changes in related diagnostics. The earth water is seen to decrease throughout the year, the result of the annually averaged drying; the reduction is on the order of 25% of the control run values. The drought index shows a consistent tendency towards a dryer climate throughout the year. Table 2 shows the change in distribution of dry and wet periods. In the control run very dry periods occurred 3% of the time, with very wet periods occurring 17%; in the doubled CO_2 climate dry periods now occur 35% of the time, with wet periods only 3%. This indicates the dramatic change toward increased dryness experienced in this grid box. As shown in the accompanying figure this change maximized in the fall. In a different doubled CO_2 experiment run, that used a different representation of sea ice (a key factor in climate models), analysis of this region hydrologically using the Palmer drought index produced similar results, with the largest effect in the spring. This difference demonstrates that the specific results for any particular grid box and month are to some extent dependent upon the unique parameterization representation of a climatic process in the model. At best, the monthly results can be taken as indicative of overall tendencies for change, not as reliable predictors.

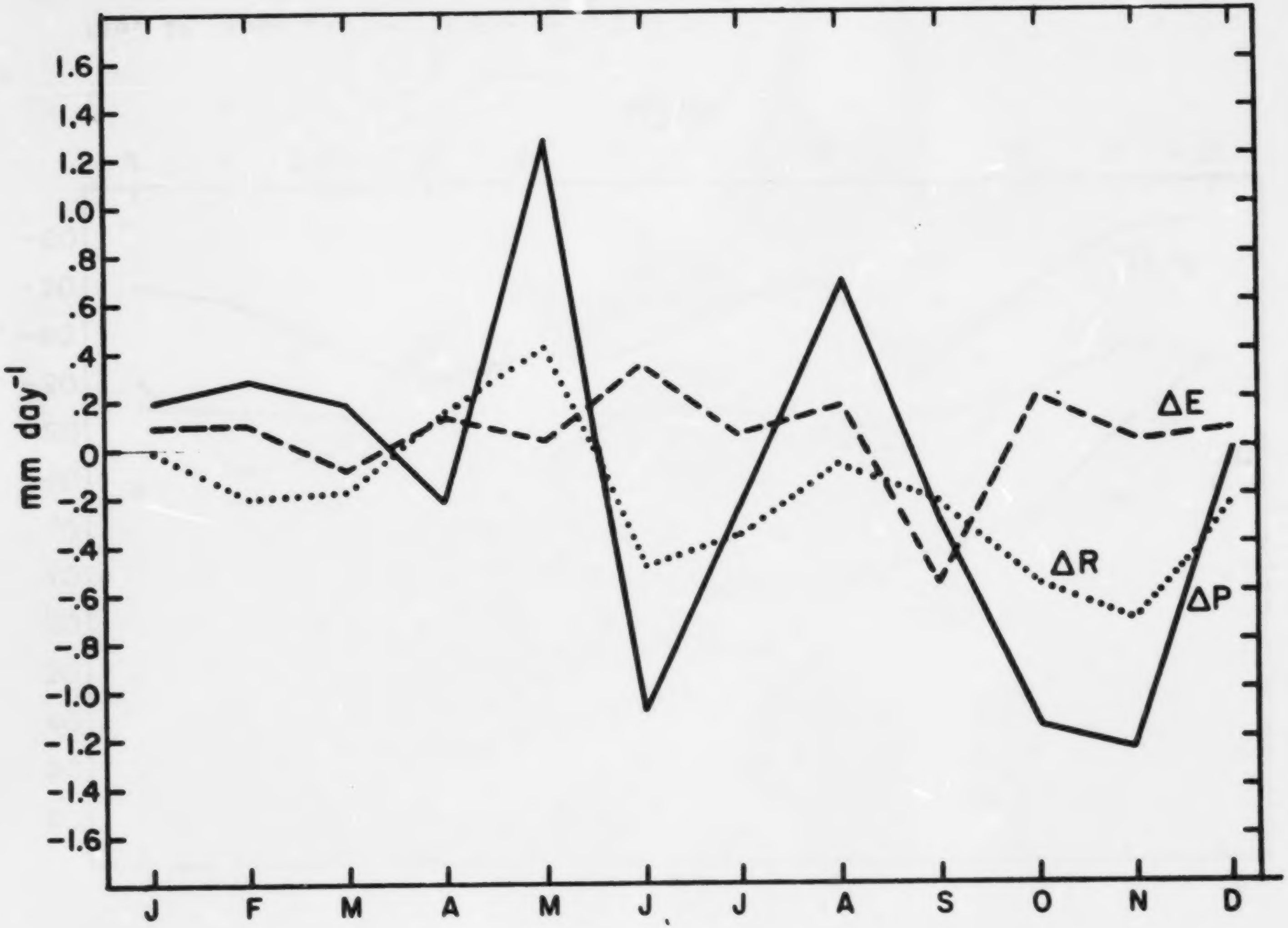

· Fig. 21. Same as Fig. 15 for grid box 14.

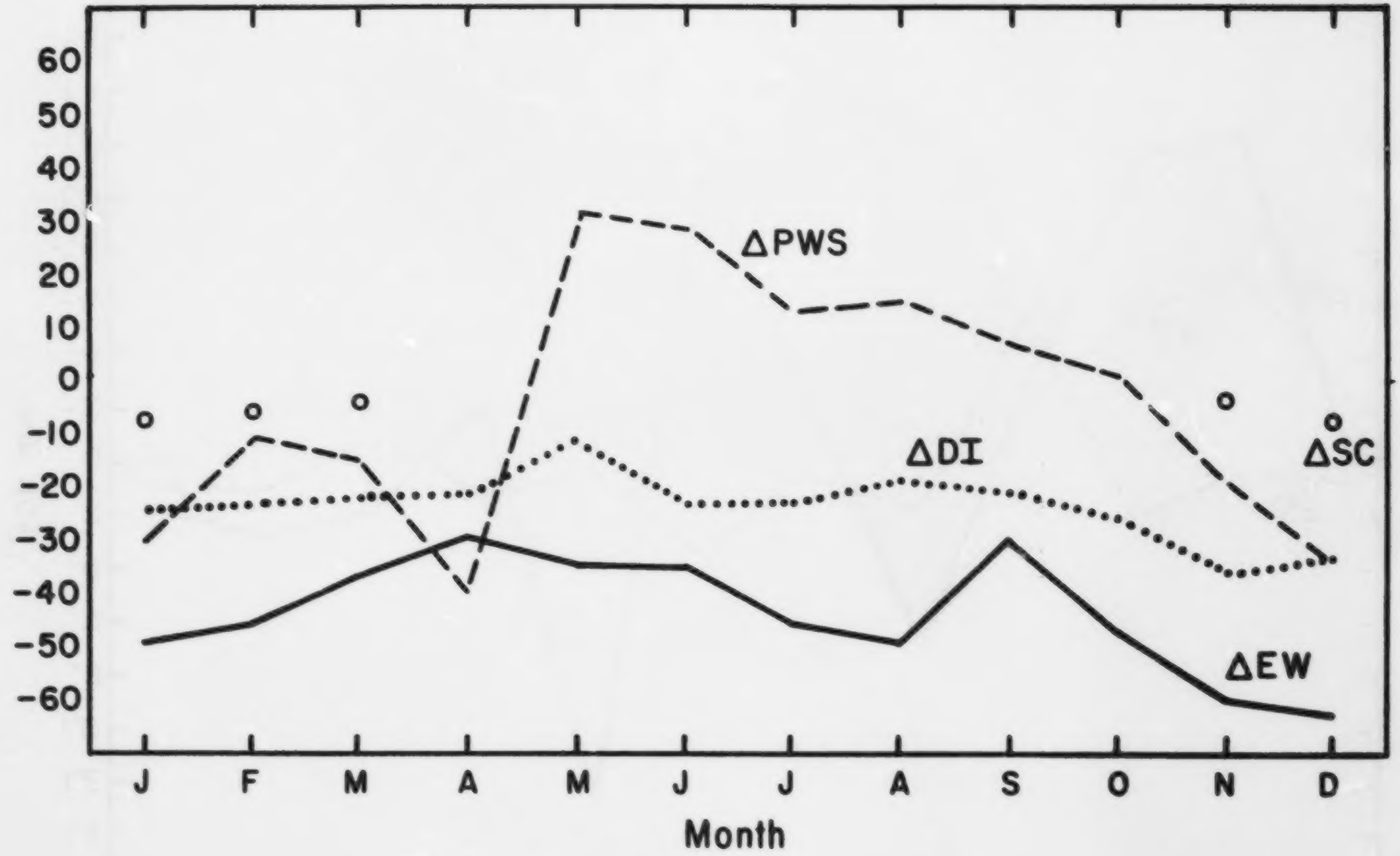

Fig. 22. Same as Fig. 16 for grid box 14.

The plant water stress increases during the warm season, although the change in summer is small relative to that seen at the other grid boxes discussed above. The area covered by snow cover decreases by a small percentage during the winter, although the change amounts to up to a 50% decrease relative to the control run.

Summary of Changes Over The Year

To summarize the results of this section: a review of the change in the hydrologic cycle and related diagnostics for four grid boxes for each month indicates that the variation differs from one location to another. Grid box 9 shows a general increase in the hydrologic cycle, with minimum change during late summer and early fall. Grid box 16 had increased precipitation only near the solstices, with a drying in fall. Grid box 14 had a generally drier climate, with maximum precipitation decrease during fall. In contrast, grid box 17 experienced the southern considerable drying during spring and early summer, with increased precipitation during late summer and early fall. Thus no general conclusion can be drawn about variations in monthly effects on the hydrologic cycle of doubled CO_2; each grid must be reviewed separately.

If one combines the extremely and severely dry percentages for the various grid boxes one can display the results, as in Fig. 22a, of the number of months in a 30 year period in which there is potential for drought. The results are shown for the four grid boxes, both for the control run and the doubled CO_2 run. As can be seen, there is potential for substantial increase in a particular grid box; again, these results should be viewed as indicating the types of changes possible in the hydrologic cycle, rather than as applying to any particular grid box. Fig. 22b shows the number of months of severely and extremely wet periods - there is much variation from grid box to grid box, and the potential for strong changes from the current climate.

Several other diagnostics did show common changes, due largely to the increase in temperature experienced throughout the year. The plant water stress generally

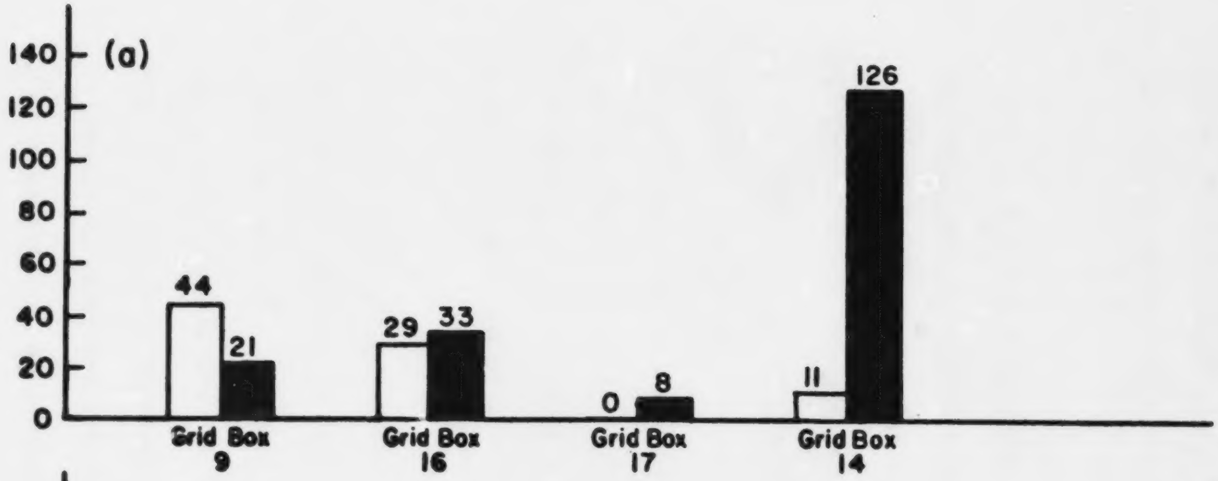

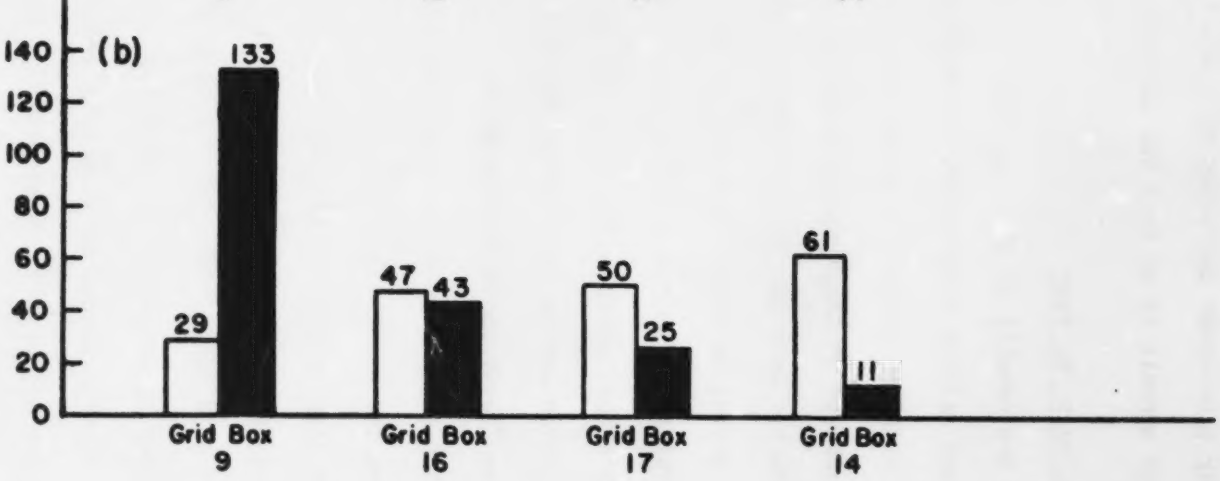

Fig. 22a. Number of severely or extremely dry months which would be expected during 30 years in four different grid boxes for the control run (blank boxes) and in the doubled CO_2 climate (blackened boxes).

Fig. 22b. Same as 22a except for the number of months extremely or severely wet.

increased during the warmer months (although even this has to be qualified for the southern plains region), and snow cover decreased during the winter, by large percentages relative to the control run.

4. Seasonal Variation

With so much variation occurring from grid box to grid box the question arises as to what the seasonal pattern of changes looks like for the region as a whole. We will review this briefly, with reference to the precipitation changes, which, from the last section, seem to be indicative of the changes seen in other areas of the hydrologic cycle, especially the earth water. We will show the results for the four seasons, defined as December through February (winter), March through May (spring), June through August (summer), and September through November (fall). This approach does not provide as much detailed information as looking at the monthly variation, but it does allow patterns to be understood more easily; it also indicates which grid box changes have larger regional applicability, and thus more inherent confidence. The presentation will be insensitive to changes when there are strong differences between early and late parts of a season, (for example, the rainfall variation in grid box 16 during early fall and late fall). Nevertheless, the structuring provided is worthwhile.

The rainfall changes in percent relative to the control run for the four seasons are shown in Figs. 23-26. Fig. 23 and 24 show that most grid boxes showed precipitation increases, or no change, during the winter and spring; a notable exception is the southern plains region in spring, as discussed above. The precipitation increases were greatest in the northern and western portions as was true for the annual average. The southern regions showed little overall change, although Florida was considerably drier during winter.

In summer (Fig. 25) the north and northwest continued to experience greater rainfall, and the southeastern region also had much more rainfall. Little change was experienced in the center of the country. In fall (Fig. 26) substantial de-

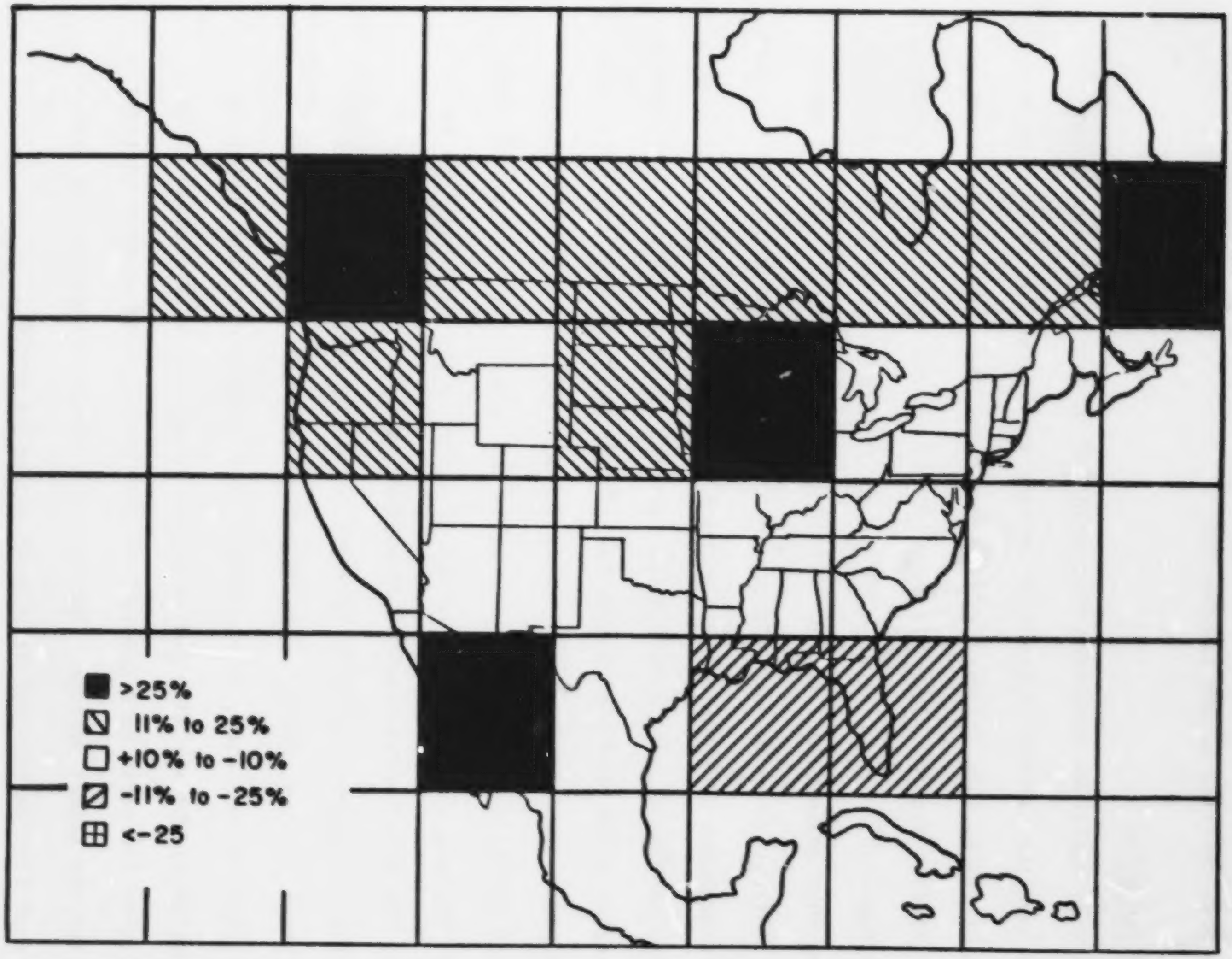

■ >25%
▧ 11% to 25%
☐ +10% to -10%
▨ -11% to -25%
⊞ <-25

Fig. 23. Change in precipitation during winter between the doubled CO_2 run and the control run. The change is given in % relative to the control run, indicated by the shading in the legend.

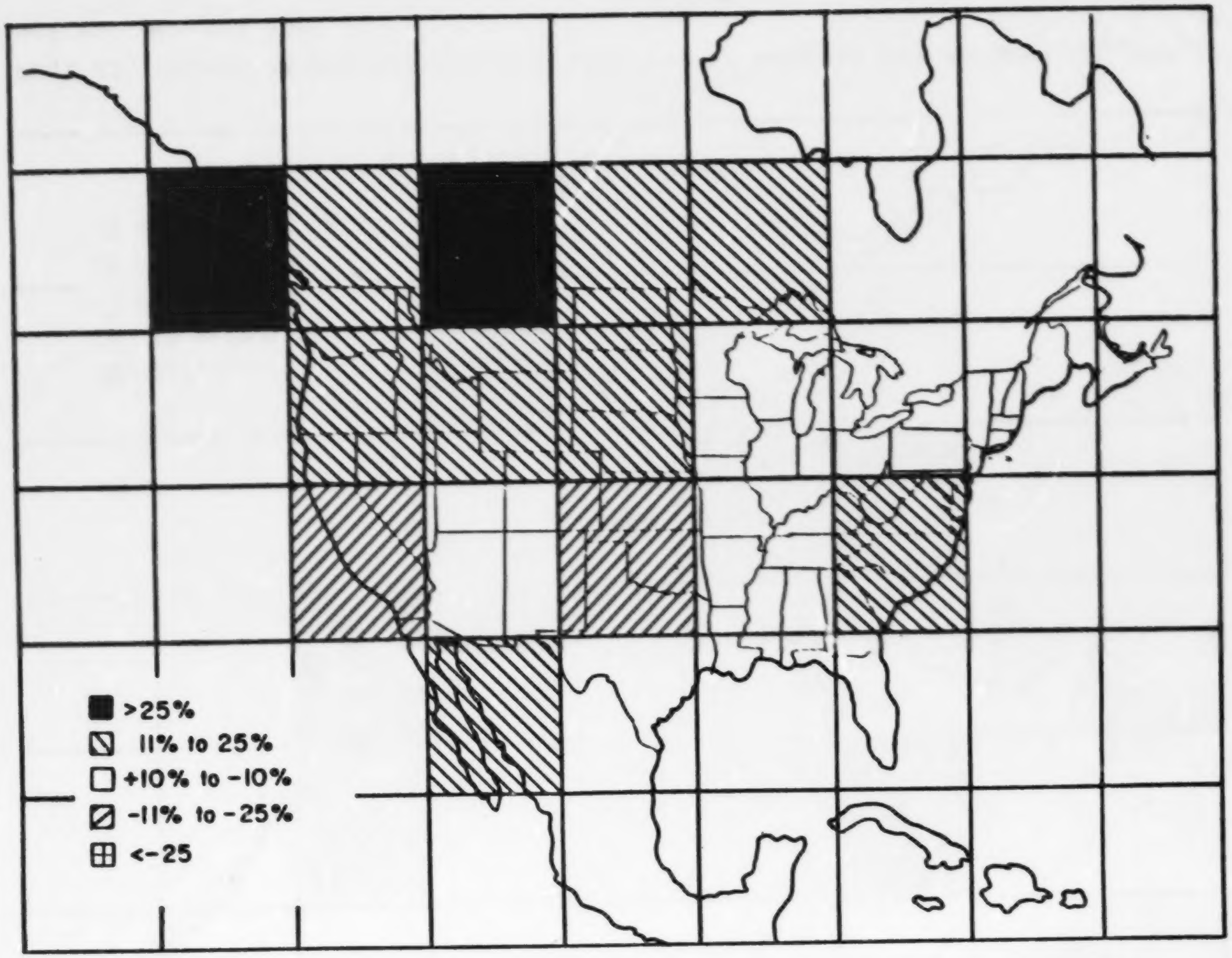
■ >25%
▧ 11% to 25%
□ +10% to -10%
▨ -11% to -25%
⊞ <-25

Fig. 24. Change in precipitation during spring between the doubled CO_2 run and the control run.

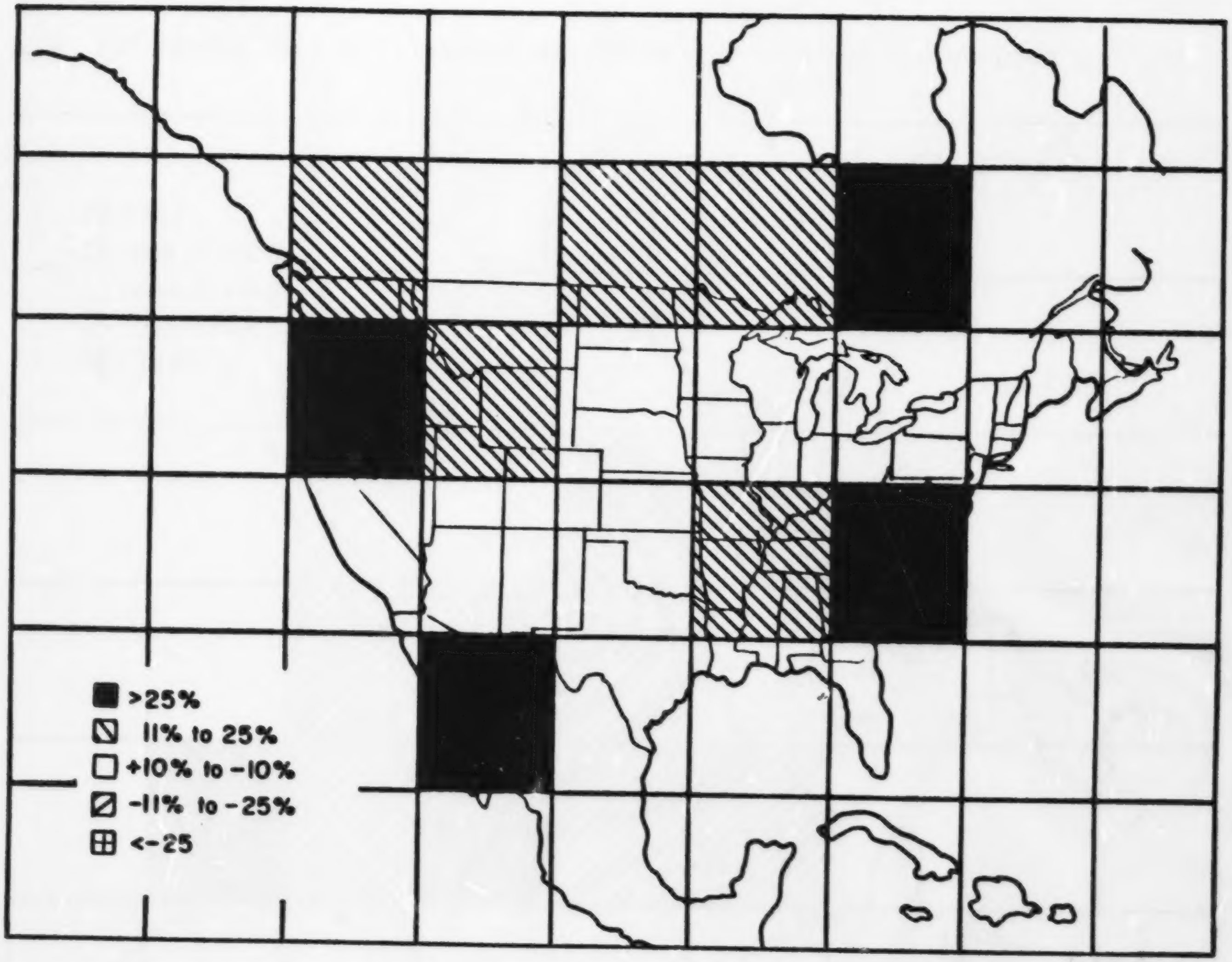
>25%
11% to 25%
+10% to -10%
-11% to -25%
<-25

Fig. 25. Change in precipitation during summer between the doubled CO_2 run and the control run.

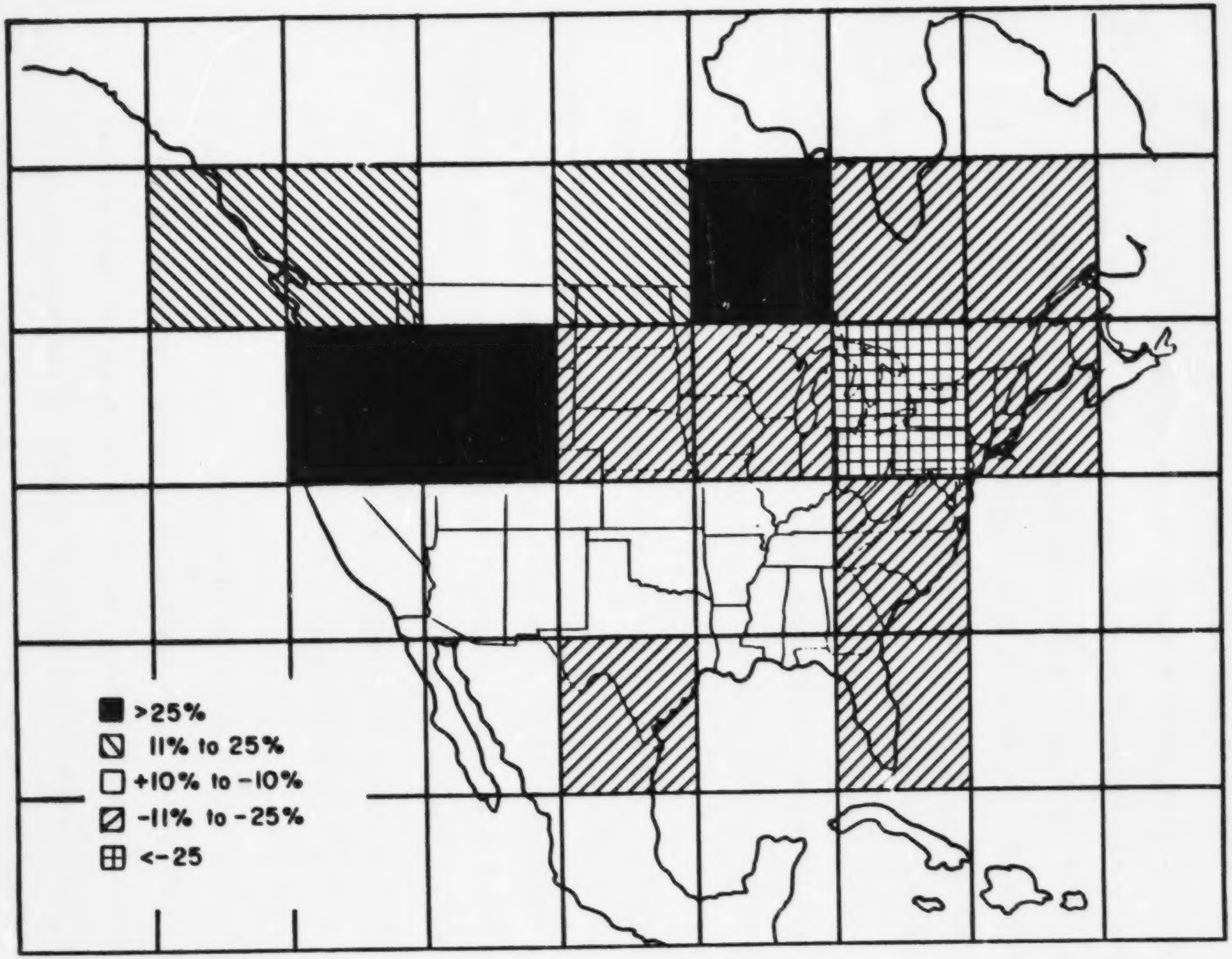
■ >25%
▧ 11% to 25%
☐ +10% to -10%
▨ -11% to -25%
⊞ <-25

Fig. 26. Change in precipitation during fall between the doubled CO_2 run and the control run.

creases in rainfall occur over much of the country, with the northwest being a major exception. The more detailed review showed that even the Colorado River grid received less rainfall through part of the fall. The areas which avoided this loss of precipitation, parts of Canada, Mexico and the northwestern United States thus experienced increased rainfall throughout the year. It should be remembered that in all grid cells evaporation increases; therefore it would be incorrect to assume that increases in precipitation mean greater water availability, although decreases can be assumed to mean reduced water availability.

It is beyond the scope of this report to explore in great detail the reasons for the changes noted above. In general the increased precipitation to the north is associated with the warmer temperatures; more water can be held by a warmer atmosphere, and with increased evaporation from the ocean, vapor is transported northward and condenses at higher latitudes. This same influence is apparently felt in the northwestern sections, where increased evaporation off the ocean is advected onto land by the prevailing west winds. The precipitation change at any grid box and in any season, however, results from a complex interaction between temperature changes in that season, changes in moisture availability due to changes in atmospheric dynamics and ground water changes (which are affected by what has happened in preceding months), and changes in the atmospheric stability and jet stream position which are associated with global scale circulation effects (e.g. Hadley cell reaction, etc.).

Manabe et al. (1981) concluded in an experiment with 4 times the current CO_2 level, that a substantial drying would occur in spring and summer in mid to upper mid latitudes. The results shown in Figs. 24 and 25 do not indicate this effect. Although the increase in CO_2 amount is greater in the Manabe et al. experiments, the global warming was similar to that reported here. This again serves to illustrate the uncertain nature of the results for specific areas and seasons at this stage of global climate modeling.

II. DIFFERENCE OF PRECIPITATION BETWEEN WARM AND COLD PERIODS IN THIS CENTURY

Purpose

In the previous sections we investigated the changes in the hydrologic cycle indicated by the model for the doubled CO_2 climate, and then discussed some consequences of these changes. The hydrologic cycle was significantly altered by the global warming (of 4°C) associated with a doubling of CO_2; the question addressed here is whether any evidence exists in the historical record that the hydrological cycle changes as global temperature changes?

This section investigates whether changes in precipitation patterns can be observed in the United States between periods of prolonged global warming and cooling. The results of this analysis are useful for two related purposes:

- for testing the hypothesis that global warming will yield significant changes in the patterns of hydrology
- as a potential benchmark for the pattern of change associated with a small temperature increase, which will be useful in evaluating the planned transient experiment discussed in section III.

The results cannot be used to validate or invalidate the doubled CO_2 results from the GCM experiment reported in Section I, however. That experiment represented a climate in equilibrium, after a much larger warming, not the transitional changes in patterns that would lead to the new equilibrium. It is possible, for example, that a region which would eventually get drier for doubled CO_2 may at first get wetter as the "typical path" of storms tends to shift eastward as the world warms. This could lead to the region becoming more in the center of the storm track for a small CO_2 change, while later with a larger CO_2 change it could be on the periphery.

Past Research That Is Relevant

The possible influence of global warming on regional precipitation patterns has been investigated recently by Wigley, et al. (1980), Williams (1980), Pittock and Salinger (1982), and Jager and Kellogg (1983). Their approach was to compare the precipitation in the warmest years with the average precipitation (Williams, and Jager and Kellogg) or with the precipitation of the coldest years (Wigley, et al. and Pittock and Salinger). However, as pointed out by Pittock and Salinger, the use of individual years to represent warm and cold climatological periods is open to serious question, since a one year transient response may have quite different characteristic than a warm period of several decades. This suggests that investigating the changes in precipitation patterns between periods of prolonged global warming and cooling would be worthwhile.

One other study should be noted. An analysis of long-term averaged data of temperature and precipitation over the United States has recently been done by Diaz and Quayle (1980). Their main interest was in the possible relationship between changes of temperature and precipitation and the changes in the corresponding variances.

Summary of Results

We find that there is a significant increase in the precipitation during the warm epoch (defined below) in the eastern half of the United States, particularly in the Southeast. The changes in precipitation in this region have a significant correlation with the changes in the global temperature. There are also precipitation changes in Western Canada and over the basin of the Colorado river. However the changes in the latter region have low statistical significance and thus the relationship between these changes and the global temperature is less certain.

Methodology

We had to perform the following tasks:

- determine appropriate cold and warm periods for study based on global temperature data,
- establish the areal extent over which the temperature and precipitation trends of a given station can be taken as representative
- combine trends at individual stations to obtain regional trends.

This section reports on the procedures used to accomplish these tasks:

Cold and warm periods. Examination of the global temperature (see Fig. 27) shows that the coldest period in the past century was 1880 to 1920, while 1940 and 1960 was a warm period. Because of data limitations in station coverage we choose the period 1900 to 1920 as the cold period, thus yielding comparable station coverage in the cold and warm periods. The global temperature difference between the two periods was about 0.3°C. The number of stations within each grid box of our medium resolution general circulation model over the U.S.A. are shown on the Figs. 28 and 29 for the periods 1900-1920 and 1940-1960.

Establishing stations reliability. The difference between the number of stations in each grid box during these two time intervals is generally small and the distribution of stations is reasonably uniform. The average number of continental stations is 4.4 per grid box during the cold period 1900-1920 and 5.3 station per grid box during the warm period 1940-1960.

Correlation of trends at different stations. In order to gain an indication of how well these station distributions permit analysis of regional precipitation trends, it is necessary to establish the area for which a given station provides a representative precipitation trend. For this purpose we used the correlation coefficient between the two sets of time series data, calculating,

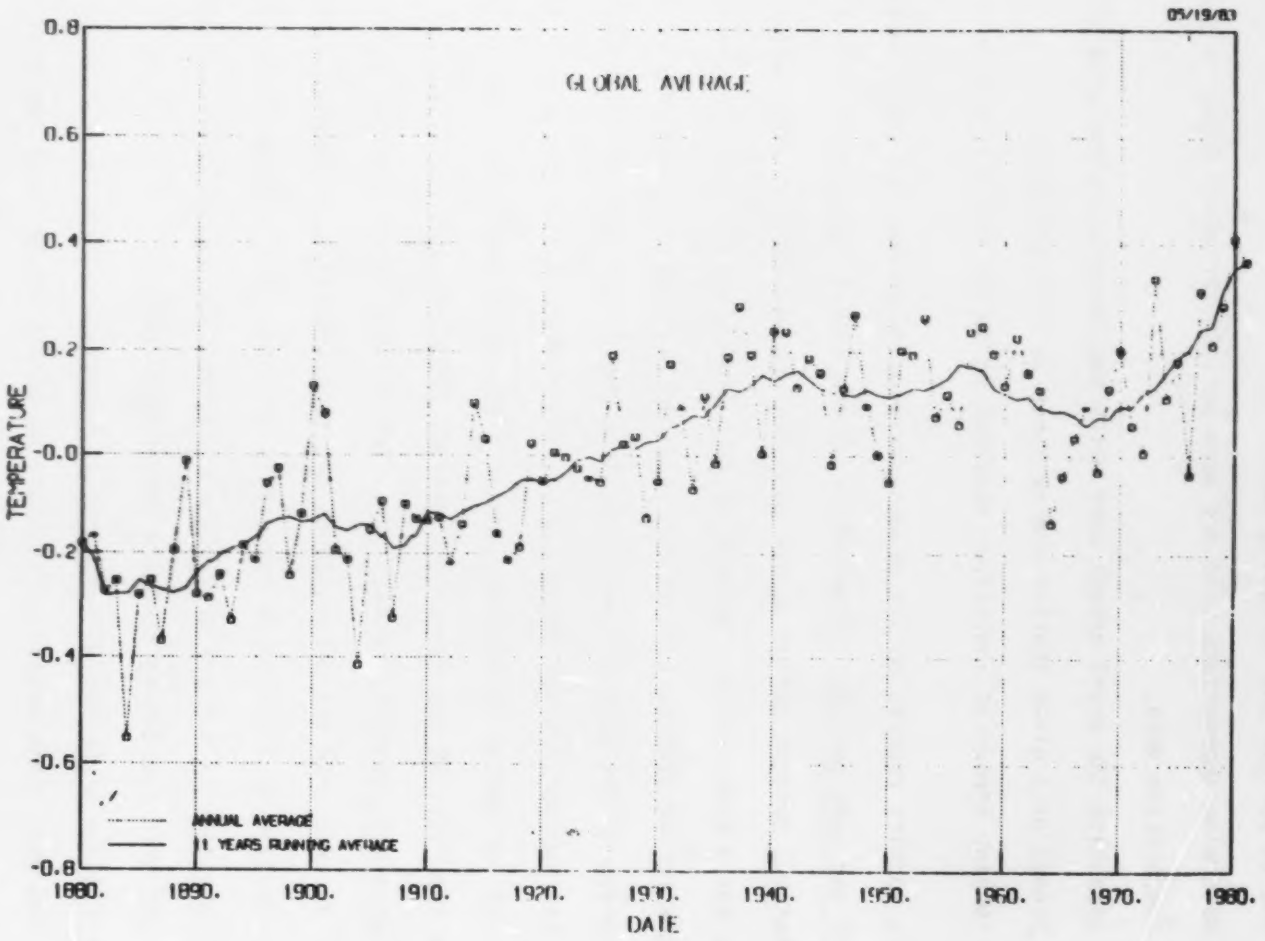

Fig. 27'. Global temperature (deviation from the mean) as a function of year from 1880-1980.

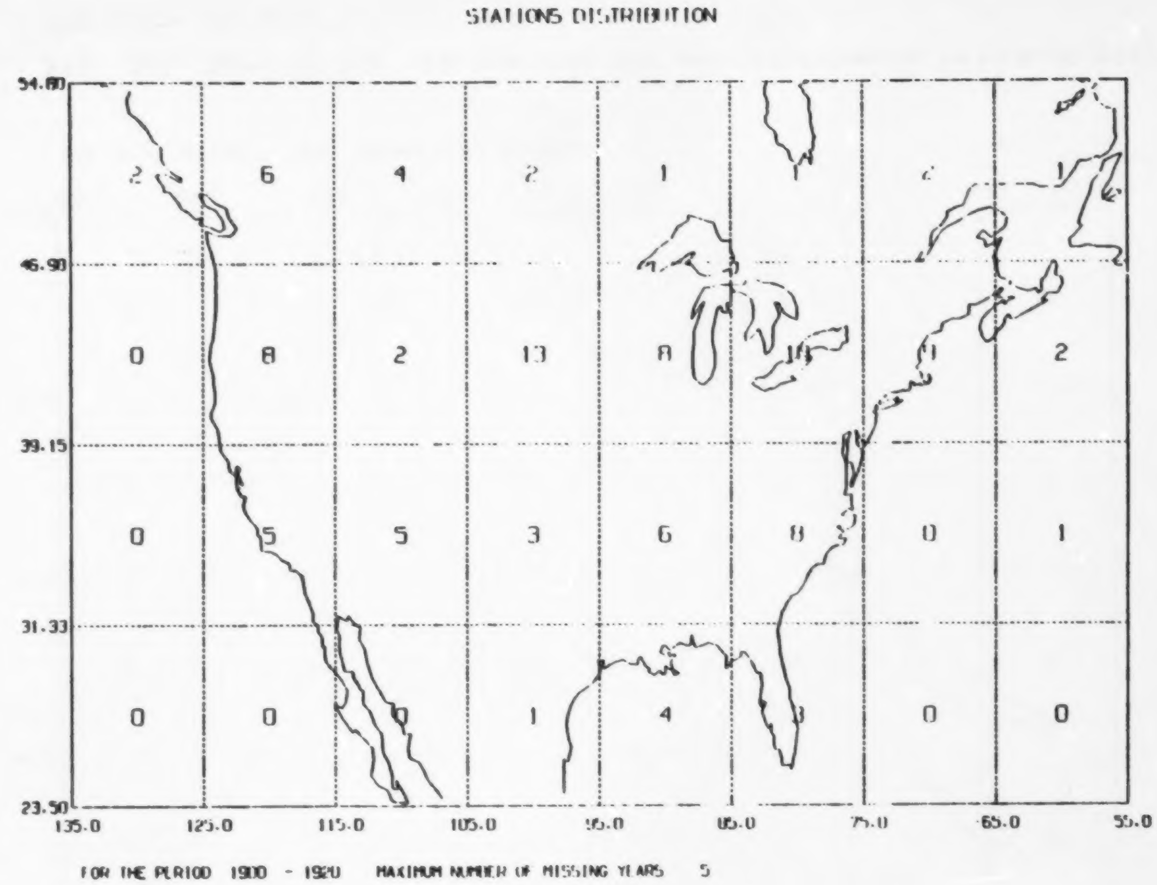
STATIONS DISTRIBUTION
54.80
46.90
39.15
31.33
23.50
135.0
125.0
115.0
105.0
95.0
85.0
75.0
65.0
55.0
2
6
4
2
1
2
1
0
8
2
13
8
10
1
2
0
5
5
3
6
8
0
1
0
0
0
1
4
8
0
0
FOR THE PERIOD 1900 - 1920 MAXIMUM NUMBER OF MISSING YEARS 5

Fig.28 . Distribution of stations in the grid boxes of our GCM during the period between 1900 and 1920, the cold period. Only those stations were counted which had no more than five years missing in the precipitation record.

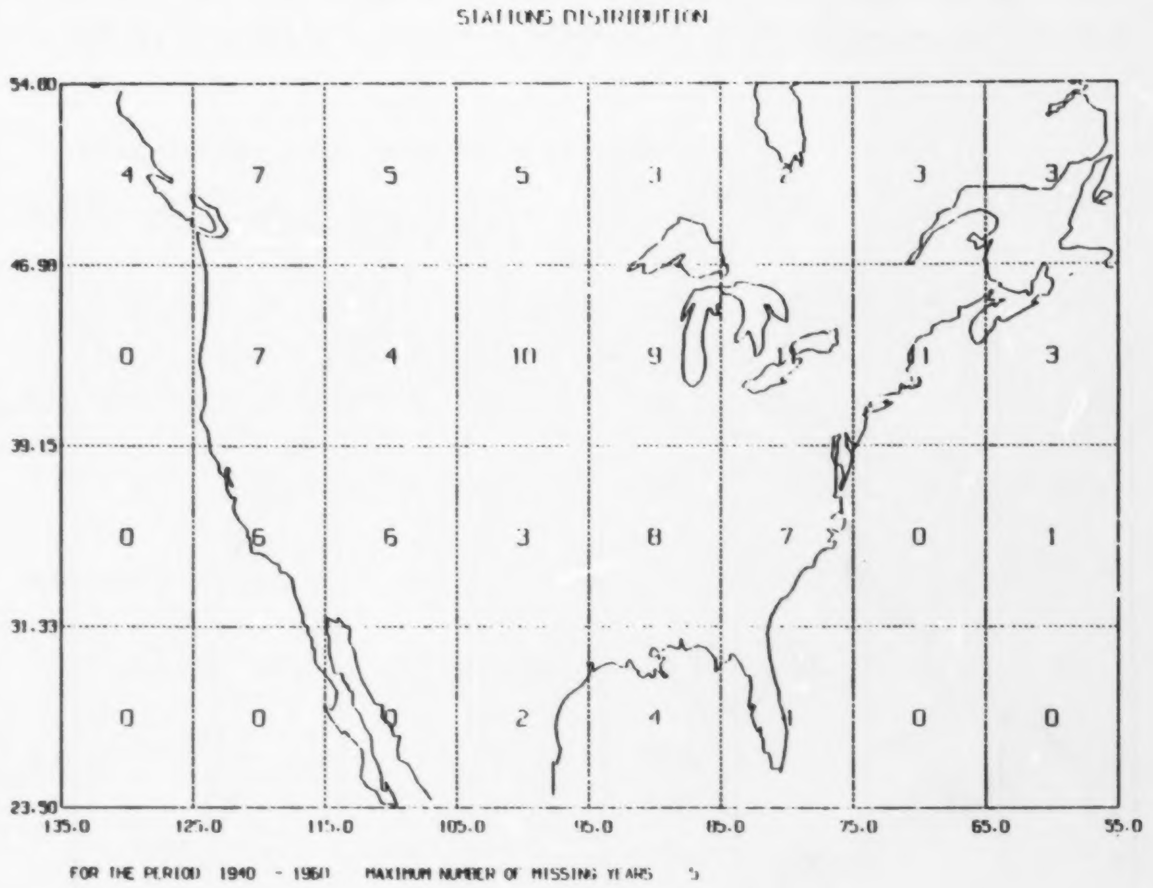
STATIONS DISTRIBUTION
54.00
46.98
39.15
31.33
23.50
135.0
125.0
115.0
105.0
95.0
85.0
75.0
65.0
55.0
4 7 5 5 3 2 3 3
0 7 4 10 9 11 11 3
0 6 6 3 8 7 0 1
0 0 0 2 4 1 0 0
FOR THE PERIOD 1940 - 1960 MAXIMUM NUMBER OF MISSING YEARS 5

Fig. 29. Same as Fig. 28 but for the period between 1940 and 1960, the warm period.

the correlation coefficients between all pairs of stations in a given region. This was done for the time series of both temperature and precipitation; the results are shown in Figs. 30 and 31. To simplify the graphical representation, it is restricted to four grid boxes of our GCM model which include the Colorado river basin and to stations with separation of 500 km or less.

The correlation coefficients were calculated for the period 1880-1980 for temperatures and for the period 1880-1979 for precipitation, with only those pairs of stations having more than 20 years of overlap included. The dashed lines in the figures connect stations between which the correlation is calculated, with the symbol in the middle of the line indicating the value of the correlation coefficient. For example, [] means that the correlation coefficient is between 0.6 and 1. Thus, [] indicates that we can state with a 99% or better confidence that there is a linear association between the temperature (or precipitation) trends at the two stations, with the linear association accounting for between 36 percent and 100 percent of the variation. The symbol Δ indicates that the probability for this association is better than 0.9. In the case of the symbol ○ the probability of this association is only better than 0.6, which means that there is a possible linear relationship between the measurements at two stations, but such can not be stated with high confidence and the relationship can not account for most of the variation.

As can be seen in Fig. 30, correlation between the temperature trends of nearby stations located in the Great Plains is excellent, and even in the Rocky Mountains this correlation is good. In contrast, as can be seen in Fig. 31, correlation between the precipitation time series measured at different station is fair to poor, and this conclusion is the same over plains and over mountains. The averaging method, described below, takes the poorer correlation for precipitation trends into account by decreasing the area for which a station is assumed to provide representative coverage.

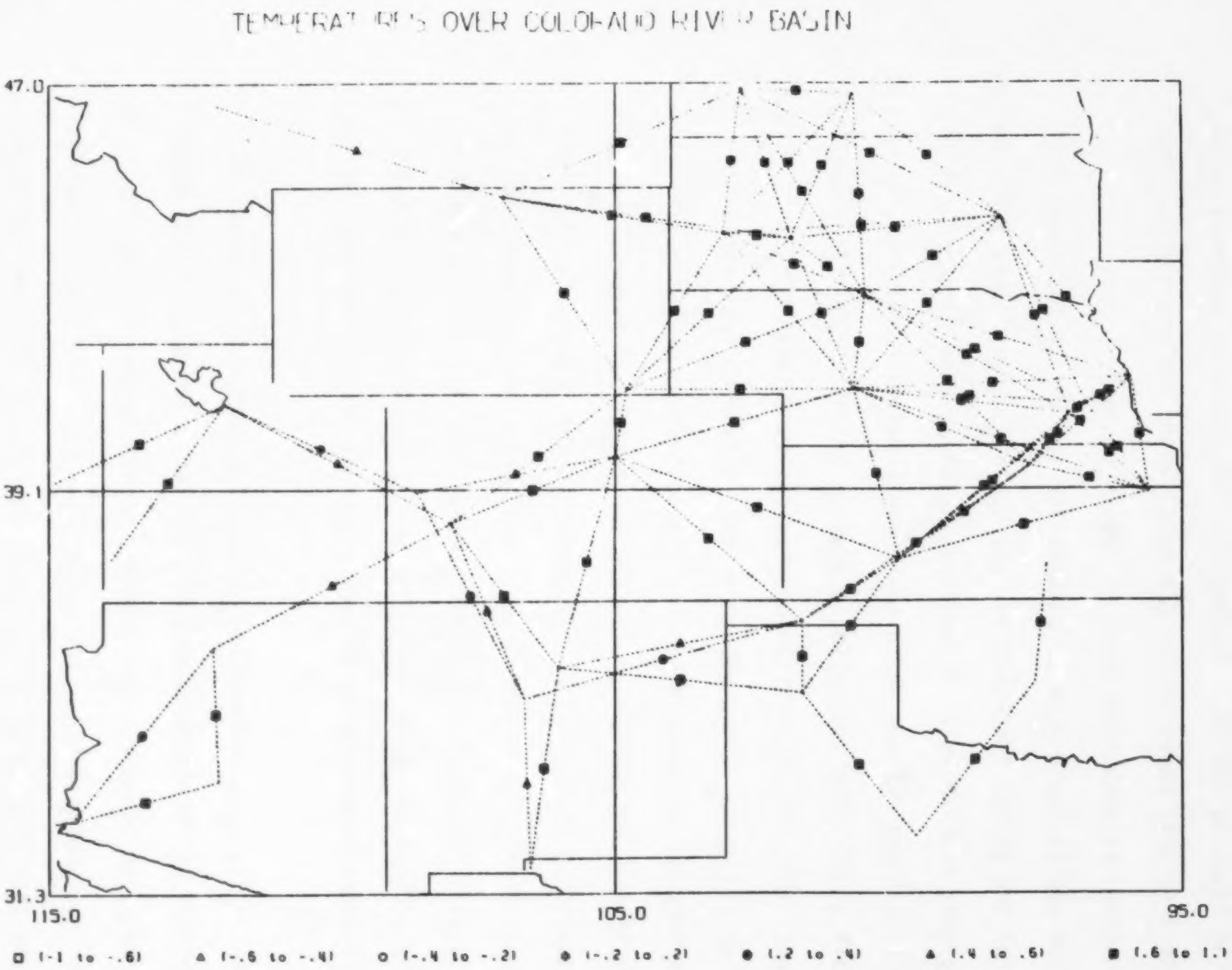
TEMPERATURES OVER COLORADO RIVER BASIN
47.0
39.1
31.3
115.0
105.0
95.0
(-1 to -.6)
(-.6 to -.4)
(-.4 to -.2)
(-.2 to .2)
(.2 to .4)
(.4 to .6)
(.6 to 1.)

Fig. 30. Correlation for temperature trend time series between stations located in the four grid boxes of the GCM. Colorado is in the center. Dashed lines are drawn between the stations, while a symbol in the middle of a line indicates the value of the correlation coefficient. Correlation coefficients were calculated over the period between 1880 and 1980. Maximum distance between the stations is 500 km.

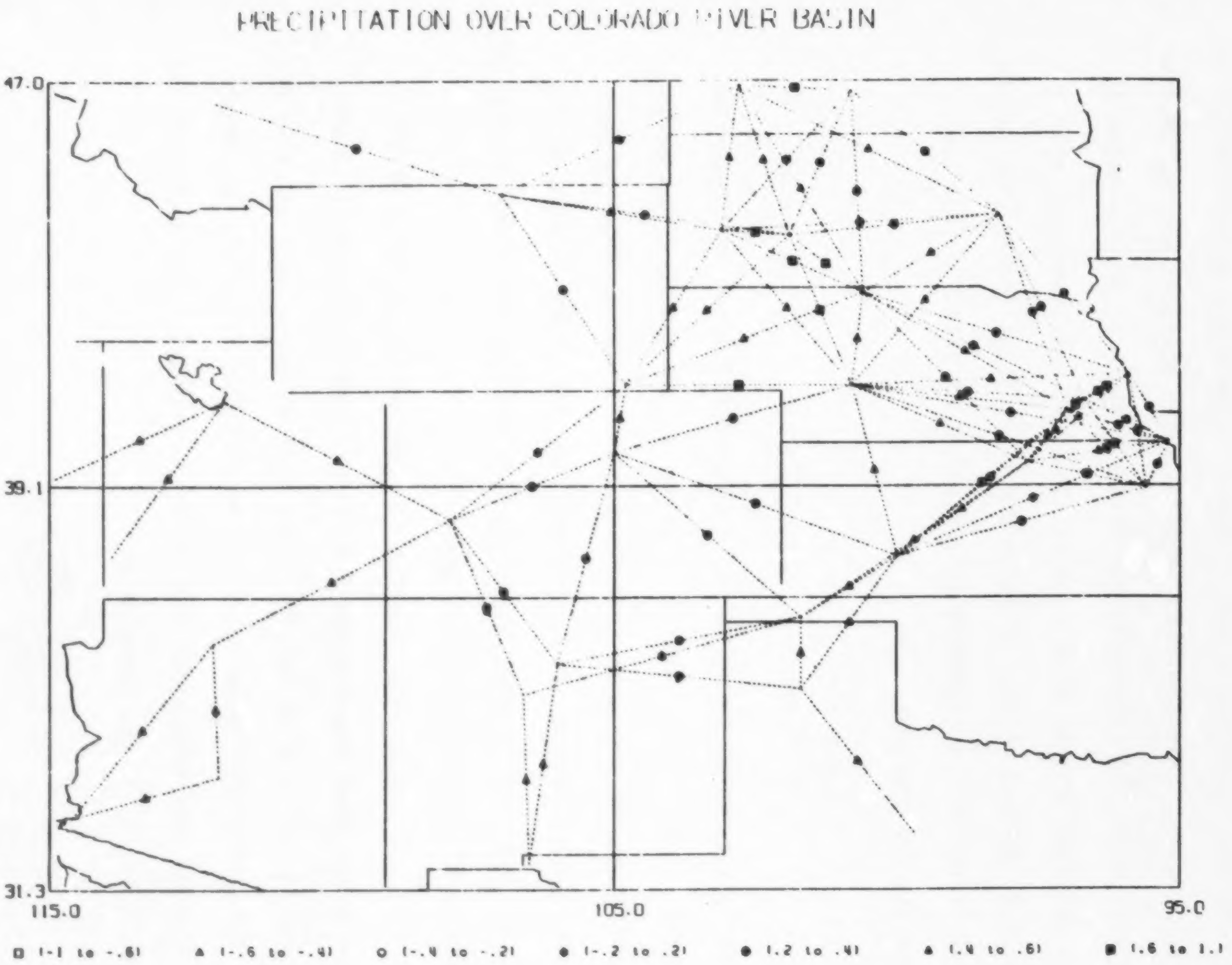
PRECIPITATION OVER COLORADO RIVER BASIN
47.0
39.1
31.3
115.0
105.0
95.0
□ (-1 to -.6)
▲ (-.6 to -.4)
○ (-.4 to -.2)
● (-.2 to .2)
● (.2 to .4)
▲ (.4 to .6)
■ (.6 to 1.)

Fig. 31. Same as Fig. 30 but for precipitation trends.

Combining station data to obtain regional trends. A method was developed to use data from stations to extract a mean change of temperature and precipitation for an arbitrary region. This procedure involves: (1) dividing the region into a large number of cells, and (2) computing the temperature or precipitation in each cell as a weighted average of all nearby stations, i.e., stations within a circle of radius R, defined below. If there are no stations inside this circle the temperature in the cell is undefined. The weight is taken to be a linear function of the station distance, i.e.

$$W = \begin{cases} 1-d/R & d<R \\ 0 & d>R \end{cases}$$

The radius R defines a region inside of which the temperature or precipitation is likely to have a trend similar to that measured at the station. The weight function is similar to the structure function of Gandin (See P. Morel (1973)). This linear dependence of weight on station distance was chosen because of its simplicity and because large scatter of correlation coefficients shown on Fig. 32 does not warrant a more complicated function.

We use correlation coefficients between the time series measured at different stations to estimate the distance R which we assume to be equal to the distance at which the correlation between these time series is statistically not significant. The appropriate value for R can be estimated from Fig. 32, which shows the correlation coefficient for 1000 pairs of stations. The solid line is an empirical analytic fit to the correlation,

$$r = 1 - \frac{d^{1/2}}{18.3 + 0.7\, d^{1/2}} \quad ,$$

where d is in kilometers. There is significant positive correlation out to distances of ~500 km for precipitation.

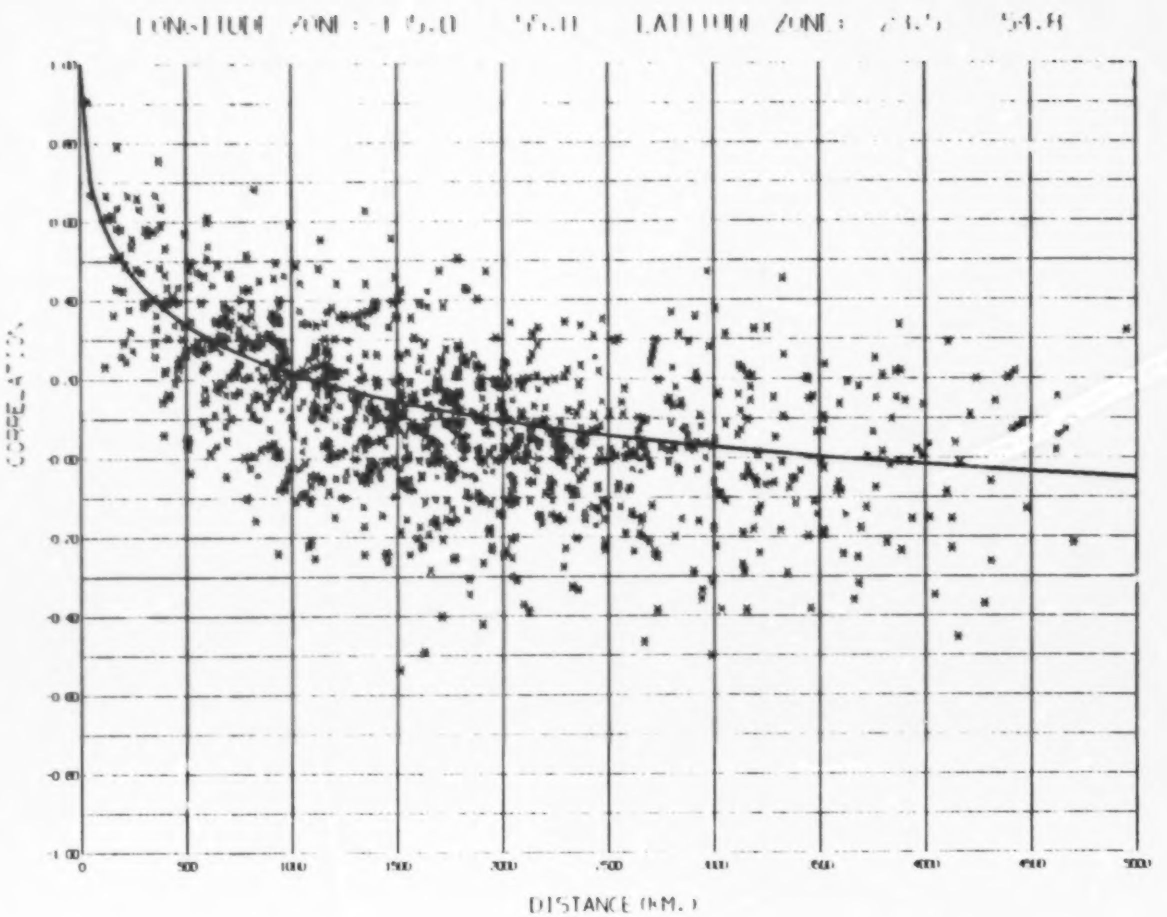

Fig. 32. Correlation coefficients between the precipitation trends of stations located in the region shown on Fig. 28, as a function of distance between the stations.

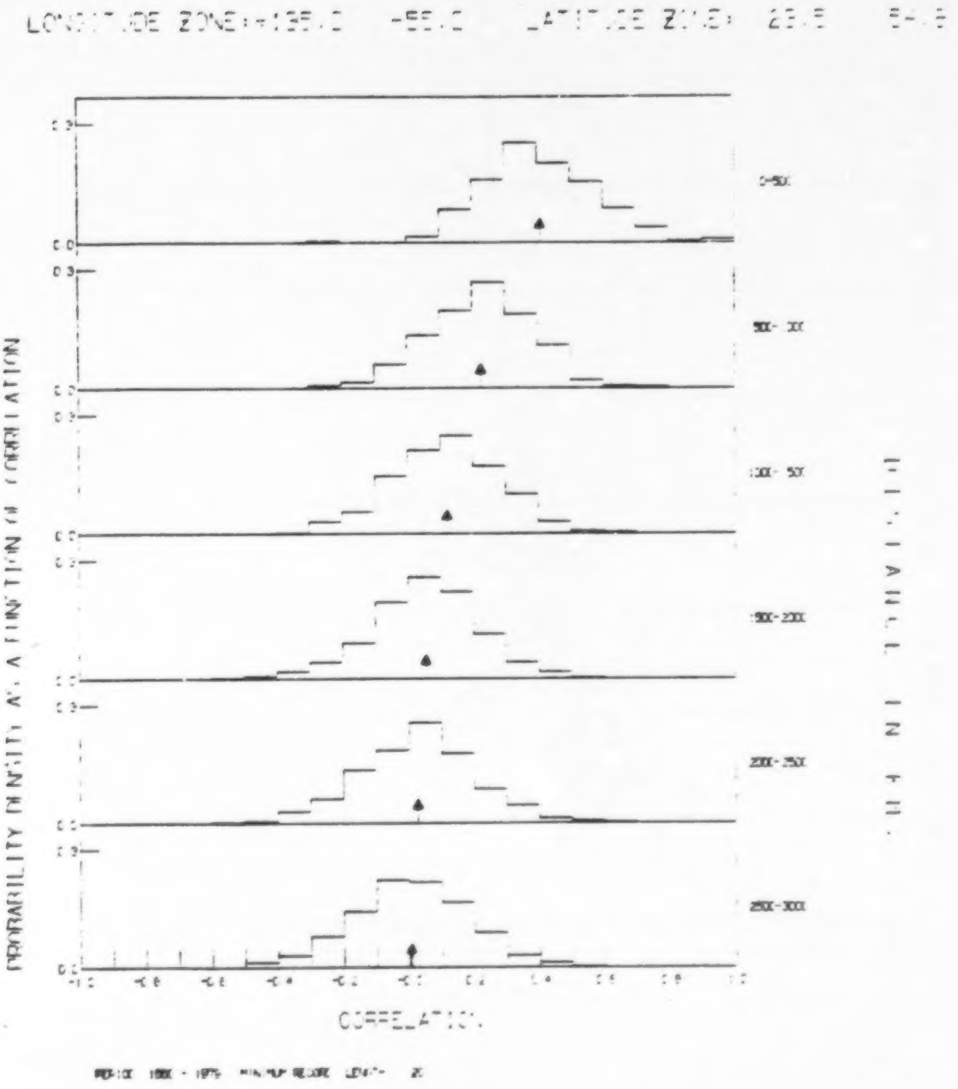

Fig. 33. Histogram for the correlation coefficients for precipitation trends between the stations as a function of distance. The distances have been divided into intervals of 500km as shown on the right of the figure.

This is illustrated in another way in Fig. 33, which is based on all the stations located in the United States. This figure was obtained by dividing station separations into groups at intervals of 500 km. The resulting histograms serve as an estimate to the probability density of the correlation coefficients. These distributions are approximately symmetric. The average value for the correlation coefficient is indicated by the arrow.

For stations separated by 500 km or less the average correlation is 0.42, the standard deviation is 0.18, and more than 99% of all the correlation coefficients are positive. For separations between 500 and 1000 km the average correlation is 0.23, the standard deviation is 0.16 and 95% of the stations are positively correlated. The correlation becomes progressively poorer for the stations separated by a larger distance.

We choose the radius R = 500 km, on the basis of the above results. This yields an area coverage of 76% of the complete region shown on Fig. 28 for the cold period (1900-1920) and an area coverage of 80% for the warm period (1940-1960), i.e., these percentages of the region have at least one station within the correlation radius R. The coverage of land area is significantly higher, as illustrated in Figs. 34 and 35 in which circles of the radius R=500 km are drawn around each station. This choice of the radius is also consistent with the resolution of our GCM, which has grid box diameters of about 1000 km.

Results

We used the above averaging procedure to compute precipitation trends in all the grid boxes shown in Fig. 28. The time series in each box was then averaged over the cold and warm periods. The difference between the average values for warm and cold periods is plotted in Fig. 36, the units being mm/year.

Two distinct regions of precipitation change are apparent in Fig. 36. There is a region of very large increase in precipitation located over the eastern part

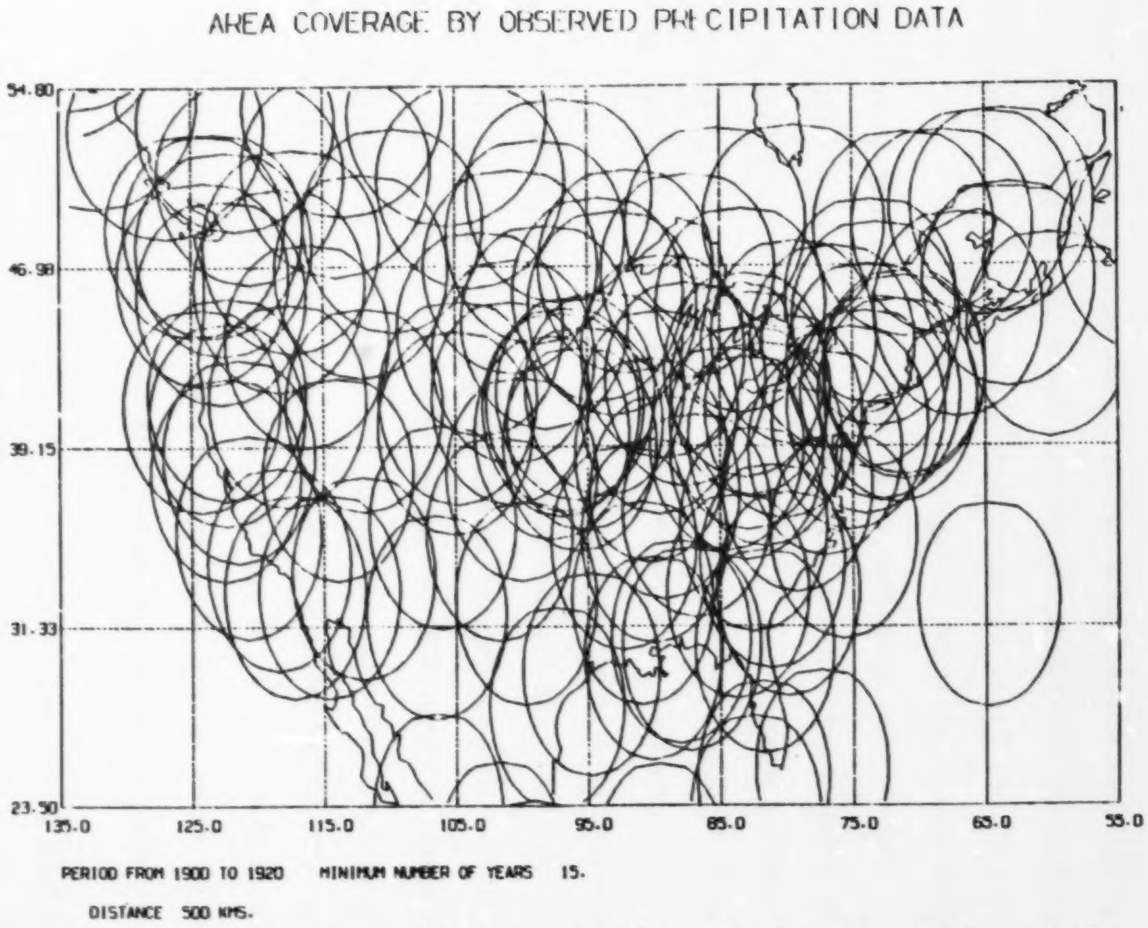
AREA COVERAGE BY OBSERVED PRECIPITATION DATA
54.80
46.98
39.15
31.33
23.50
135.0
125.0
115.0
105.0
95.0
85.0
75.0
65.0
55.0
PERIOD FROM 1900 TO 1920 MINIMUM NUMBER OF YEARS 15.
DISTANCE 500 KMS.

Fig. 34 . Area covered by the stations during the cold period.

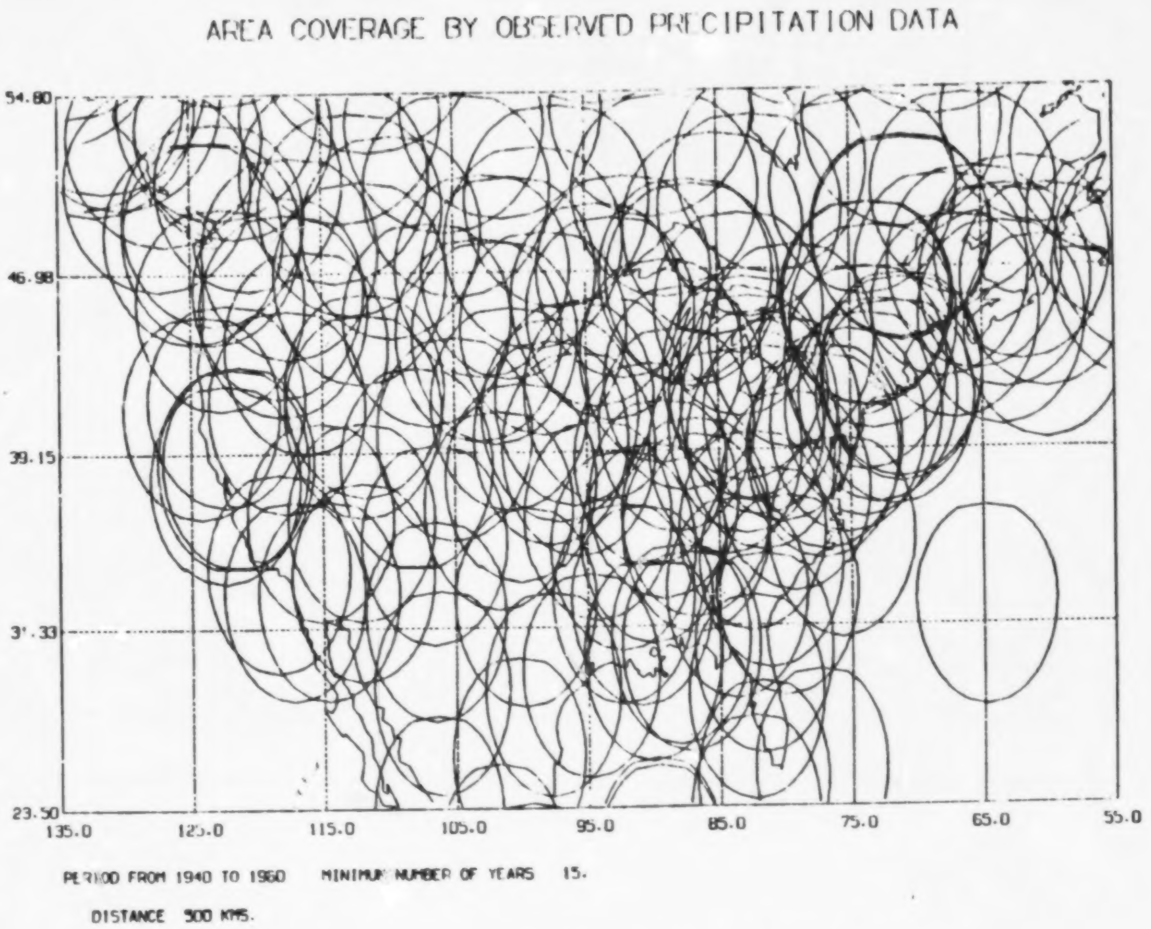
AREA COVERAGE BY OBSERVED PRECIPITATION DATA
54.80
46.98
39.15
31.33
23.50
135.0
125.0
115.0
105.0
95.0
85.0
75.0
65.0
55.0
PERIOD FROM 1940 TO 1960 MINIMUM NUMBER OF YEARS 15.
DISTANCE 500 KMS.

Fig. 35. Area covered by the stations during the warm period.

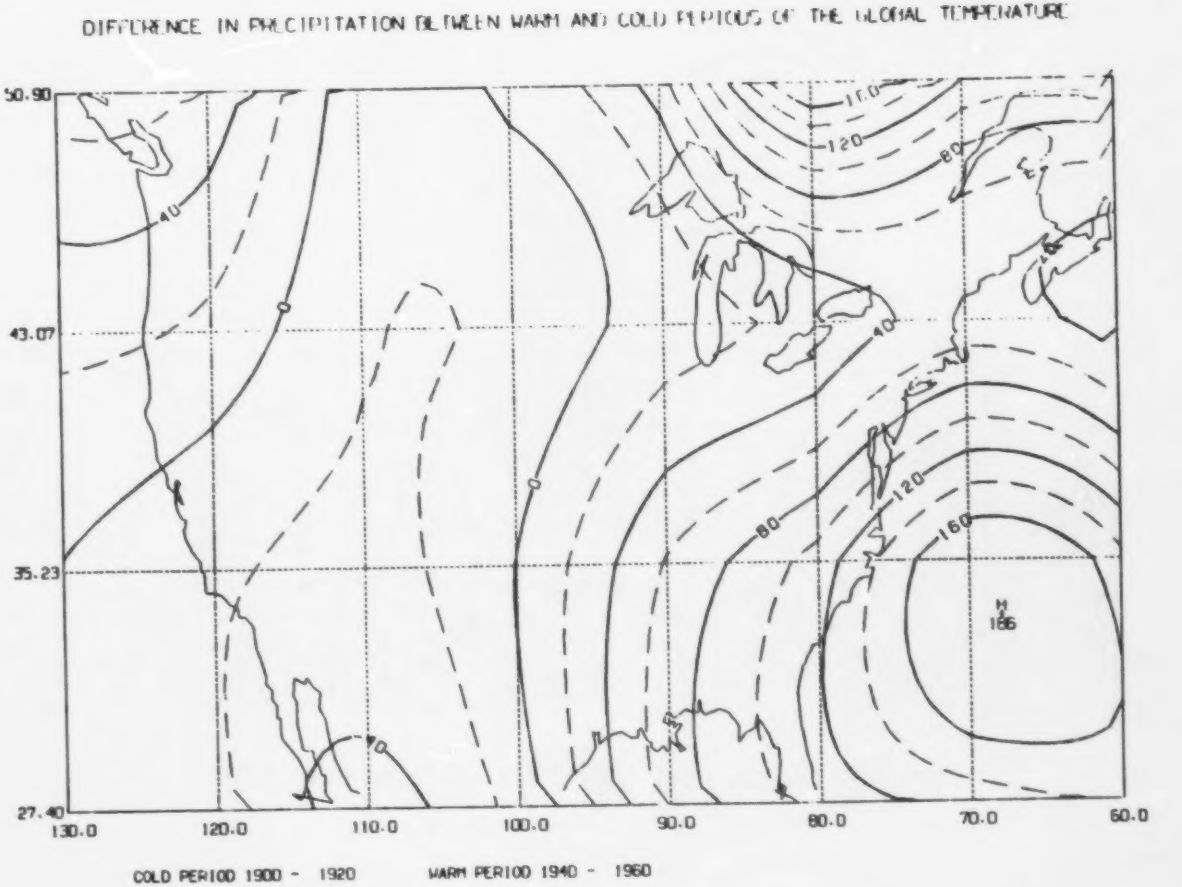
DIFFERENCE IN PRECIPITATION BETWEEN WARM AND COLD PERIODS OF THE GLOBAL TEMPERATURE
50.90
43.07
35.23
27.40
130.0
120.0
110.0
100.0
90.0
80.0
70.0
60.0
40
0
0
0
40
80
120
160
80
120
160
H
186
COLD PERIOD 1900 - 1920
WARM PERIOD 1940 - 1960

Fig. 36. Precipitation during warm period minus precipitation during cold period (mm yr^{-1}).

of the U.S.A. and over Canada, with two apparent maxima: one over Bermuda and a second over the southern tip of Hudson Bay, in Canada.

The remaining large region has very little change in precipitation between the warm and cold periods. Located west of the Mississippi valley, it covers the region of the Great Plains and Rocky Mountains. Two additional, less significant regions of change appear in Fig. 36. One of these, located in the northeast, shows an increase in precipitation. It could be an extension of the region of precipitation increase located in the eastern part of the U.S.A. and connected to it through northern Canada. The second is a region of decreased precipitation, which is of a particular interest because it includes the Colorado river basin.

Comparison to results of other researchers

In order to compare our results with those of Diaz and Quayle we computed the precipitation change between the time periods (1955 - 1977) and (1895 - 1970), which are their time periods C and A. The results of this computation are shown on Fig. 37. Their results for precipitation change have a broad similarity with ours. Thus both results show a precipitation increase in the Southeast and Northwest, and a precipitation decrease over the remaining part of the western coast. We also show a precipitation decrease over the Midwest, although our decrease appears to be smaller. There are however some significant differences between the two results in the Northeastern part of the United States. Some of these difference are partially due to the fact that their resolution of 5°x5° is smaller than our resolution of 8°x10°. For instance, instead of their precipitation decrease over the northern part of Maine and precipitation increase over the New York state, we have a broad region where the precipitation increase is small and almost constant. The difference between our results and theirs is further accentuated by differences in date bases and averaging procedures used by us and by Diaz and Quayle. While we

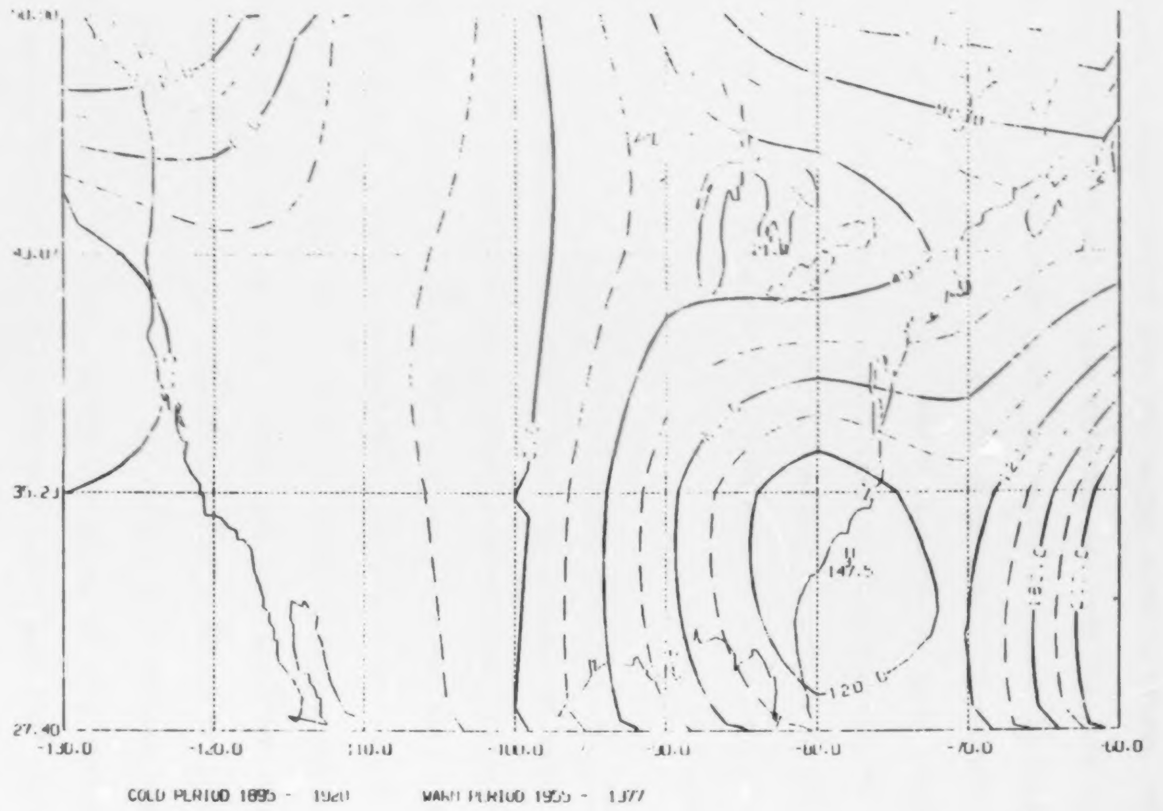
40.00
35.20
27.40
-130.0
-120.0
-110.0
-100.0
-90.0
-80.0
-70.0
-60.0
147.5
120
90.0
COLD PERIOD 1895 - 1920
WARM PERIOD 1955 - 1977

Fig. 37. Precipitation change between the periods 1955-1977 and 1895-1920.

use the measurements from individual stations which we then average over the grids shown on Fig. 28, they use average precipitation for each of the 48 United States which they then interpolate over their 5°x5° grid.

Statistical significance of our results

To study the statistical significance of the precipitation changes as a function of global temperature we first isolated the region of significant precipitation change by applying statistical significance tests to the precipitation changes in individual grid boxes. First, in order to determine the appropriate test for the precipitation change between the warm and the cold periods, we used the F test to find out if the variances of the precipitation time series in each grid box were the same during the cold and the warm periods. This hypothesis had to be rejected only in three grid boxes at the 90% confidence level. Therefore we assumed that variances were the same during the warm and cold periods and applied the appropriate one sided t test to the precipitation time series to isolate regions of statistically significant precipitation change. The criterion was set at the 90% confidence level. The four regions with significant precipitation change are shown on Fig. 38.

Next we examined the time series of the precipitation for these four regions. The time series of precipitation over the eastern United States is particularly interesting. The eleven year running mean (solid line in Fig. 39a) is very similar to the global temperature trend as computed by Hansen et al. (1981), i.e., it increases during the period 1910 and 1940, flattens out during the period between 1940 and 1960 and has maxima in 1940 and 1960. The correlation coefficient between the eleven year running means of temperature and precipitation is 0.85, and even if we assume that the time series have only eight data points (i.e. one point per decade), then the correlation between the precipitation in the eastern United States and the global temperature is significant at a 99% confidence level. The precipitation time series in the region of little precipitation change (Fig.

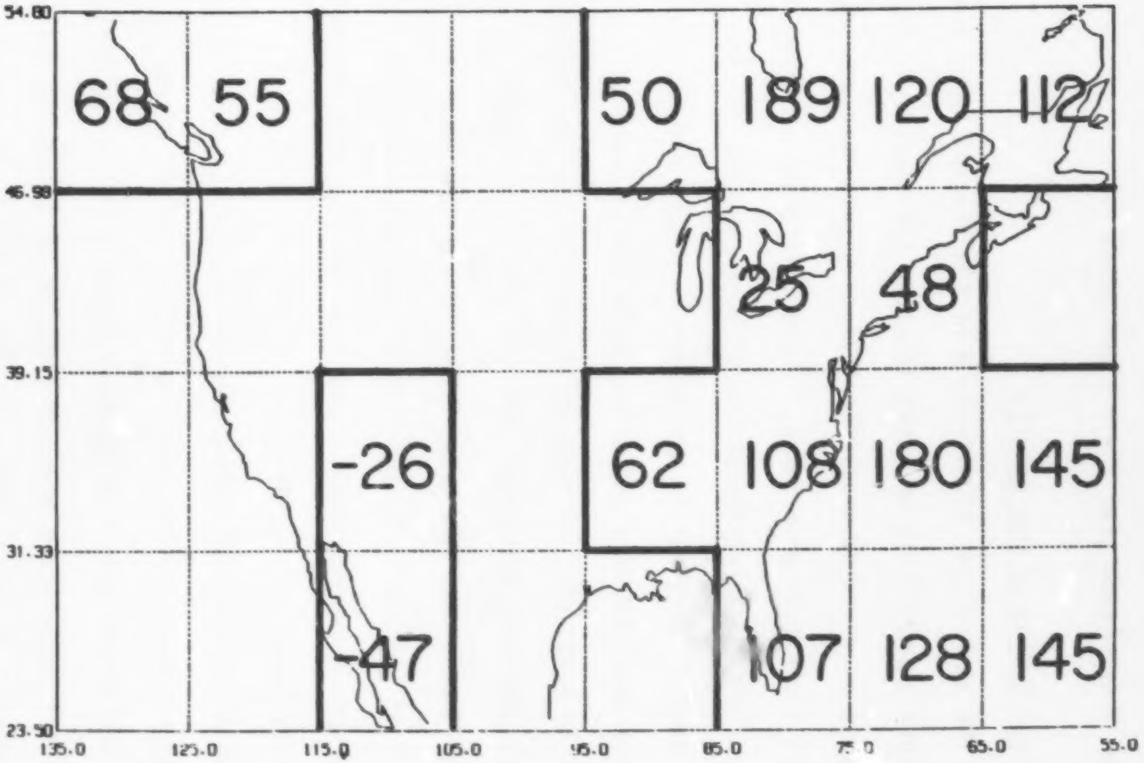
54.80
46.98
39.15
31.33
23.50
135.0
125.0
115.0
105.0
95.0
85.0
75.0
65.0
55.0
68
55
50
189
120
112
25
48
-26
62
108
180
145
-47
107
128
145

Fig. 38. Same as Fig. 36 with the change for each grid box (mm/year). Only changes significant at the 90% confidence level are shown.

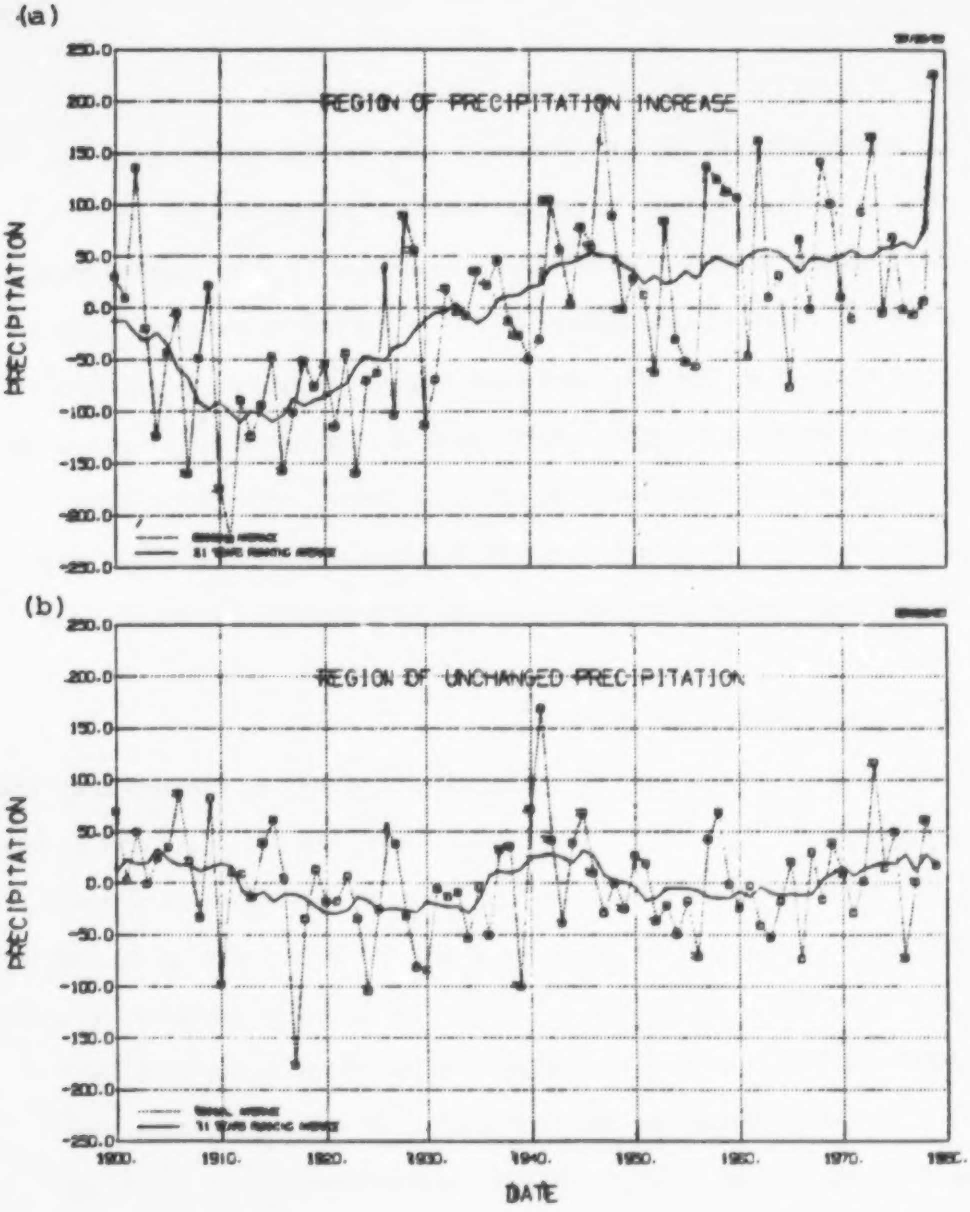

Fig. 39. (a) Averaged precipitation over the region of significant precipitation increase, in the eastern portion of the continent.

(b) Averaged precipitation over the region with no precipitation changes.

39b) has negligible correlation with the global temperature trend (correlation coefficient ~0.1). The precipitation time series of the Northwestern region is very noisy (Fig. 40a). However it does shows an increase during the period between 1910 and 1960; the correlation coefficient between the 11 year running means of global temperature and regional precipitation is 0.6, which is marginal since this represents a correlation at the 88% confidence level. Finally the precipitation curve over the Colorado basin (Fig. 40b) shows a decreasing long range trend. It is negatively correlated with the global temperature trend, with correlation coefficient -0.5. The sense of the correlation is consistent with the slight tendency toward drying in this region with the increased temperatures in the doubled CO_2 experiment discussed in the previous section of this report, however, the correlation is too weak to permit firm comparison.

By comparing our results with those by Wigley et al. (1980) we can see that the change in the Eastern United States is broader and includes the region of the precipitation increase computed by Wigley et al. on the basis of individual warm years. It also appears that their precipitation increase along the West coast of the United States is a warm year transitory phenomenon not reflected in the climatological mean.

Finally, we note that the precipitation change found in the eastern United States is quite large. Corresponding to the change of 0.27°C in the global temperature, the precipitation change is 11 cm/yr which represents 10% of the total precipitation in the region. If the global temperature trend and rainfall changes are indeed causally connected, the implication may be substantial; note that the temperature difference between these two periods is small compared to the projected warming during the next several decades as a result of CO_2 and trace gas warming. Closer examination of these relationships as the current warming trend progresses is obviously warranted, as well as comparison of 3-D global climate model simulations with the observed patterns of precipitation change. The preparation for one such modeling experiment is described in the next section.

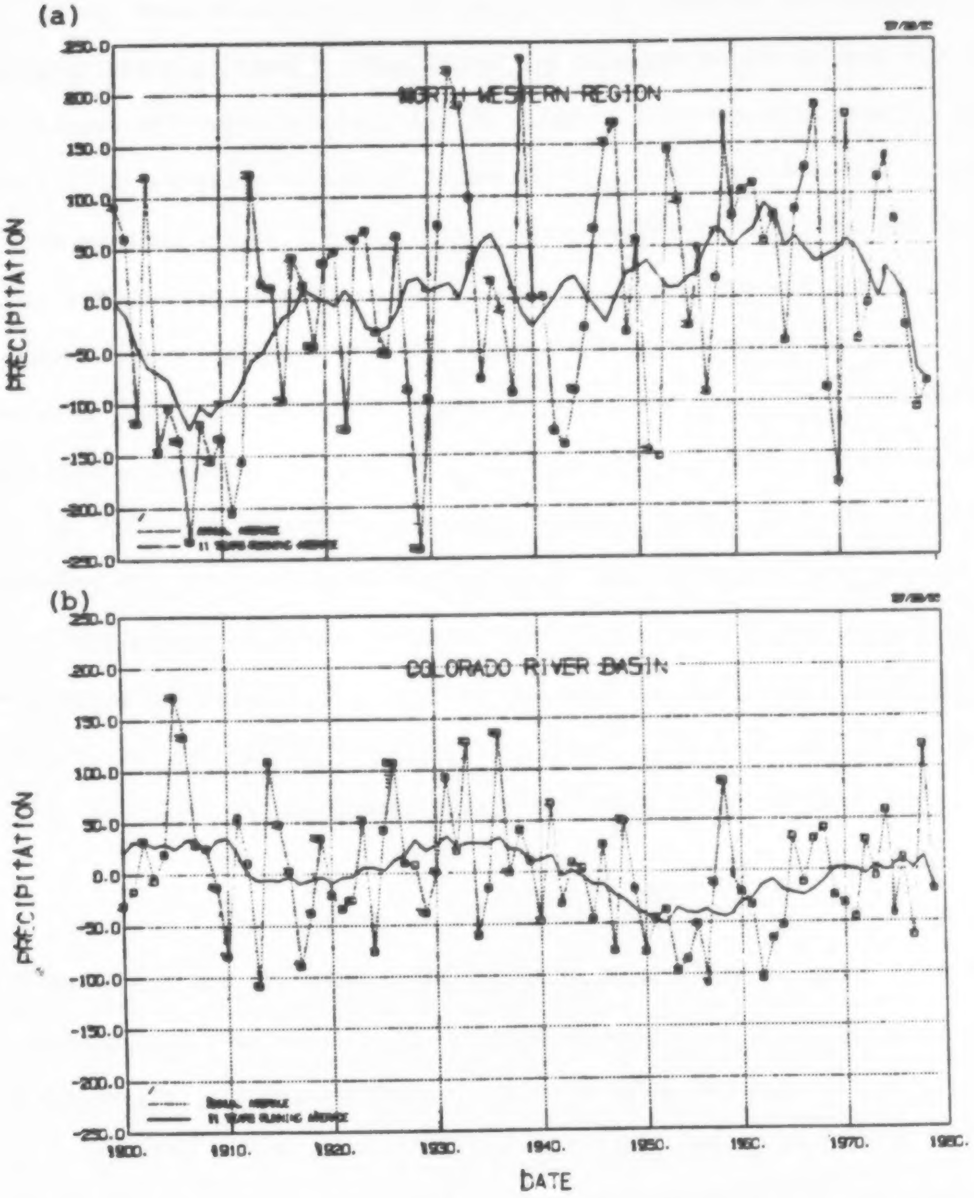

Fig. 40. (a) Averaged precipitation over the northwestern region.
(b) Averaged precipitation over the Colorado River Basin.

III. Future Refinements to Climate Models

In the previous two sections we discussed the difference between the climate in the doubled CO_2 atmosphere and the present climate, and the observed differences between warm and cold climates in the past century. The results in some instances seem contradictory. For example, in the slightly warmer historical climate, the east coast received more rainfall, while in the much warmer doubled CO_2 climate, the east coast was drier. As mentioned earlier, however, these results are not necessarily contradictory -- the doubled CO_2 experiment results do not describe the transitional phases of climate, they focus only on equilibrium conditions after CO_2 has doubled. In order to adequately anticipate transitional climates and decide upon the appropriate responses it will be necessary to know how the system will react as the climate warms, with magnitudes of warming intermediate between the historical rise and the projected doubled CO_2 equilibrium effect. This requires that GCMs be used for experiments in which carbon dioxide (and other greenhouse gases) is allowed to increase gradually with time, and the response of the system determined as a function of time.

The Goddard Institute for Space Studies is in the process of doing its first "transient" run, in which we start with the climate of 1958 and alter the atmospheric composition in a continuous manner. It is important to emphasize, however, that one run with one model will not provide a statistically reliable solution to this question. Many such runs with different models will be required. Furthermore, uncertainties associated with global climate modeling, particularly of physical processes such as ocean atmosphere coupling (whose importance is illustrated by El Nino events), cloud dynamics, sea ice representation, and accurate hydrological/biological interactions, all need to be examined. In addition, as is evident in the presentation so far, model resolution would need to be increased if answers are to be provided on a finer spatial scale. Nevertheless, this first transient run will allow us to begin examining the evolution of the warming. Simulations with increasingly realistic models will be possible in the future, if appropriate model development and related observational studies are carried out.

Use of GCMs holds much promise as a tool for projecting future climatic change from increases in greenhouse gases. These models, however, are still in their development stage and require considerable refinement if they are to achieve their full potential. This chapter highlights critical physical processes that need to be better represented if we are to reduce current uncertainties in estimating the responsiveness of the climate system to increases in greenhouse gases. It also discusses other possible refinements to the models aimed at providing annual or "transient" changes in climate as greeenhouse gases increase over time and at improving estimates for individual grids.

Three kinds of uncertainties affect the reliability of output from general circulation models: how responsive will the climate system be to increases in greenhouse gases (eg. how much will the temperature rise for a particular increase in CO_2); how will regional climates change; and how will changes occur over time given specified increases in various greenhouse gases.

Sensitivity of Climate System

The range of estimates from GCM's is quite large. For a doubling of atmospheric CO_2 levels, Manabe et al. estimate a 2°C rise, Washington et al. estimate a 4.2°C rise, and Hansen et al., a rise of 4.1°C. Differences between the high and low estimates can be attributed to how the GCMs simulate clouds, and secondarily to initial sea ice conditions.

Cloud behavior is particularly difficult to model. Existing databases and theory do not provide an adequate basis for defining their appropriate treatment. Thus, additional research will be needed to develop a more comprehensive database and to improve scientific capability to model clouds more reliably. Until this analysis is completed, large uncertainties will persist in calculating thermal responsiveness of the climate system to increases in greenhouse gases.

Improvements will also be needed in knowledge about sea ice and ocean dynamics that could affect such ice. Since sea ice reflects large amounts of sunlight, changes in it could be important to the total radiation absorbed by earth, and thus the climate system's responsiveness to perturbation.

Uncertainties Concerning Regional Climates

Regional climates are sensitive to patterns of general circulation. In particular, sea surface temperature is a key factor influencing the movement of weather systems. For example, the 1982-3 Nino involved a very large change in sea surface temperature that caused weather in many parts of the world to follow highly unusual patterns. The cold weather (for continental U.S.) of 1976 and 1977 was possibly influenced by unusually warm water off the Bering Staights that may have influenced the polar jet streams to first go north, then dip south.

Global warming on the scale anticipated from increases in greenhouse gases is likely to alter ocean circulation and thus sea surface temperatures. Current GCMs generally have very simple oceans, which only passively respond to changes in heat. Ocean circulation is not ordinarily modeled as a dynamic process. Thus, GCMs underestimate variations in sea surface temperature that could alter weather patterns, failing to adequately predict this vital aspect of the climate system. Until changes in ocean circulation are modeled so that they respond to temperature, the regional projections produced by GCMs will be less reliable than desired. Research must be expanded in this area to collect data that can be used to incorporate more realistic treatment of the oceans.

Of less importance, but still of significance, will be improvements in modeling ground hydrology and the response of plant life to alterations in climate and to the photosynthetic effects of rising CO_2. Both the water holding capacity of land and the efficiency of water use by plants will be altered by rising CO_2 and climate change. Since these are important determinants of regional climate, this feedback loop needs to be modeled in GCMs. In the long term GCMs will need representations of these processes or they will not be able to forecast regional climate change accurately.

Timetrend of Temperature Change

Finally from the perspective of users the most important aspect of climate change will be the transitions through time, not the "ultimate" climate after CO_2 has doubled. Appendix A discusses key parameters used in an initial transient run underway at the Goddard Institute for Space Studies.

APPENDIX A

ESTIMATING ANNUAL CHANGES IN TEMPERATURES

The Goddard Institute for Space Studies is now in the process of performing a transient run with its GCM in which the year by year changes in climate are simulated for past and expected changes in greenhouse gases and aerosols.

Trace Gas and Aerosol Perturbation

In this section we describe the parameterizations developed for the time evolution of trace gases for the period 1958 to 2030 which will be used in our transient global climate model experiment. First we consider the parameterization for CO_2 and other trace gases such as Fluorocarbon 11 (F11), Fluorocarbon 12 (F12), Methane (CH_4) and Nitrous Oxide (N_2O). Since increase in these gases is slow compared with their mixing time over the globe, we can take these gases as being uniformly mixed.

For the CO_2 concentration between 1958 and 1980 we use the annually averaged amount of CO_2 at Mauna Loa as measured by Keeling et al. (1982). Projection of the CO_2 concentration into the future is extremely uncertain, depending especially on the postulated growth of energy demand and the availability of different fuels. For these reasons it is worthwhile to consider a range of scenarios, for example, as discussed by Hansen et al. (1981). Table 3 shows the CO_2 trends obtained with their 'fast growth' (~3 percent/year), slow growth (~1½ percent/year) and no growth energy scenarios, as well as the CO_2 trend which we will use in our 3-D transient experiment. The latter was supplied to us by EPA, being constructed on the basis of a moderate growth of energy use with changes of the airborne fraction of CO_2 accounted for on the basis of a simple carbon cycle model (loc. cit.). This EPA scenario is quite similar to the slow growth scenario of Hansen et al. (1981).

Table 3. Different CO_2 Scenarios

Year	EPA Scenario	Growth Rate		
		Fast	Slow	NO
1980	339	339	339	339
1990	352	356	354	352
2000	373	384	373	366
2010	396	429	395	378
2020	420	504	422	394
2025	433.75	554	438	401
2030	448	614	453	408
2040	478	753	490	424
2050	513	893	532	440

Minor gases included in our transient run are F11, F12, CH_4 and N_2O. Concentrations of fluorocarbons were obtained using estimates for their release for the period 1950 to 1980 by the Chemical Manufacturer Association (1981). The annual release of fluorocarbons during the years 1980-2030 is assumed to be constant and equal to the average value of their release during the decade 1971-1980, i.e. 283.5 millions of kilograms of F11 per year and 367.5 millions of kilograms of F12 per year.

The annual release of fluorocarbons for the period prior to 1950 was estimated by assuming this release to be a linear function of time.

$$\text{Annual release} = A_k(\text{years} - Y_k^o)$$

Here k=11,12 and stands for fluorocarbon F11 and F12. The proportionality constants A_k and the years Y_k^o , at which the annual release is equal to zero, were determined in such a way that the annual release in 1950 and the total amount released up to 1950 calculated using the expression above were equal to the values reported in the CMA report. The residence times of fluorocarbons are not well known, the main sink being the stratosphere. Here we estimate these residence times t_k to be 75 years for F11 and 150 years for F12. Thus, for the year m the concentration $C_k(m)$ as a function of the annual release $R_k(m)$ is given by:

$$C_k(m) = f_k \sum_{e=1940}^{m} e^{-(m-e)/t_k} R_k(e) \text{ .} \qquad \text{(A)}$$

According to our estimate the annual release for both fluorocarbons during the year 1940 was zero. The constant f_k relates the mixing ratios C_k in ppbv of fluorocarbons to their annual release R_k (in millions kg/year). These constants of proportionality were determined by comparing the computed concentrations with observed globally averaged values of F11 and F12 for the years 1977-1979 as reported by NOAA (1979) and (1980) in Geophysical Monitoring for Climatic Change No. 7 and No. 8. Global average concentrations were computed from the results of measurements of concentrations at five stations. Locations of these stations and the measured values are summarized in Tables 4 and 5. We assumed the concentrations to be zonally uniform and fitted expresssions

$$C_k(\lambda,\phi) = \sum_{e=1}^{5} a_e \sin^{e-1} (\phi)$$

to the data in Table 4. Here ϕ denotes latitude and λ longitude. The global averages are shown in the last column of Table 4. The constants of proportionality f_k were obtained by fitting expressions (A) to the data, yielding $f_{11} = 4.6395.10^{-5}$ and $f_{12} = 5.3279.10^{-5}$ ppb/(millions kg/year).

Table 4. Concentrations of Fluorocarbons (ppbv)

Year	Station					
	BRW	NWR	MLO	SMO	SPO	GLOBAL
	Fluorocarbon 11 (CCl_3F)					
1977	0.159	0.155	0.148	0.140	0.139	0.145
1978	0.172	0.168	0.162	0.153	0.154	0.159
1979	0.182	0.175	0.174	0.164	0.175	0.171
	Fluorocarbon 12 (CCl_2F_2)					
1977	0.292	0.275	0.270	0.256	0.248	0.262
1978	0.302	0.296	0.291	0.273	0.271	0.282
1979	0.301	0.301	0.296	0.276	0.306	0.290

Table 5. Locations of the Stations

Name	Abrev.	Longitude	Lattitude
Point Barrow	BRW	130.60°W	70.32°N
Niwot Ridge	NWR	105.63°W	40.05°N
Mauna Loa	MLO	155.58°W	19.53°N
American Samoa	SMO	170.56°W	14.25°S
South Pole	SPO	24.80°W	89.98°S

The corresponding fluorocarbon scenarios are shown in Fig. 41. Scenarios for Methane and Nitrous Oxide were constructed using estimates of Lacis et al. (1981). Concentrations for CH_4 and N_2O, in 1958, are respectively 1.4 and 0.295 ppmv. Between 1958 and 1970 the concentration of N_2O remains unchanged while that for CH_4 increases by 0.6%/yr. During the decade between 1970 and 1980 concentrations for CH_4 and N_2O change respectively by 0.96% and 0.2%. Finally, after 1980, we estimated the CH_4 increase to be 1.5% and N_2O increase to be 0.3%. The time variations of CH_4 and N_2O are shown in Figs. 42 and 43.

Atmospheric aerosols produced by volcanic explosions are shortlived, lasting no more than a few years. Also the spread of volcanic dust in space is highly

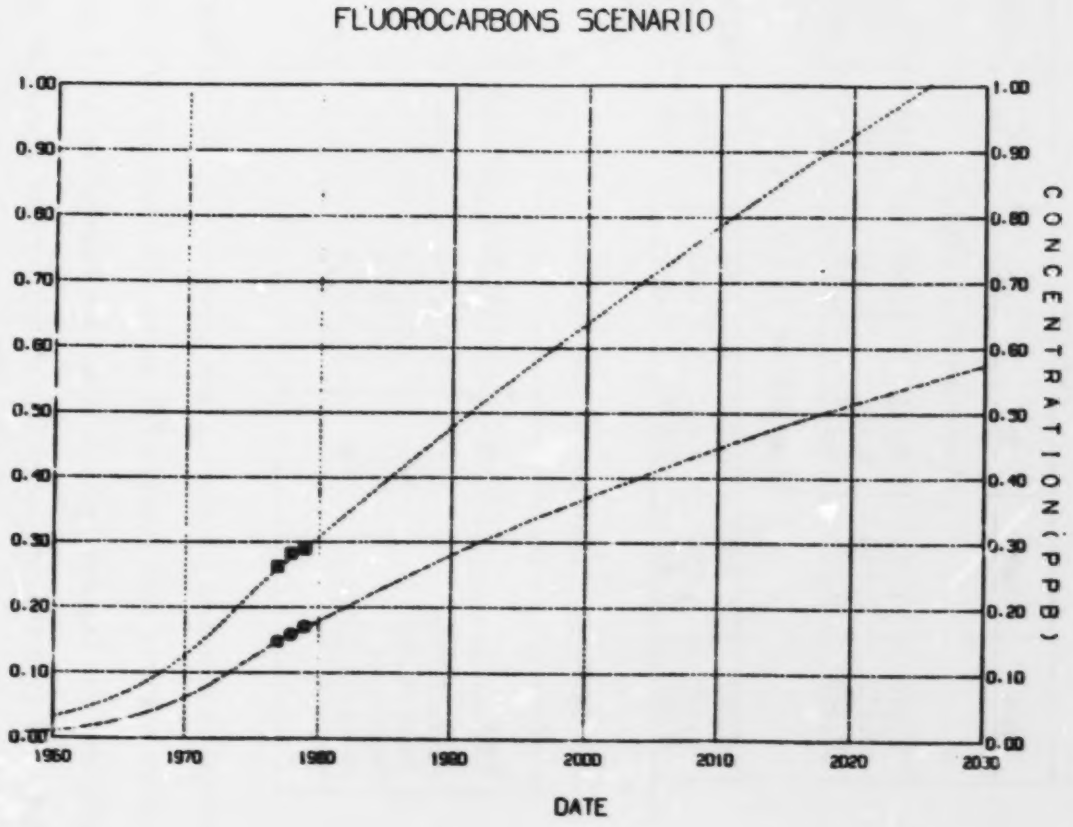

Fig. 41. Fluorocarbon scenarios. The observed values are also shown by circles for F11 and squares for F12.

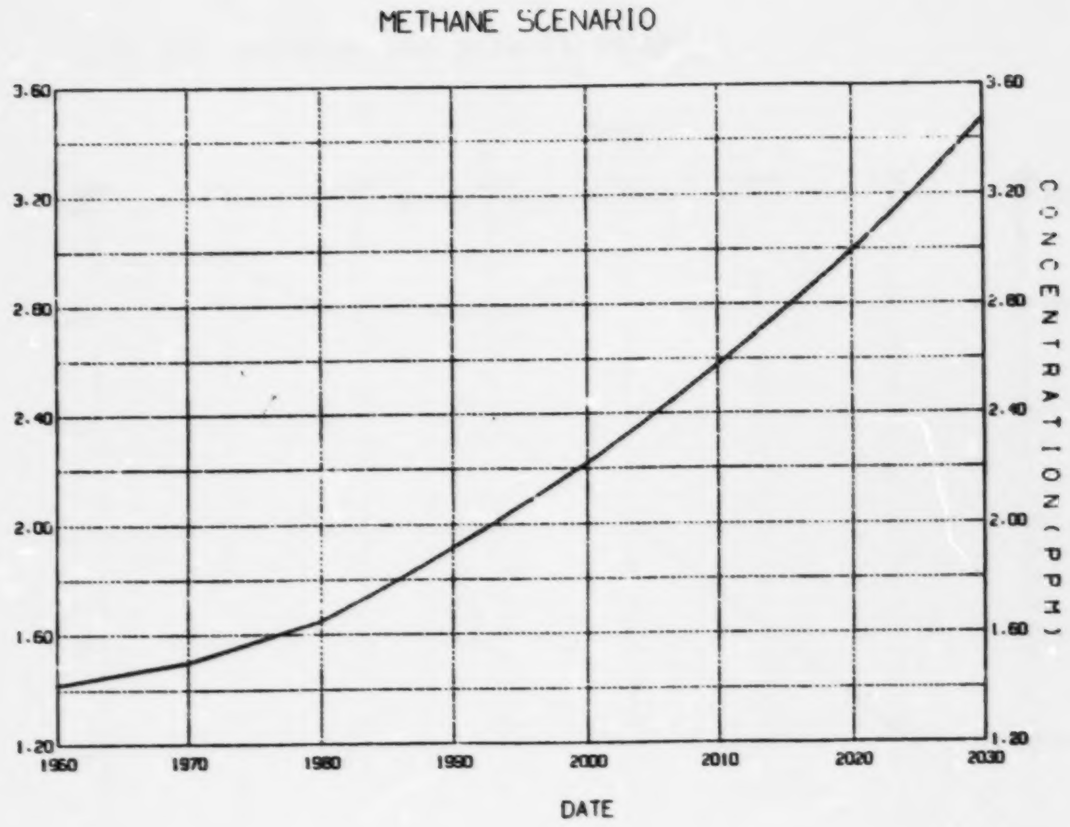

Fig. 42. Scenario for methane.

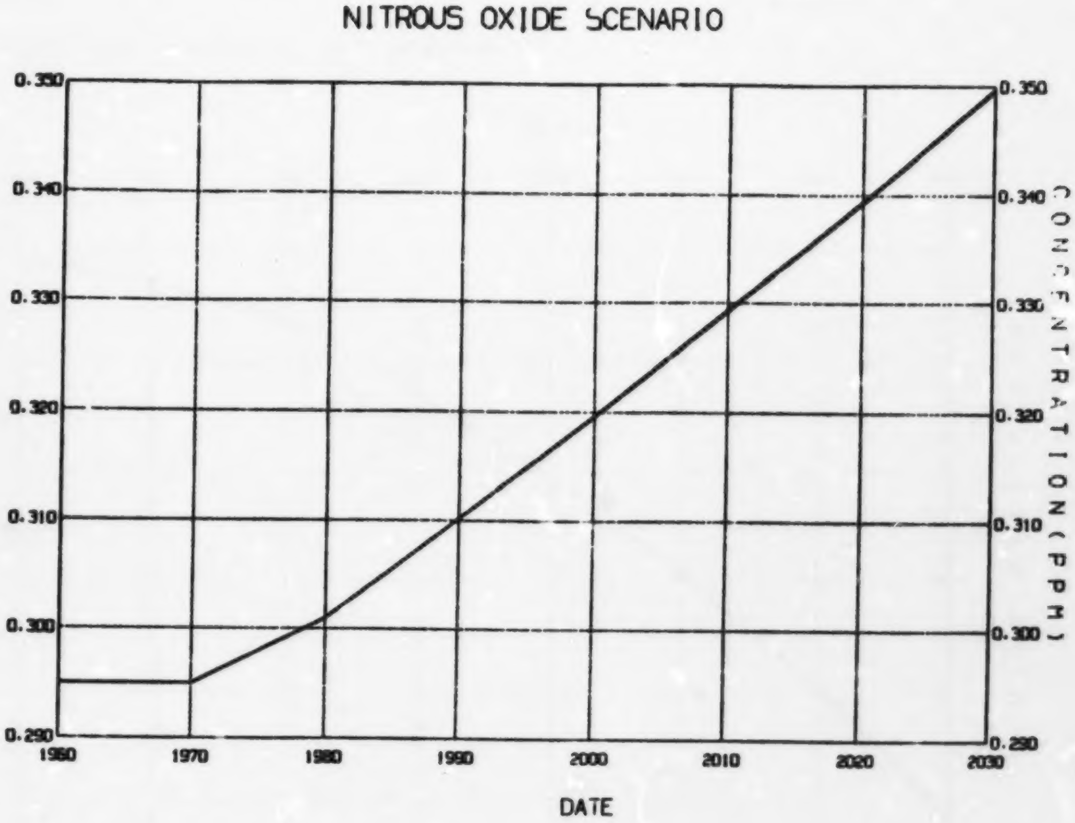

Fig. 43. Scenario for nitrous oxide.

nonuniform. For instance: dust from volcanoes that erupt in the polar regions tends to be confined to these regions; also volcano Agung erupted near the equator, but most of its dust went into the Southern Hemisphere; more recently the stratospheric aerosols from the volcano El Chichon remained confined for a long time to a latitudinal belt between the equator and 30°N. Therefore, the specification of the volcanic aerosol distribution has to be done at least on a monthly basis and the optical depth has to be a function of position over the globe. A list of volcanos since 1956 that are thought to have produced substantial aerosol amounts is summarized in Table 6.

Table 6. List of Climatologically Significant Volcanoes

Name	Date	Latitude	Longitude	Lambs DVI	Scaling Factors X10^8
Bezymjannaja	3/30/1956	56.0°N	160.5°E	30	0
Volcanos in Chile	5/20/1960	39-45°S	72.5°W	100	?
Gunung Agung	3/17/1963	8.5°S	115.5°E	800	846
Awu	8/12/1966	3.5°N	125.5°E	150	162
Fernandina	6/12/1968	0.5°S	92.0°W	75	123
Fuego	10/18/1974	14.3°N	90.5°W		83
Soufriere	4/17/1979	13.3°N	61.2°W		0
St. Helens	5/18/1980	46.2°N	122.2°W		0
Alaid	4/27/1981	50.8°N	155.5°E		0
El Chichon	4/2/1982	17.3°N	92.8°W		?

We used our medium resolution 9-layer general circulation model (Hansen et al. (1983)) and our tracer model (Russell and Lerner (1981)) to determine the dispersion of the volcanic dust over the globe for each of these volcanoes. First, winds for the entire globe and for several years were generated by the General Circulation Model. Then the same amount of dust from every volcano shown in Table 6 was injected into the stratosphere of the model at the location and time indicated in the table, and the tracer model was used to study the diffusion of the volcanic cloud over the globe. Dust entering the troposphere was assumed to be instantly removed. Therefore the exchange of air parcels between the stratosphere and troposphere served as a sink for the stratospheric dust.

The main scattering and absorbtion of solar radiation is by sulfuric acid aerosols, which are produced from gas-to-particle conversion of the gases SO_2, H_2S, and CSO injected by volcanos. The conversion time in the stratosphere between these gases and sulfuric acid is estimated to be of the order of six months. Therefore, in order to take into account this conversion time, we multiplied the computed density of the volcanic dust by a function

$$F(t) = \begin{cases} t/\tau & t<\tau \\ 1 & t>\tau \end{cases}$$

where t is the time elapsed since the eruption and τ is assumed to be equal to six months.

In order to determine the optical depth due to the aerosol injected by each volcano we used the solar irradiance transmission measured at Mauna Loa for the period 1958 to 1979 (NOAA 1979). The τ so obtained contains scattering, due to Rayleigh aerosol as well as absorption by different atmospheric gases. In order to isolate the optical depth due to the volcanoes, we used the fact that no major eruption affecting the atmospheric transmission at Mauna Loa occurred in the several years prior to Agung. Thus by subtracting the average value for the optical depth between the years 1958 and 1963 the effect of scattering due to all other components of the atmosphere but the volcanic aerosol was removed. This residual optical depth is plotted in Fig. 44. Eruption dates of the volcanos listed in the table are indicated by arrows on the figure. Volcanos in Chile are located too far to the south of the equator to have a significant impact at Mauna Loa. However, Agung, Awu, and Fuego are clearly visible. Although any signal from Fernandina is barely discernable in the noise, it was introduced in order to represent the slow decrease in optical depth after the explosion of Awu. The scaling factors between the computed density and the optical depth to be used in the model run were obtained by imposing the condition that the computed and observed optical depths at Mauna Loa should be equal.

The tracer model was integrated for 36 months after the Agung eruption at which point the volcano Awu exploded. The computed optical depth due to Agung was subtracted from the observation and the computed density due to Awu as well as the residual observed optical depth were integrated for 22 months, when the volcano Fernandina exploded. The scale factor for Fernandina was obtained in the same way as the scale factor for Awu. The optical depth due to the volcano Fuego was not contaminated by previous eruptions, and thus the scale factor was simply obtained by integrating the computed and observed τ over a period of 32 months. The computed optical depth at Mauna Loa is plotted as a solid line in Fig. 44. The agreement between observed and computed optical depths for Awu and Fuego is very good, and the signal from Fernandina is buried in the noise. However, in the case of Agung the observed maximum in the optical depth is delayed by about a year from the computed maximum. The imprecision in representing the time dependence of aerosol opacity after Agung may be due to unrealistic transport by the tracer model; however, the model did result in 20%

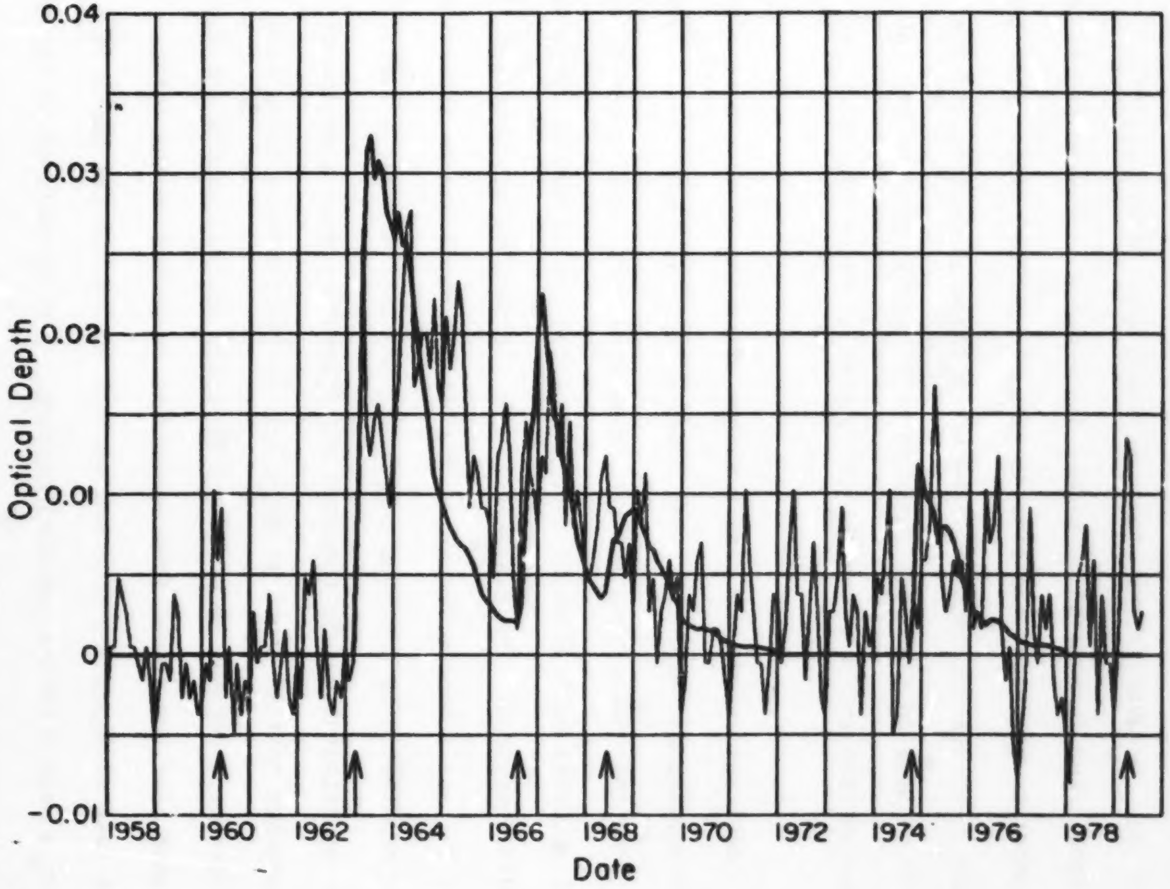

Fig. 44. Optical depth as measured at Mauna Loa Observatory (dashed line) after removal of average value from 1958 to 1963. Also shown is the computed optical depth (solid line). The arrows refer to the volcanos listed in Table 6.

of the aerosol going into the Northern Hemisphere in agreement with observations. Perhaps the assumed 6-month decay time is inaccurate for an eruption as large and which penetrated as high as Agung did.

According to M.P. McCormick et al. (1981) the effect of the explosion of Soufriere on climate should be negligible, and as estimated by Jager et al. (1982) the same is true for the two volcanos Mt. St. Helen and Alaid. Thus, the only volcano to be included since 1974 is El Chichon, for which the data just now are becoming available.

Increasing Our Confidence in the Result

As noted in the first part of this section, this run will provide only one estimate of the climate change due to the gradual increase in carbon dioxide and other trace gases. Much work needs to be done to increase our confidence in the result. The elements of the climate system that are currently poorly modeled, or not modeled at all, must be investigated closely, both theoretically and observationally. The highest priority must be given to understanding the ocean circulation, and how it may respond to the climate change. This will require a large increase in observations of the ocean, from both ships and satellites, for it is impossible to confidently model a system when it is uncertain whether the model is producing realistic simulations. Programs are already under way to produce a cloud climatology data set for the same reasons. Understanding of these and other parts of the geophysical system will depend on increased observational capability of both the particular aspect and of its interaction with the atmosphere.

We may expect that firm results about the climate's sensitivity will yield only to long-term analysis. The results obtained in the above sections, and those to be produced in the transient experiment, are only a beginning of attempts to understand and model how climate will change in the years to come.

References

Arakawa, A., 1972: Design of the UCLA General Circulation Model. Tech. Rep. No. 7, Dept. Meteor., University of California, Los Angeles, 116 pp.

Berry, F., E. Bollay and N. Beers, Eds., 1973: Handbook of Meteorology. McGraw-Hill, 1068 pp.

Chemical Manufacturers Association (CMA): World Production and Release of Chlorofluorocarbons 11 and 12 through 1980. CMA Report, July 29, 1981.

Diaz, M. F. and Quayle, R. G., 1980: The Climate of the United States since 1895: Spatial and Temporal Changes, Mon. Wea. Rev., 108, p. 246-266.

Hansen, J., Johnson, D., Lacis, A., Lebedeff, S., Lee, P., Rind, D., Russell, G., 1981: Science, 213, 957-966.

Hansen, J., Russell, G., Rind, D., Stone, P., Lacis, A., Lebedeff, S., Reudy, R. and Travis, L., 1983: Efficient Three-Dimensional Global Models for Climate Studies, Models I and II. Mon. Wea. Rev. 111, in press.

Jager, H., Reiter, R., Carnuth, W., Funk, W., 1982: The Aerosol Increase with Stratosphere due to Volcanism During 1980 and 1981, observed by Lidar at Garmish-Parturkirchen, presented at The Symposium on the Application of Lidar to Radiation and Climate. IAMAP Third Scientific Assembly, Hamburg, Federal Republic of Germany, 1981.

Jager, J. and Kellogg, W.W., 1983: Anomalies in Temperature and Rainfall during Warm Arctic Seasons, Climatic Change 5, 39-60.

Keeling, C.D., Bacastaw, R.B., Whorf, T.P., 1982: Measurements of the Concentration of Carbon Dioxide at Mauna Loa Observatory, Hawaii, pp 377-385, in Carbon Dioxide Review, 1982, W.C. Clark, Ed., Oxford Univ., Press, New York.

Korzoun, V., et al., 1977: Atlas of World Water Balance. The UNESCO Press, Paris.

Lacis, A., Hansen, J., Lee, P., Mitchell, T., Lebedeff, S., 1981: Greenhouse Effect of Trace Gases, 1970-1980, Geophysical Research Letters, 8, 1035-1038.

Lamb, H.H., 1970: Volcanic Dust in the Atmosphere, Phil., Trans. Roy Soc. London, 266B, 425-575.

McCormick, M.P., Kent, G.S., Yue, G.K., Cunnold, D.M., 1981: Sage Measurements of The Stratospheric Aerosol Dispersion and Loading From the Soufriere Volcanoes, NASA TP-1977.

Miller, J., Russell, G. and Tsang, L., 1983: Annual Oceanic Heat Transports Computed from an Atmospheric Model, Dynamics of Atms. and Oceans, 7, 95-109.

Morel, P., 1973: Space and Meteorological Data Analysis, p. 471 - in Dynamic Meteorology, P. Morel, Ed., D. Reidel Publishing, Co., Boston, U.S.A.

National Academy of Sciences, 1979, 1981: Carbon Dioxide and Climate, A Scientific Assessment, Washington, D.C.

NOAA, 1979: Geophysical Monitoring for Climatic Change No. 7., Summary Report 1978, B.G. Mendonca, Ed., Environmental Research Laboratories, Boulder, Colorado.

NOAA, 1980: Geophysical Monitoring for Climatic Change No. 8., Summary Report 1979, G.A. Herbert, Ed., Environmental Research Laboratory, Boulder, Colorado.

Pittock, A.B., Salinger, M.J., 1982: Towards Regional Scenarios for a CO_2-Warmed Earth, Climatic Change 4, 23-39.

Russell, G.L. and Lerner, J.A., 1981: A New Finite-Differencing Scheme for the Tracer Transport Equation, J. Appl. Meteor, 20, 1483-1498.

Schutz, C. and Gates, W., 1971: Global Climatic Data for Surface, 800mb, 400mb, Reps. R-915-ARPA, R-915/1 ARPA, R-1029-ARPA, Rand Corp., Santa Monica.

Wigley, T.M.L., Jones, P.D. and Kelly, P.M., 1980: Scenario for a Warm, High-CO_2 World, Nature, 283, 17-21.

Williams, J., 1980: Anomalies in Temperature and Rainfall During Warm Arctic Seasons as a Guide to the Formulation of Climatic Scenarios, Climatic Change 2, 249-260.

*U.S. GOVERNMENT PRINTING OFFICE : 1984 O-421-082/518